**BERGISCHE UNIVERSITÄT WUPPERTAL**

Dissertation im Fach
Geographie

mit dem Titel

# The potential of passive infrared thermography for the detection of microbial hot spots and hot moments at high spatial and temporal resolution

zur Erlangung des akademischen Grades
Doktor der Naturwissenschaften (Dr. rer. nat.)

durch die Fakultät für Human- und Sozialwissenschaften
der Bergischen Universität Wuppertal

vorgelegt von
Melanie Katharina Schwarz
aus Recklinghausen

Wuppertal, im Juni 2021

The PhD thesis can be quoted as follows:

*Look.*

# Contents

# List of Figures

# List of Tables

# Nomenclature

**List of Abbreviations**

**ALC**      Ambient Laboratory Conditions

**ANOVA**  Analysis of Variance

**C**         Carbon

$^{14}$**C**      Radiocarbon

**CaCl$_2$**    Calcium Chloride

**C$_{mic}$**     Microbial Carbon

**C/N**      Carbon-to-Nitrogen Ratio

**CO$_2$**      Carbon Dioxide

**C$_P$**       Partition Coefficient

**CV**       Variation Coefficient

**CHC**     Controlled Air Humidity Conditions

**DFG**     Deutsche Forschungsgemeinschaft (German Research Foundation)

**E$_P$**       Partition Entropy

$f$         Focal Ratio

**FIR**      Far Infrared

**G$_M$**      Mixed Glucose Solution

**G$_P$**      Pipetted Glucose Solution

| | |
|---|---|
| **IR** | Infrared |
| **IRT** | Infrared Thermography |
| **KOH** | Potassium Hydroxide |
| **LIR** | Longwave Infrared |
| **M** | Mixed |
| **MUF** | 4-Methylumbelliferyl-$\beta$-D-Glucopyranoside |
| **O$_2$** | Dioxygen |
| **p** | Level of Significance |
| **P** | Pipetted |
| **PP** | Polypropylene |
| **PPF** | Polypropylene Foil |
| **R$^2$** | Correlation Coefficient |
| **SD** | Standard Deviation |
| **SOC** | Soil Organic Carbon |
| **SOM** | Soil Organic Matter |
| **T** | Temperature |
| $T(hm)$ | Mean Temperature of hot moment |
| $T(max)$ | Maximum Temperature of hot moment |
| $T(min)$ | Minimum Temperature of hot moment |
| **UV** | Ultraviolet |

**VWC**        Volumetric Water Content

**WHC**        Water Holding Capacity

**WRB**        World Reference Base

### Greek notations and other symbols

$A$            Amplitude

$\alpha_\lambda$            Emitted Radiant Power

$\boldsymbol{\beta}$            Beta Ray

$c$            Specific Heat Capacity

$\epsilon$            Specific Emissivity

$\boldsymbol{\gamma}$            Gamma Ray

$\lambda$            Outgoing Thermal Radiation

$\lambda_b$            Black-Body Thermal Radiation

$m$            Mass

$\boldsymbol{\mu}$            Mean of $\Delta T$

$n$            Number of Pixels

$\o$            Mean of Property

$R$            Mineralized $CO_2$ Amount

$S$            Equidistant Data Point

$\sigma$            Stefan-Boltzmann constant

$\sigma^2$         Variance of Time Series

$\boldsymbol{\sigma}$         Phase Angle

$t$         Time

$Q$         Thermal Energy

$\Delta Q$         Thermal Energy Change

$Q_R$         Respiration Energy Release

$\Delta T$         Temperature Change

$\varphi$         Gaussian Function

$w_{i,j}$         Areal Proportion

$x$         Argument of a Function

$Y_{i,j}$         Given Value

$Y_{scale}$         Scaled Value

# Abstract

The detection of soil surface temperatures allows various statements to be made about soil microbial activity. Such activity can be expressed as catabolic activity in form of heat generation, which is already used as an equivalent to microbial growth rates in established measurement methods (e.g., microcalorimetry). Accordingly, passive infrared thermography (IRT) that measures heat from measurement object surfaces is a promising technique for the non-contact and non-invasive detection of soil microbial activity. Passive IRT records the heat generation on surfaces in temporal and spatial high resolution. Therefore, high-resolution thermal imaging can be used to map the dynamics of microbial growth rates.

The goal of the present thesis is the development of a non-invasive measurement approach of microbial heat production in soils. Accordingly, the systematic development of a laboratory analytical and data processing procedure to capture spatial and temporal variability of catabolic heat generation on soil surfaces is addressed. A component of the method development includes undisturbed soil samples in addition to the conventionally used disturbed samples. The results show that passive IRT has great potential and multiple possibilities of application in microbiological soil research, hence, it can be used to predict energy and metabolic turnover, especially of carbon. After substrate application, a temperature increase of more than 1 K was detected, which can be attributed to hot spots and hot moments of microbial activity, in so-called hot movements. Furthermore, IRT offers the possibility to approximate soil surface moisture and its change over time in an active measurement procedure so that soil physical properties can be considered in addition to the microbiological component. The simultaneous detection of moisture and other soil surface properties using established measurement methods is used to evaluate and explain passive IRT derived data.

The results of this thesis make a decisive contribution to the research of microbial dynamics in soil and provide future studies with a technical basis to map microbiological and physical energy fluxes in soil. The thesis contributes to obtaining deeper insights into metabolic processes in soils.

*Keywords: Passive infrared thermography, heat production, catabolism, microbial activity, spatio-temporal analysis*

# Kurzfassung

Die Erfassung der Bodenoberflächentemperatur ermöglicht es eine Vielzahl an Aussagen über mikrobielle Aktivität im Boden zu treffen. Diese Aktivität kann als katabolische Aktivität in Form von Wärmeentwicklung ausgedrückt werden, die in etablierten Messverfahren (z.B. Mikrokalorimetrie) bereits als Äquivalent zur mikrobiellen Wachstumsrate verwendet wird. Daher ist die passive Infrarot-Thermografie (IRT), die die Wärme von Messobjektoberflächen misst, eine vielversprechende Technik für die berührungslose und nicht-invasive Erfassung der mikrobiellen Aktivität im Boden. Die passive IRT erfasst die Wärmeentwicklung von Oberflächen in zeitlich und räumlich hoher Auflösung. Daher kann die hochauflösende Wärmebildtechnik genutzt werden, um die Dynamik der mikrobiellen Wachstumsraten abzubilden.

Das Ziel der vorliegenden Arbeit ist die Entwicklung einer nicht-invasiven Messmethodik der mikrobiellen Wärmeproduktion in Böden. Dementsprechend wird die systematische Entwicklung eines laboranalytischen und datenverarbeitenden Verfahrens zur Erfassung der räumlichen und zeitlichen Variabilität der katabolischen Wärmeentwicklung auf Bodenoberflächen angestrebt. Ein Bestandteil der Verfahrensentwicklung ist neben den konventionell verwendeten gestörten Proben auch ungestörte Bodenproben. Die Ergebnisse zeigen, dass die passive IRT ein großes Potential und zahlreiche Einsatzmöglichkeiten in der mikrobiologischen Bodenforschung zur Vorhersage von Energie- und Stoffumsätzen, insbesondere von Kohlenstoff, bietet. Nach der Substratapplikation wurde ein Temperaturanstieg von mehr als 1 K erfasst, der auf hot spots und hot moments der mikrobiellen Aktivität, in sogenannten hot movements, zurückgeführt werden kann. Darüber hinaus bietet die IRT die Möglichkeit, die Feuchtigkeit der Bodenoberflächen und deren zeitliche Veränderung in einem aktiven Messverfahren anzunähern, so dass neben der mikrobiologischen Komponente auch bodenphysikalische Eigenschaften berücksichtigt werden können. Die gleichzeitige Erfassung der Bodenfeuchtigkeit und weiterer

Bodenoberflächeneigenschaften mittels etablierter Messverfahren werden zur Auswertung und Erklärung der Messdaten der passiven IRT herangezogen.

Die Ergebnisse dieser Arbeit leisten einen entscheidenden Beitrag zur Erforschung der mikrobiellen Dynamik im Boden und bieten zukünftigen Studien eine technische Grundlage, um mikrobiologische und physikalische Energieflüsse im Boden abzubilden. Die Arbeit trägt dazu bei, tiefere Einblicke in Stoffwechselvorgänge in Böden zu erhalten.

*Schlagworte: Passive Infrarot-Thermography, Wärmeentwicklung, Katabolismus, mikrobielle Aktivtät, räumlich-zeitliche Analyse*

# 1 Introduction

## 1.1 General Motivation

The pedosphere is a place of diverse processes and dynamics that occur predominantly at the microscale and initially appear invisible. These microscale processes include soil organic matter (SOM) decomposition, transformation, and sequestration in soils and contribute to biogeochemical cycling, climate change, and ecosystem sustainability (Lal, 2004; Liang et al., 2017). Since soil biomass carbon (C) stocks exceed atmospheric C by significantly more than three times, SOM decomposition is of great significance in light of climate change prediction (Ciais et al., 2014; Lal, 2004; Lützow et al., 2006). In this context, metabolic processes by microorganisms cannot be neglected because SOM decomposition and soil C cycling are a product of microbial growth and activity (Bölscher et al., 2016; Liang et al., 2017; Schimel and Schaeffer, 2012). Microbial processes have two crucial, opposing functions in regulating terrestrial C dynamics: releasing C to the atmosphere via their catabolic activities but also preventing C release by stabilizing it into forms that are not easily decomposable (Chakrawal et al., 2020; Liang et al., 2017; Schimel and Schaeffer, 2012). These processes occur at the microscale and are embedded in a complex and dynamic system that makes an enormous and overarching contribution to the global C cycle (Ciais et al., 2014; Lal, 2004; Schlesinger and Andrews, 2000).

The degradation of SOM has a significant effect on the surface and subsurface physical, biological, and chemical soil properties (LaRowe and Van Cappellen, 2011; Tecon and Or, 2017). However, microorganisms require an adequate amount of SOM, in which soil organic carbon (SOC) is also included, to maintain microbial functioning and physiological processes (Billings and Ballantyne Iv, 2013; Liang et al., 2017). Therefore, microbial activity is strongly linked to the availability and quality of C. Nevertheless, C limitations are widespread in soils restricting

biotic factors in soils, as the composition of microbial communities (Drotz et al., 2010; Kuzyakov and Blagodatskaya, 2015). In addition to the influence of C, abiotic factors, such as soil moisture, oxygen availability, soil or ambient temperature, chemical soil reactions (e.g., pH) are restricting microbial activity and process rates (Kuzyakov and Blagodatskaya, 2015; Tecon and Or, 2017; Vos et al., 2013). The tremendous dynamic nature of soil processes and the rapid changes in microbial community function are the consequence of such abiotic and biotic factors resulting in great diversity and ecological functioning of soil microbes (Tecon and Or, 2017; Torsvik et al., 1996). Thus, microbiological and physical soil processes cannot be separated from each other in studies on microbial dynamics as they are mutually dependent.

In order to record the microbial dynamics in the soil, Hesselink van Suchtelen (1931) already carried out a variety of calorimetric studies in the late 1920s and highlighted the relationship between heat development in soils and microbial activity. Calorimetry provides heat flow information on microbial metabolic processes to study very accurately microbial involvement in soil carbon dynamics (Barros et al., 1995; Herrmann et al., 2014; Sparling, 1981), and has been applied to microbial biomass detection, microbial behavior, and substrates conversion in soil sciences (Barros et al., 1995; Critter et al., 1994; Ljungholm et al., 1979; Sparling, 1981). The technique enables non-destructive measurement (of disturbed soil samples), analyses of small volumes of soil material, high reproducibility and sensitivity, and the chance to study different simultaneous processes without including further measurement methods (Vor et al., 2002). Nevertheless, calorimetry neglects spatial dynamics and diversity in soil processes (Kluge et al., 2013; Kuzyakov and Blagodatskaya, 2015). However, measuring the heat generated by a soil has proven to be a promising approach to gain deep insights into the metabolic processes of microorganisms (Kuzyakov and Blagodatskaya, 2015; Vor et al., 2002).

Nowadays, non-visible parts of soil processes, such as heat generation, can be detected and analyzed using spectroscopic analysis techniques using the infrared part of electromagnetic spectrum (Meola and Carlomagno, 2004; Usamentiaga et al., 2014). These parts of the spectrum conceal a wealth of information and properties of processes that provide deeper insights into the characteristics of our dynamic environment, especially of soil characteristics (Lehmann et al., 2008; Schmidt et al., 2011; Viscarra Rossel and Webster, 2012). Infrared thermography (IRT) offers promising potential in the longwave range of the spectrum to record thermal energy generated in the soil in a high spatial and temporal resolution. In addition to the advantages of calorimetry, this technique, as a proximal sensing elaboration method, offers the possibility to analyze undisturbed soil samples and observe full dynamics even in real-time (Bagavathiappan et al., 2013; Meola and Carlomagno, 2004).

This thesis recognizes the importance of determining microbial activity and additional physical and biological soil properties in a high spatial and temporal perspective. It aims to advance the scientific understanding of the relationship between soil properties by using IRT as a state-of the-art and non-contact measurement approach. Exploiting the potential of observing soil surface temperatures as an approximation of soil microbial activity is one of the main challenges of the thesis.

Fig. 1.1 illustrates the structure of this thesis. The following section 1.2 gives a detailed overview of the current state of the art and the scientific basis. In section 1.2.1, the physical basis of IRT is introduced concerning detecting heat on measurement object surfaces and necessary physical equations and units, which need to be considered for detecting soil properties. In section 1.2.2, the microbiological aspects and processes producing heat are clarified regarding the processes in soils. In section 1.2.3, the essential influencing parameters are described and how they affect the measured surface temperature and the physical properties of soils. These need

to be considered for a complete discussion of the functionality of IRT as a measurement approach for soil biological properties, as microbial activity. Open research questions are identified in section 1.3, from which the scope and specific aims of the thesis are derived.
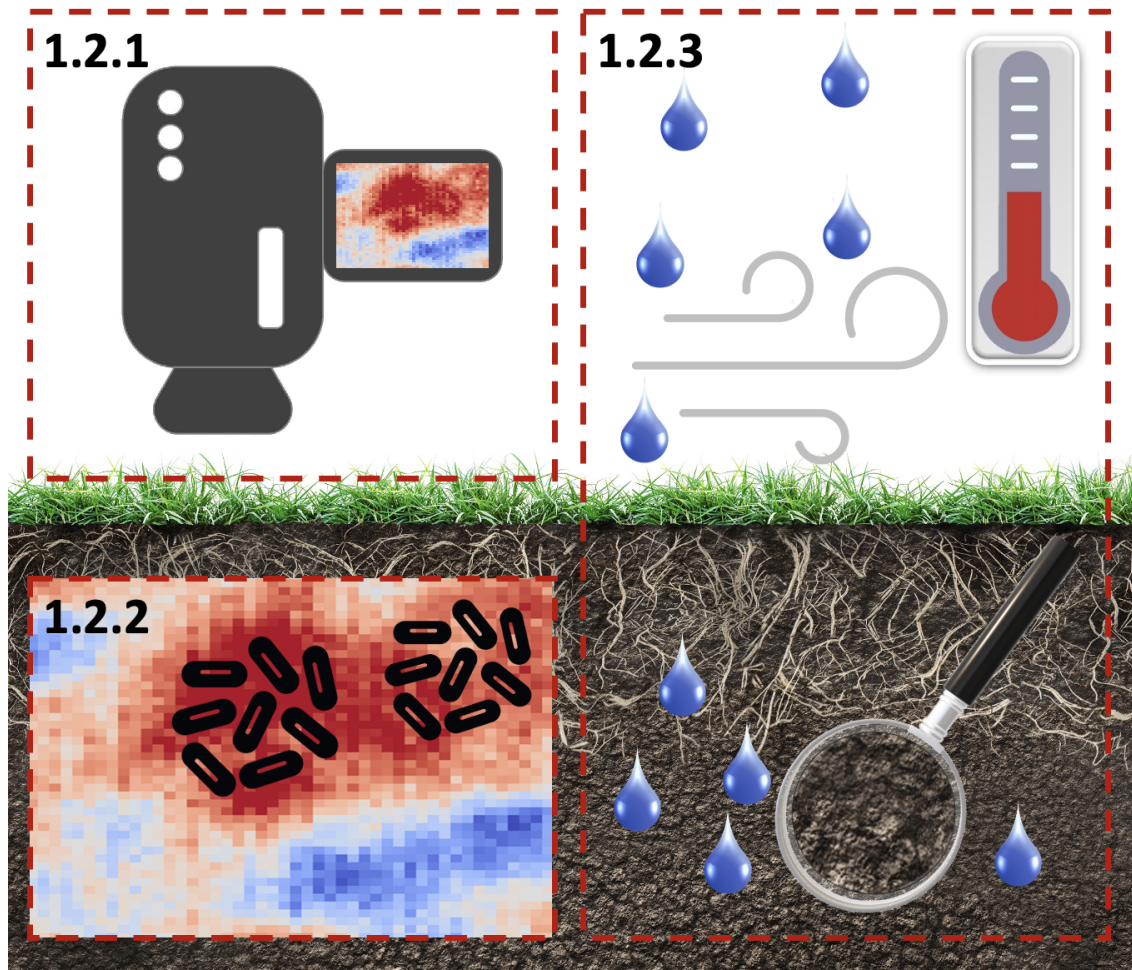


**Figure 1.1:** *The outline of section 1.2. The red outlined boxes are referring to the subsections, respectively. In section 1.2.1, the physical basis of the IRT technique is introduced, answering the question, how infrared thermography works and what exactly is measured. The processes generating heat in soils are addressed in section 1.2.2, and in section 1.2.3, the soil properties and ambient conditions are discussed regarding how they affect the measured surface temperature of soils.*

## 1.2  State of the Art

### 1.2.1  How infrared thermography works and what exactly is measured

Over the last two decades, IRT has become a technically advanced and versatile measurement method for detecting longwave thermal radiation (Bagavathiappan et al., 2013; Theodorakeas et al., 2015). The surface temperature, i.e., the recorded outgoing surface radiation of an objects surface, can be used to investigate various issues – these range from building inspections over medical applications to scientific questions. Modern IRT systems allow image series and subsequent data analyses; they are no longer purely image recording equipment (Grudzielanek and Cermak, 2015; Meola and Carlomagno, 2004; Usamentiaga et al., 2014). Thus, dynamic processes can be analyzed and examined and described by statistical methods.

IRT is based on the measurement of thermal radiation from measurement objects surfaces. All objects with a temperature above absolute zero (absolute zero = 0 K = temperature at which no more molecular movement occurs) emit thermal radiation. Thermal radiation is classified in the infrared part of the electromagnetic radiation spectrum. The IRT system, used in this work, measures in the longwave infrared (LIR), from 7.5 $\mu$m to 14 $\mu$m (Fokaides and Kalogirou, 2011; Grudzielanek and Cermak, 2015; Ranjit et al., 2015). IRT cameras do not measure the surface temperature of measurement object surfaces directly but determine it indirectly without contact by measuring the intensity of the outgoing thermal radiation. The measurement of the intensity of the outgoing thermal radiation [$\lambda$] is calculated using the Stefan-Boltzmann formula, where $\sigma$ is constant (5.670 W m$^{-2}$ K$^{-4}$) and T is the absolute temperature [K] of the measurement object (Balaras and Argiriou, 2002; Usamentiaga et al., 2014):

$$\lambda = \sigma * T^4 \tag{1.1}$$

The intensity of the longwave thermal radiation of objects thus depends directly on their absolute temperature.

The properties of the radiation of longwave thermal radiation vary significantly for different surfaces. These differences must be considered for the comparability of radiation measurements on different surfaces. Usually, the model of a black body is used for this purpose. A black body has a constant absolute temperature, and the radiant power absorbed by it is equal to the radiant power emitted by itself ($\alpha_\lambda = 1$) (Balaras and Argiriou, 2002; Usamentiaga et al., 2014). The specific emissivity ($\epsilon$) of a real object in relation to that of the black body ($\lambda_b$) is called the substance-specific emissivity $\epsilon$:

$$\epsilon = \frac{\lambda}{\lambda_b} \tag{1.2}$$

The emissivity thus expresses how great the capacity of a body to emit longwave thermal radiation is. It depends on various factors, such as color, surface properties, and physical properties of the body's material (Balaras and Argiriou, 2002).

The change in the measured radiated longwave radiation can also be expressed in terms of heat $\Delta Q$ (J) by considering the mass m (kg) to be heated and the material properties, considering the specific heat capacity c (J k$^{-1}$ K$^{-1}$). In contrast to temperature as a static variable, heat describes the amount of energy released, which is needed for temperature change ($\Delta T$) (Avdelidis et al., 2004; Bristow, 1998; Grinzato et al., 1998):

$$\Delta Q = c \times m \times \Delta T \tag{1.3}$$

Thereby, the specific heat capacity strongly depends on the soil properties. On the one hand, the water content of the soil has a significant influence on the properties of the soil. With increasing water content, the specific heat capacity increases to the soil's saturation point (Abu-Hamdeh, 2003; Abu-Hamdeh and Reeder, 2000). On the other hand, the density and the composition of the soil in terms of sand, clay, and silt content affect the specific heat capacity (Abu-Hamdeh, 2003; Ochsner et al., 2001; Ren et al., 2003). Since the specific heat capacity decreases with increasing sand content and increases with higher silt or clay content (Ochsner et al., 2001; Ren et al., 2003).

In the context of soil science research, the soil texture differences (Abu-Hamdeh and Reeder, 2000; Ochsner et al., 2001; Ren et al., 2003), surface structure (An et al., 2017; Ranjit et al., 2015), SOC contents (An et al., 2017; Ochsner et al., 2001; Sanchez et al., 2011), but also soil moisture (Antonucci et al., 2011; Sanchez et al., 2011; Villaseñor-Mora and González-Vega, 2015) have an impact on emissivity and specific heat capacity. Thus, information about these soil properties can also be obtained by IRT if a constant emissivity is chosen for a soil surface, but especially if temperature changes are caused by active heating of the surface (Antonucci et al., 2011). It is important to distinguish between heat production by metabolization processes (section 1.2.2) and the physical properties of the soils (section 1.2.3), which influence the measured surface temperature with varying emissivity and specific heat capacity.

### 1.2.2 What processes generate heat in soils

Soil heat production as a proxy for soil microbial activity has increasingly come into focus over recent decades (Chakrawal et al., 2020). The measurement of the effects of substrate addition on heat dissipated in soils was one of the earliest examples by

Ljungholm et al. (1979) using heat as a surrogate for microbial activity. After years of trying, a method of measuring soil calorimetry has emerged as a valuable tool because of its non-destructive measurements (Barros et al., 2007; Braissant et al., 2010; Critter et al., 1994; Sparling, 1981). The key force that generates heat is the metabolization of SOM and the resulting release of energy from microbial and enzymatic activity. Here, the catabolic breakdown of the substrate has the primary influence, and anabolic reactions contribute little to overall equilibrium (Barros et al., 1995). In fact, catabolic processes release energy by breaking down complex molecules in the soil. This energy can then be measured as heat energy (Barros et al., 1995; Drotz et al., 2010; Liang et al., 2017). Whereas in anabolic processes, energy is consumed when substances are broken down, and cannot be measured thermally or by soil respiration. However, these processes can then be captured, e.g., by the synthesis of microbial biomass (Drotz et al., 2010).

However, the heat generation in soils is involved in all phases of soil C turnover (Barros et al., 2011). The magnitude of soil C storage is largely influenced by the equilibrium between the C consuming microbial activity, indicated by $CO_2$ release, and the anabolism, contributing to aged biomass (Liang et al., 2017). Here, the turnover of the substrate, especially of C, distinguishes between the fast-growing microorganisms that use readily available substrates and the slow-growing ones that use the available resources more efficiently, even without substrate limitation in the soil (Blagodatskaya et al., 2007; Ekschmitt et al., 2005; Herrmann et al., 2014). Since both types, r- (high reproduction rate) and K-strategists (low reproduction rate), are abundant in soil, changes in the growth rate of the entire population, following the addition of easily available substrate (e.g., glucose), can indicate the shift in dominance of both types. The fast-growing r-strategists have a highly variable population size depending on substrate availability. This particularly addresses microorganisms that are dormant at substrate limited soil conditions (Blagodatskaya

and Kuzyakov, 2013) which use various survival strategies to become active again after environmental conditions were improved (Heitkötter and Marschner, 2018a; Joergensen and Wichern, 2018). In fact, microorganisms can only grow rapidly when substrate availability is high, especially easily available substrates, and can thus acquire a dominant population size. In contrast, the slow-growing K-strategists have a more constant population size. They dominate microbial communities in population, especially in substrate-limited environments (Barnard et al., 2013; Fierer et al., 2007; Herrmann et al., 2014). Consequently, r-strategists can react quickly to new organic inputs or rapid increase of water content in dry soils. Their growth increases based on the availability of easily available substrates from dead biomass (Blagodatskaya and Kuzyakov, 2008; Unger et al., 2010), because their metabolic contribution is stimulated (Blagodatskaya and Kuzyakov, 2008; Rousk et al., 2015). By adding easily available C, such as glucose, to the soil, metabolization by r-strategists will dominate in the first hours and days (Blagodatskaya et al., 2007). The addition of water to dry soils results in the so-called Birch effect (Birch, 1958) which leads to increased microbial activity for only a few hours, as the labile substrates are rapidly consumed (Borken et al., 2003; Kieft et al., 1987; Unger et al., 2010). Both substrate addition and rewetting lead to a heat pulse in the soil as an indication of the catabolic activity, which is caused in particular by the strong growth of the r-strategists.

However, the fact that soil microbial activity is not distributed uniformly in the soil matrix but concentrates on spatially isolated hot spots is generally accepted (Ekschmitt et al., 2005; Heitkötter and Marschner, 2018a; Nunan et al., 2003; Tecon and Or, 2017). While hot spots are usually characterized by high process and microbial growth rates at a spatial perspective, the microbial group structure between and in hot spots is highly variable (Kuzyakov and Blagodatskaya, 2015; Tecon and Or, 2017). Thus, the heat production from spatially distinct hot spots cannot be

linked to various microbial hot spot communities using the common calorimetric approaches for bulk soil samples. This results in an incomplete and incorrect determination of the relationship between the metabolic activity and related heat production of the various microbial hot spot populations (Heitkötter and Marschner, 2018a; Ruamps et al., 2011). Besides the spatial detection of these aggregated microbial colonies, their dynamics may be of great significance if the increased microbial activity is further restricted to hot moments for short-term events (Blagodatskaya and Kuzyakov, 2013; Kuzyakov and Blagodatskaya, 2015; Tecon and Or, 2017). The main drivers of biotic hot moments are root exudation, litterfall and root death, root ingrowth in a new soil volume, and activities of burrowing animals (Kuzyakov and Blagodatskaya, 2015). Consistent with the theory that r-strategists exhibit a rapid response of a few hours to a few days when readily degradable substrates are available, these are the main drivers at hot moments. This temporal aspect can then be measured as heat due to the catabolic activity by calorimetry. However, the spatial analysis is completely omitted so that hot spots cannot be detected.

Nevertheless, hot spots are able to form out of hot moments but do not necessarily vanish at the end of these; they can persist due to higher levels of microbial activity compared to ambient soil conditions (Blagodatskaya and Kuzyakov, 2013; Kuzyakov and Blagodatskaya, 2015). Biotic hot moments, which form due to labile C input, always lead to the formation or maintenance of hot spots (Kuzyakov and Blagodatskaya, 2015). These can then be determined by zymography which determines enzyme activity. However, the spatial and temporal combination of information is strongly limited (Heitkötter and Marschner, 2018b,a; Spohn et al., 2013; Spohn and Kuzyakov, 2014). To capture temporal and spatial aspects of microbial activity, techniques such as calorimetry and zymography are used in combination (Zhang et al., 2020). However, these methods are still in their early stages and neglect small-scale processes and short-term microbial activity changes. The het-

erogeneity in the soil environment is the main reason determining the microbial degradation of the organic substrates is limited so far, and the technical challenges are great.

A first technical approach to meet this challenge and fulfill the technical requirements is offered by IRT. The high temporal and spatial resolution of this measurement technique allows the detection of the heat generated on soil surfaces by the catabolic activity in the soil, which is caused in particular by r-strategists. Kluge et al. (2013) have shown first promising results in this regard, where microbial activity was recorded in both temporal and spatial perspectives. Temperature differences of up to 0.5 K were recorded due to microbial growth after substrate application and then compared with measurement techniques such as respirometry and calorimetry. However, physical influences induced by spatial emissivity and specific heat capacity variations must be considered (Abu-Hamdeh, 2003; Abu-Hamdeh and Reeder, 2000; Alnefaie and Abu-Hamdeh, 2013; Mira et al., 2007) but have not been so far. It must be taken into account that the water content of the soil also influences microbiological processes. The microbial activity has a demonstrable relationship with soil moisture because in a dry regime microbial activity is significantly lower compared to a moist regime (Barnard et al., 2013; Borken and Matzner, 2008). The same effect applies to the ambient temperature. With increasing temperature and additional high soil moisture, increased microbial growth rates occur, which is clearly reflected in the catabolic heat development (Rey et al., 2005; Steinweg et al., 2012).

### 1.2.3 How soil properties and ambient conditions affect the measured surface temperature

Differences in soil physical properties affect the measured surface temperature by techniques, such as IRT. Spatial differences in texture, soil color, soil density, sur-

face structure, but also temporal changes in soil moisture content, the emissivity, and the specific heat capacity influence the measured surface temperature, as well (Abu-Hamdeh, 2003; An et al., 2017; Antonucci et al., 2011; Barreira and Almeida, 2015; Wallbrink et al., 2007). In addition, changes in the ambient conditions, such as humidity or air temperature, have a strong influence on the surface temperature (Bagavathiappan et al., 2013; Fokaides and Kalogirou, 2011).

The texture of a soil significantly changes its specific heat capacity. Particle size matters because heat can be transferred depending on the contact areas between the individual soil particles. For this purAbu-Hamdeh (2003) has studied the determination of soil thermal properties and examined how the thermal properties change with different soil textures, depending on soil water content. They found that soils with higher clay content, and therefore smaller particle size, have a higher specific heat capacity than sandy soils independent of water content. These findings result from the adsorption of water, which appears to form thicker coatings around particles in clayey soils compared to sandier ones containing quartz (Abu-Hamdeh, 2003; Bristow, 1998; Ren et al., 2003). In laboratory studies, Alnefaie and Abu-Hamdeh (2013) investigated the specific heat capacity of soils as an effect of bulk density and further considering soil texture. According to their results, the specific heat capacity increases with increasing density due to the larger contact areas and, therefore, higher heat transfer between the individual soil particles (Abu-Hamdeh and Reeder, 2000; Alnefaie and Abu-Hamdeh, 2013; Ochsner et al., 2001). Thus, the temperature of soils is kept at a constant level for a longer time with a higher specific heat capacity and warm up or cool down more slowly if internal or external influences on soil temperature change.

In the case of methods for the spatial detection of thermal surface properties of soils, the structure is also decisive. Such structures can include cavities but also ele-

vations, which cause diffuse reflection of thermal radiation. Within cavity structures, incoming thermal radiation gets more adsorbed by higher reflectivity (Quinn, 1967; Usamentiaga et al., 2014). Quinn (1967) researched cavity emissivity and pointed out that the deeper the cavity, the higher the emissivity, causing near-black-body radiation. Thus, the emissivity would be almost 1 and, therefore, the surface would be characterized by higher apparent temperature.

Another factor influencing the measured surface temperature is soil color, which changes the emissivity of soils (An et al., 2017). The hypothesis about soil coloring is that the color of a soil is essentially determined by the sum of the following key soil constituents: SOC content, iron oxides, silicates, and carbonate minerals (Heil et al., 2020; Sánchez-Marañón et al., 2004). Here, the brightness of the color is decisive and determines the emissivity (An et al., 2017). The darker the color, e.g., at high organic carbon contents, the higher the emissivity (Heil et al., 2020; Schwertmann, 1993). As a result, the apparent surface temperature also increases with, e.g., higher SOC contents.

However, soil moisture has the most significant impact on thermal soil properties. Different water contents lead to variations in the specific heat capacity. Thus, with increasing soil moisture, the physical soil properties are affected, but additionally soil color, which influences the emissivity. Zanetti et al. (2015) investigated the relationship between soil moisture and soil color. They determined that the color of the soil tends to become darker with increasing water content. This changes the emissivity, and one would assume a higher apparent soil temperature. However, opposing effects are overriding the impact of emissivity change, such as evaporative cooling (Kerridge et al., 2013), which provides cooling of the soil surface by removing the energy required for evaporation (An et al., 2017; Benasher et al., 1983). In contrast to dry soils, moist soils are characterized by cooler surfaces in thermal images (Qiu and

Ben-Asher, 2010). Therefore, the surface temperature of soils changes at different soil moisture levels. When soils dry out, the surface temperature increases because the evaporative cooling decreases or is absent when the soil is dry (Antonucci et al., 2011; Kerridge et al., 2013).

Another influence of increased water content in soil samples is the change in specific heat capacity. A higher water content buffers the temperature change, which might be caused by internal or external processes and state changes. The buffer effect results from the high specific heat capacity of water, leading to a higher need for energy to heat moist soil (Antonucci et al., 2011; Bagavathiappan et al., 2013; Bristow, 1998). Internal effects and processes are caused by microbial activity and the corresponding catabolic processes that produce heat (see section 1.2.2), and external influences can be the change in ambient temperature, e.g., induced by the diurnal cycle of air temperature.

Changes in the ambient environmental conditions impact measured surface temperatures since IRT is sensitive towards their variations. A rise in ambient air temperature contributes to a higher measured temperature of the objects under investigation. The intensity of the change depends on the measured object's surface properties, particularly on the specific heat storage capacity. The lower the heat capacity, the higher the susceptibility to changes in the ambient environment (Grudzielanek and Cermak, 2015). Thus, air drafts and direct heat radiation affect the measured temperature values of the objects (Bagavathiappan et al., 2013). A change in ambient air temperature also affects relative humidity. The higher the temperature increases, the lower the relative humidity becomes. With regard to the investigation of moist soils, it should be noted that with decreasing relative humidity, the drying out of the moist soil progresses more quickly. If the air humidity is constantly high, a constantly low drying of the soil can be assumed. Consequently,

the evaporative cooling and, as a result, the measured surface temperature are affected by the stability and air humidity level (Barreira and Almeida, 2015; Grinzato et al., 1998; Jones, 1999).

In summary, numerous influences affect the thermal properties of soils. Especially for temporal and spatial measurements of the surface temperature, as is the case with infrared thermography, these factors must be included to avoid misinterpretations. It is expected that hot spots and hot moments in thermal images will be measured as temperature increases in time and space. However, these can be over- or under-interpreted by the influencing factors mentioned above. Therefore, it is always important to know and consider as many influencing variables as possible.

IRT was only used in a few cases as a measurement technique in the context of soil science research. There are many open questions and challenges in non-contact sensing of soil thermal properties caused by physical processes and conditions on the one hand and soil biological metabolic processes on the other hand.

## 1.3 Open Questions, Aims and Outline

As outlined in the previous sections, IRT is a promising tool for the detection of heat production in soils induced by microbial activity. The main knowledge gaps concerning the application of IRT can be ascribed to three sources of uncertainty:

a. Can IRT be applied for the detection of microbial hot spots and hot moments in soils?

b. Does IRT enable the possibility to record physical soil properties?

c. Is passive IRT capable of detecting microbial characteristics in undisturbed samples?

In this dissertation, those open research questions will be addressed. The focus is on a method development with regard to the general applicability of the technique with different soil treatment and the use of disturbed and undisturbed soil samples, the comparison with established methods in terms of time (respirometry) and space (zymography), but also the recording of physical soil surface properties such as moisture or physical structure. In the following, the method development is divided into three studies addressing each fulfilling technical requirements and challenges:

I What technical requirements are needed to detect physical and biological soil properties and can IRT be used to determine a short-term effect of microbial activity after rewetting events?

Understanding thermal images obtained by IRT and untangling key determinants regarding the physical soil properties is one of the major challenges concerning IRT as a measurement approach for microbial activity. As outlined in section 1.2.3, soil properties such as moisture and its distribution in the soil matrix or surface structural patterns affect the physical properties as well as the measured temperature. In section 2, this issue is addressed using an active heating approach, known as active IRT, to detect the heating and cooling phase of rewetted soil surfaces. Depending on the soil moisture, the specific heat capacity of the samples differs (c.f. section 1.2.1 & 1.2.3), so it can be assumed that the heat signal can be used as an approximation for soil water content.

As outlined in section 1.2.2, metabolization processes in soils increase at labile substrate availability, which produces heat due to catabolic activity by microorganisms. Rewetting dry soils can achieve such an effect. So far, IRT has not been used to detect microbial activity after rewetting. Nevertheless, the rapid growth of microorganisms due to soil rewetting is expected to generate heat that can be made visible thermally. In section 2, this objective is accomplished by running a selected number of samples in a passive IRT approach after rewetting.

II What environmental conditions and data preprocessing need to be considered to detect substrate-induced increases in microbial activity in the form of hot spots and hot moments in disturbed soil samples?

It has already been investigated that substrate-induced increase in microbial activity is detectable in disturbed soil samples using passive IRT (Kluge et al., 2013). However, no systematic study on the influence of ambient environmental conditions has been conducted that identifies an optimal incubation procedure for determining microbial activity with a further linkage to the data preprocessing to extract such influences from the time series of the thermal acquisition (c.f. section 1.2.3). In section 3, these gaps in methodological structure and procedure are addressed using variations in ambient conditions regarding relative air humidity and a sequence of data preparation steps to obtain a temperature profile caused by microbial activity that is as unaffected as possible. The amount of heat energy released by microbial activity is validated by including soil respiration data and considering the combined temporal and spatial aspects of the thermal images.

III Can infrared thermography be used for the temporally and spatially coupled

observation of the substrate-induced increase in microbial activity on undisturbed samples, and what are the main determinants?

Microbial activity in undisturbed soil samples is frequently studied by relating hot spots to spatial enzyme activity determined by zymography (Heitkötter and Marschner, 2018b,a; Spohn et al., 2013). However, hot moments in a high-temporal resolution (maximum of 30 minutes) (Spohn and Kuzyakov, 2014) and the methodical combination with hot spots is limited and not captured in its full complexity (Kuzyakov and Blagodatskaya, 2015). In section 4, hot spots and hot moments are addressed by the detection of surface temperature using passive IRT under stable ambient conditions. Since bivariate statistics do not enable comparing the magnitude and relevance of hot spots and hot moments to those of spatial physical and biological soil properties, multivariate statistics were applied to investigate the spatio-temporal complexity of the soil matrix and the internal processes. To include influencing factors that control both the thermal properties of soils and biological processes, as outlined in section 1.2.3, measurements from zymography, photography, and active infrared thermography were included.

The three work packages build the frame of the work and are addressed in the following three sections (2 - 4). In the final section (section 5), an overall discussion and suggestions for future research are discussed. The framework and the outlined scientific agenda of this thesis are summed up schematically in Fig. 1.2. The research discussed in this study has already been published in a scientific journal or submitted for publication. (c.f. Appendix 5.3 List of publications).
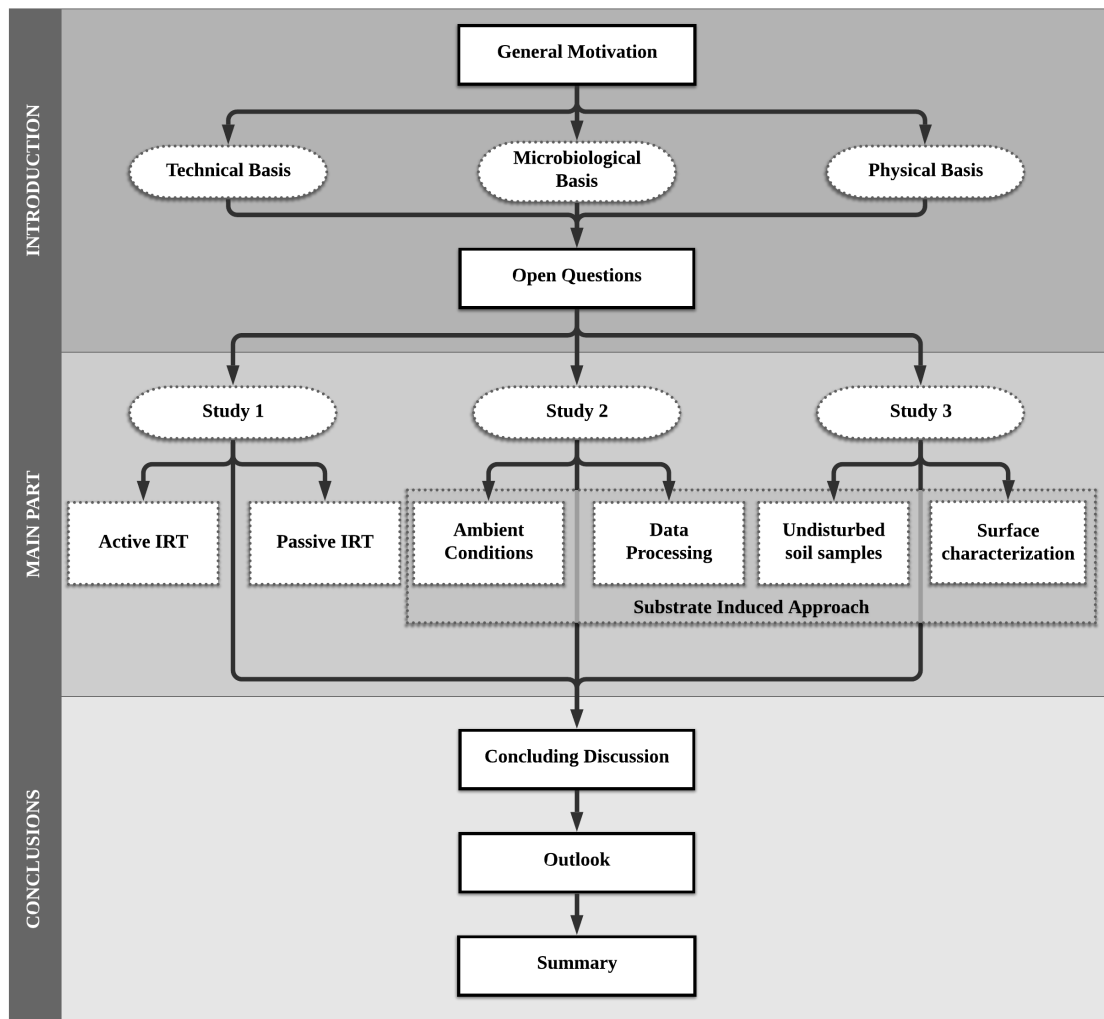
**Figure 1.2:** *The flowchart diagram represents the structure of the thesis to cover the outlined topic of each section. Arrows indicate the direction of information flow for each section. The upper part represents the introduction of the thesis with sections and subsections. The center part refers to the main part with focus on the three studies with the corresponding approaches applied in each one. The bottom part represents the final conclusions of the thesis with sections.*

# 2 Research Study I

**The potential of active and passive infrared thermography for identifying dynamics of soil moisture and microbial activity at high spatial and temporal resolution**

Co-Authors: Julian Heitkötter, Jannis Heil, Bernd Marschner, Britta Stumpe
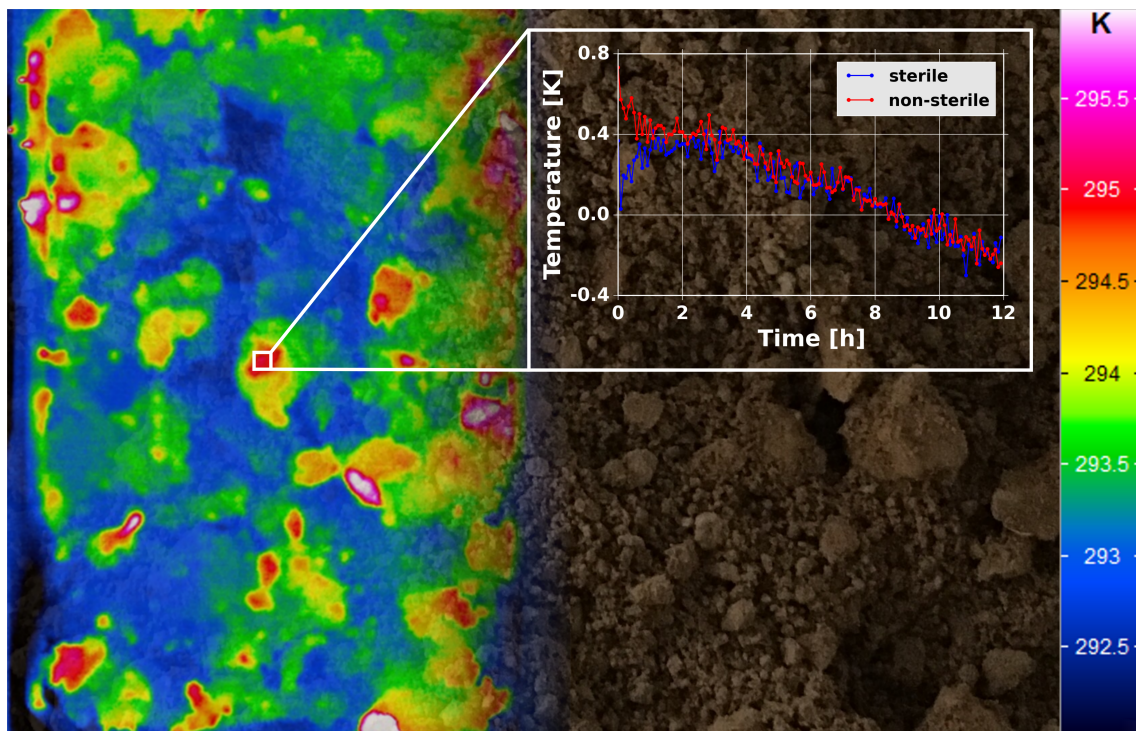
## 2.1   Introduction

The spatial and temporal heterogeneity of soil properties at the microscale have increasingly moved into the focus of many studies, since the microscale has a great potential to reveal new insights into soil processes (Dechesne et al., 2007; Grundmann and Debouzie, 2000; Nunan et al., 2003; Vos et al., 2013; Young and Crawford, 2004). However, while soil physical properties have been intensively studied at the microscale (Heeraman et al., 1997; Heng et al., 2010; Hirmas et al., 2016; Hummel et al., 2001; Lehmann et al., 2008; Moran et al., 2000; Pierret et al., 2003), the soil microbial heterogeneity at this scale is only poorly understood (Kuzyakov and Blagodatskaya, 2015; Tecon and Or, 2017; Vos et al., 2013). This is mainly due to methodical limitations, since it is much more challenging to develop mapping tools that display microbial activities (Kluge et al., 2013; Kuzyakov and Blagodatskaya, 2015; Pausch and Kuzyakov, 2011; Schmidt and Eickhorst, 2014). Especially real-time methods that can simultaneously describe soil physical as well as biological parameters and dynamics are not available at the microscale.

In this context, infrared thermography (IRT) seems to be a promising tool (Kluge et al., 2013). IRT measures thermal energy radiated from object surfaces. The emitted energy detected by an IRT camera is mainly a function of surface temperature, which is transformed into a visible image (Meola and Carlomagno, 2004). Passive and active IRT are the two basic approaches of the IRT technique (Bagavathiappan et al., 2013; Theodorakeas et al., 2015). Passive IRT monitors the thermal radiation emitted by the surface of the test body under natural condition whereas, for active IRT, the test body is thermally irradiated by an external energy source to produce an intensive thermal contrast on the test body surface.

During the past decade, both passive and active infrared thermography techniques have become powerful and effective tools in a wide range of applications,

since these techniques show numerous advantages. One of the main advantages of IRT is that it only requires an infrared camera with little other instrumentation. Other important advantages are that infrared thermography, as a remote sensing technique, can be used without physical contact to the test objects and their destruction (Bagavathiappan et al., 2013; Usamentiaga et al., 2014). Additionally, IRT provides a real-time temperature map of the test surfaces with a scan speed of up to 1600 Hz in a high thermal and spatial resolution. Modern IRT systems show a thermal sensitivity better than 0.02 K and a spatial image resolution with $>1.5$ megapixels (Meola and Carlomagno, 2004).

Based on these benefits, passive and active IRT have a broad range of applications ranging from life sciences and medicine to engineering and industry (Meola and Carlomagno, 2004). Most common industrial applications for passive IRT are building insulation diagnostics as well as mechanical and electrical inspections for locating defects (Bagavathiappan et al., 2013; Fokaides and Kalogirou, 2011; Utne et al., 2012). For example, IRT inspections of buildings can be used to detect heat losses and missing or damaged thermal insulations in walls and roofs (Fokaides and Kalogirou, 2011; Grinzato et al., 2011). The most common application of active IRT is industrial material testing for the detection of defects and fine cracks (Busse et al., 1992; Hain et al., 2009; Huth et al., 2002; Ranjit et al., 2015; Theodorakeas et al., 2015; Wu and Busse, 1998).

Although IRT has been used for many environmental investigations (Antonucci et al., 2013; Grudzielanek and Cermak, 2015; Jones, 1999), it has rarely been used in soil science, especially at the microscale. Generally, all soil properties associated with thermal surface radiation can potentially be assessed with IRT approaches. Thus, especially water content and microbial activity may be detectable using IRT techniques in soils due to increasing volumetric heat capacities with increasing wa-

ter contents (Abu-Hamdeh, 2003; Antonucci et al., 2011) and to heat production of microorganisms during respiration (Barros et al., 2011; Kluge et al., 2013; Sparling, 1981), respectively.

Concerning the soil water content, there are many studies using passive IRT as a remote sensing tool to identify water content of landscapes at large scales (Bittelli, 2011; Njoku et al., 2003; Verstraeten et al., 2006). So far, only Antonucci et al. (2011) showed that active IRT is also a useful technique for assessing soil water contents at smaller scales. In their laboratory study, they used active IRT to heat various soil samples with different initial temperatures and water contents. Total water contents of the soil samples were calibrated against the temperature variations with correlation coefficients of up to 0.74. However, the study of Antonucci et al. (2011) did not consider the possibility of active IRT to detect the spatial distribution as well as the dynamics of soil water content on the soil surfaces.

The possibility of using IRT approaches for detecting the microbial activity of soil samples has only been assessed by Kluge et al. (2013). The authors used the passive IRT approach to determine the spatial distribution of soil microbial activity on soil sample surfaces after glucose application. They showed that a substrate-induced increase of the surface temperature from the stimulated microbial activity was detectable. However, they did not determine the spatial distribution of soil moisture. Soil moisture will not only influence the measured surface temperatures but also alters the process rates of microbial activity (Baldrian et al., 2010; Barros et al., 1995; Skopp et al., 1990). Thus, for a better understanding of interactions between soil physical properties and biological processes at the microscale, the simultaneous determination of soil moisture and microbial activity dynamics is of special interest.

The present study evaluated the potential of active and passive IRT for the detection of soil surface temperatures with the aim to obtain soil surface properties at

high spatial and temporal resolution. The detection and calibration of soil moisture were performed with active IRT and the determination of microbial activity with passive IRT. In the first part of the study, the potential and accuracy of active IRT to determine soil moisture contents and detect structural patterns of the soil surface was investigated. In the second part, the rewetting effect of soil samples and the resulting increase in microbial activity was examined using passive IRT. Finally, active and passive IRT approaches were combined for evaluating the potential of IRT to assess microbiological and microphysical soil properties and for analyzing surface temperature changes from different perspectives.

## 2.2 Material and Methods

### 2.2.1 Soil sampling

For this study, a pool of 48 soil samples was used from different sites across North Rhine-Westphalia (Germany). The top- and subsoil samples (0–30 and 30–60 cm) cover a wide range of chemical, physical, and biological soil properties (Appendix Table A1.1). All soils were air-dried after sampling and sieved to < 2 mm.

In addition to this sample set, two samples from agricultural topsoils (A and B) and one from a forest subsoil (C), were selected for the longterm incubation experiments described in detail below. Soil properties of these samples are listed in Table 2.1. In order to obtain sterile samples of these soils A, B, and C, subsamples were exposed to a total dose of 75 kGy of $\gamma$-irradiation during three 24-hour irradiation intervals, which is considered sufficient to achieve sterility (McNamara et al., 2003; Trevors, 1996).

**Table 2.1:** *Phsyical and chemical characteristics of the soil samples for the incubation experiments.*

| Soil Sample | pH[a] | C/N[b] | SOC[b] | WHC[c] | Sand[d] | Silt[d] | Clay[d] | $C_{mic}^e$ | Basal respiration[f] |
|:---:|:---:|:---:|:---:|:---:|:---:|:---:|:---:|:---:|:---:|
| | [-] | | | | [%] | | | $[\mu g\ g^{-1}]$ | $[CO_2\ mg\ h^{-1}]$ |
| A | 6.1 | 14 | 2.5 | 50.9 | 38 | 54 | 8 | 126.7 | 2.18 |
| B | 7.1 | 13 | 3.0 | 61.5 | 7 | 85 | 8 | 171.9 | 4.10 |
| C | 3.7 | 10 | 0.4 | 50.6 | 12 | 68 | 20 | 32.2 | 0.29 |

[a] 0.01 M $CaCl_2$

[b] Vario EL Elementar Analyser (Elementar Analysesysteme GmbH, Hanau, Germany)

[c] After DIN EN ISO 11267 (2014-07)

[d] Analysette (Fritsch GmbH, Idar-Oberstein, Germany)

[e] after Vance et al. (1987)

[f] Respicond (Nordgren Innovations AB, Bygdeå, Sweden)

A high definition IRT camera (Variocam HD research, InfraTec, Dresden, Germany) combined with the associated standard lens (30 mm focal length) was used to obtain thermal images of the soil surfaces. The IRT camera has an image resolution of 1024×768 pixels. The camera distance to the soil sample surfaces was set to 50 cm resulting in a pixel resolution of 0.283 mm. The IRT camera detected the spectral range in the far infrared (FIR) of 7–14 $\mu$m with a temperature accuracy of ± 30 mK. In all experimental designs, an overall emissivity of 0.95 [−] was assumed for the soil surfaces (Axelsson, 1988; Benasher et al., 1983; Kluge et al., 2013).

### 2.2.2 Active and passive infrared thermography

For active IRT, a halogen spotlight (1500 W) was used as an external heat source to induce a clear thermal contrast on the object surfaces. The spotlight was placed at a distance of 50 cm from the object surface. Active IRT was conducted in the lock-in mode as described in Ibarra-Castanedo et al. (2009). Briefly, the halogen spotlight was illuminated with a lock-in frequency of 0.5 Hz and a 30 Hz frame rate. The thermal response of the soil surfaces was recorded during the heating and transient cooling phase. The thermal response of the heating and cooling phase of each pixel was noise corrected using a Fourier Transformation. The resulting sinusoidal waves are characterized by their amplitude and phase values (Huth et al., 2002; Vollmer and Möllmann, 2010; Wu and Busse, 1998). To calculate the amplitude $A$ and phase $\boldsymbol{\sigma}$, four equidistant data points ($S_1$, $S_2$, $S_3$, $S_4$) in a complete period of the waves are used as described in the Eqs. (2.1) and (2.2) (Busse et al., 1992; Ranjit et al., 2015):

$$A = \sqrt{(S_1 - S_3)^2 + (S_2 - S_4)^2} \qquad (2.1)$$

$$\boldsymbol{\sigma} = tan^{-1} \times (\frac{S_1 - S_3}{S_2 - S_4})$$ (2.2)

The amplitude describes the intensity of the thermal response during the heating and cooling cycle (Ranjit et al., 2015; Wallbrink et al., 2007). The water contents of the surface modify the intensity of the thermal response due to its high specific heat capacity (De Vries, 1963; Wiggenhauser, 2002). Accordingly, increasing temperature amplitudes of the soil surface indicate decreasing soil moisture contents.

The phase represents the velocity of temperature change on the specimen surface (Meola et al., 2006; Ranjit et al., 2015). Structural differences of the object influence the velocity of the thermal response. Therefore, in material science and material testing, phase angle information is commonly used to identify the depth of material defects (Busse et al., 1992; Hain et al., 2009; Huth et al., 2002; Ranjit et al., 2015; Theodorakeas et al., 2015; Wu and Busse, 1998). In this study, the phase angle [°] was used as an approximation to the soil surface structure and density. High variances in the phase image indicate high structural differences of the soil surface, as well as differences in soil density. Hence, the percentage deviations from the mean values are calculated to address the structural diversity of the soil surfaces. For example, values below the mean value indicate a high bulk density, due to the decreased velocity of temperature adjustment, which is induced by the higher specific heat capacity at denser soil samples (Abu-Hamdeh, 2003; Bristow, 1998). Values above the mean value indicate voids, pores or cavities. The thermal conductivity and density of the material decreases (Avdelidis et al., 2004; Usamentiaga et al., 2014) and thus the contrary effect can be observed, leading to higher phase angle values. Due to the possibility of mixed structures, the phase angle values cannot be assigned precisely to a specific type of structure, as high densities or elevations, to

correct the amplitude image. Therefore, the standard deviation is calculated from the deviations of the phase angle values to get a measure of the structural richness of each phase image. The phase image is widely unaffected by the surface emissivity; thus, a moisture-independent image is extracted (Huth et al., 2002; Meola et al., 2006).

Passive IRT does not require an external energy heat source since natural heat emission from surfaces is detected (Vollmer and Möllmann, 2010). Thus, passive IRT directly displays the surface temperature of an object in Kelvin [K]. In this study, passive IRT techniques were used to detect natural thermal contrast on soil surfaces which then were linked to temporal and spatial variations of microbial activity, similar to the approach of Kluge et al. (2013). In our study, microbial activity dynamics were monitored using passive IRT thermal radiation at a temporal resolution of 1 min.

The detection of thermal radiation by IRT cameras is highly sensitive towards ambient environmental influences, like air drafts or relative humidity changes (De Vries, 1958, 1963). Thus, all IRT experiments were conducted in a gas-tight glovebox to reduce ambient environmental influences. Inside the glovebox, relative humidity was adjusted to 92% using a saturated sodium chloride solution (Rockland, 1960; Young, 1967) to reduce soil drying, at a given air temperature of 22 °C, both being monitored continuously by wireless data loggers (M-Log5W-HUMIDITY, Geoprecision, Ettlingen, Germany).

### 2.2.3 Determination of soil moisture using active infrared thermography

In a first step (Experiment A1), the relationship between soil surface moisture contents and emitted heat energy using active IRT of the soil surface was evaluated.

Soils A, B, and C were rewetted to 16 different moisture contents between 15 and 75% of their maximum Water Holding Capacity (WHC). The other 48 samples were all uniformly rewetted to a gravimetric water content of 23%. A fixed water volume ensures a wide range of volumetric water contents (VWC) due to the varying soil properties (Abu-Hamdeh, 2003; Abu-Hamdeh and Reeder, 2000; Alnefaie and Abu-Hamdeh, 2013). After rewetting and thorough homogenization with a spatula, the samples were filled into vessels (2 cm diameter, 1 cm height) and the surfaces were scanned immediately via active IRT in three replicates. For each soil surface, the mean temperature amplitude was calculated and calibrated against the corresponding VWC. To evaluate the relationship between the mean temperature amplitude and the soil water content, the data were fitted using a supervised least square regression analysis from which the goodness of fit was calculated. Histograms of the surface temperature amplitude values from all pixels were computed in order to evaluate the spatial variance of the temperature amplitude values of each soil surface. The associated phase images are also depicted for the consideration of the surface structure and bulk density.

In a second step (Experiment A2), the active IRT was used to detect spatio-temporal dynamics of the surface soil moisture contents. For this, a continuous drying experiment was conducted to induce spatial and temporal variations of the surface soil moisture. For the drying experiment, 20 g of soils A, B, and C were rewetted to 40% WHC and incubated over a period of one week. Immediately after rewetting, the changes of the pixelwise temperature amplitudes were monitored via active IRT at regular time intervals. Based on the calibration functions for soils A, B, and C from experiment A1, the spatial distribution of the VWCs was then calculated for the corresponding soil surfaces. Changes in the driest and wettest areas of the soil surface were extracted using the 5th and 95th percentile of the surface water contents to identify extreme values of the spatio-temporal variability during

soil drying. The corresponding phase images are considered for further explanations by structural dependencies.

### 2.2.4 Determination of microbial activity using passive infrared thermography

In a first step (Experiment P1), microbial activities on soil surfaces were linked to surface temperatures. For this, the non-sterile soil samples A, B, and C were rewetted to 40% WHC, filled into vessels (6 cm diameter, 1 cm height), and then incubated for one week. A pre-incubation phase was avoided so that the so-called "Birch effect" of strongly stimulated microbial activity immediately upon rewetting could be observed (Birch, 1958; Kieft et al., 1987). As controls, the sterile A, B, and C soil samples were incubated. Autoclaved water was used for rewetting of the sterile samples and the equipment like spatulas, vessels, and pipettes were rinsed with ethanol in order to maintain sterile conditions. Before rewetting, water and soil samples were adjusted to 22 °C to avoid temperature artifacts induced by interactions of rewetted soil and the ambient environment. Immediately after the start of the soil incubation, scanning of the soil surfaces with passive IRT started. For each measurement, the surface temperature mean value of each sample was calculated. In order to relate temperature increases to microbial activity, differences between the surface mean values of the sterile and non-sterile samples were tested for significance using the two-sample t-test for each time step with a significance level of 95%.

In a second step (Experiment P2), the data set of experiment P1 was used to identify spatio-temporal dynamics of microbial activity on soil surfaces. Thus, so-called Hovmöller diagrams were created for visualizing and analyzing surface temperature changes over time. For each sample, transects through the center of the surfaces were selected. The temporal changes in surface temperature along these transects were plotted during the first 4 h of incubation according to Hovmöller (1949).

In a third step (Experiment P3), the influence of surface soil moisture on the spatial pattern of microbial activity was quantified in further incubation experiments using a combined active and passive IRT approach. For this experimental design, the sterile and the non-sterile soil samples A, B, and C were incubated for one week as described for experiment P1. The passive IRT procedure started immediately after rewetting. The active IRT procedure started 30 min after rewetting and was repeated only once a day to avoid effects of the external heating energy on the microbial dynamics on the soil surfaces as far as possible. A linear regression analysis was performed to explain microbial activity indicated by soil surface temperature together with surface moisture contents represented by the temperature amplitude.

### 2.2.5   Software

IRBIS3 professional (InfraTec, Dresden, Germany) was used for the camera connection, data conversion, and data export. The data preparations, calculations, and statistical analyses were performed with Python 2.7.

## 2.3   Results and discussion

### 2.3.1   Determination of soil moisture using active infrared thermography (A)

#### 2.3.1.1   Soil moisture calibration

Fig. 2.1a shows the relationship between the mean temperature amplitude and the mean VWC of all soil samples (Experiment A1). The mean temperature amplitude decreased non-linearly with decreasing VWC of the samples. An exponential function gave the best fit for the data ($R^2 = 0.72$) since the mean temperature amplitude showed a large decrease for VWCs between 0 and 30% while remaining more or less

constant at a level of 100 to 120 mK for VWCs above 30%. Thus, the mean temperature amplitude was a good approximation for VWCs of up to 30% but failed to predict VWCs above 30%. Previous studies observed that the specific heat capacity of soil tends to increase to the specific heat of water at high water contents (Alnefaie and Abu-Hamdeh, 2013; Antonucci et al., 2011; Bristow, 1998; De Vries, 1963; Ochsner et al., 2001). Thus, an increase of the temperature amplitude at lower soil water contents was explained by a decreasing specific heat capacity with lower water contents (Antonucci et al., 2011). Constant specific heat capacity at higher soil water contents was discussed by Bristow (1998). The authors argued that higher soil water contents increase the connectivity between soil particles so that the specific heat capacity becomes nearly constant.

### 2.3.1.2   Spatial surface moisture distribution

The relationship between the mean temperature amplitude and the VWC of the soil surfaces for soils A, B, and C were also fitted separately with individual exponential functions (Fig. 2.1b, c, and d). Compared to Fig. 2.1a, the $R^2$ values increased up to 0.89 using single soil samples for the calibration, which indicated that soil properties influence the temperature amplitude. Also, differences in the temperature amplitude values between soil sample A, B, and C (Fig. 2.1b–d) indicated that the specific heat capacity varies with soil texture; the clay-rich soil C is less sensitive towards temperature changes, resulting in lower temperature amplitudes at low water contents compared to soils A and B. Within this context, Abu-Hamdeh (2003) investigated the thermal properties of soils depending on density and water content under consideration of varying soil textures. Similar to our results, Abu-Hamdeh (2003) concluded that clayey soils have a higher specific heat capacity than sandy soils. The adsorption of water tends to form thicker coatings around loam particles in clayey soils leading to a higher specific heat capacity compared to quartz con-

taining sandy soils (Abu-Hamdeh, 2003; Alnefaie and Abu-Hamdeh, 2013; Bristow, 1998; Ghuman and Lal, 1985). Abu-Hamdeh and Reeder (2000) discussed that the thermal conductivity of same water contents is higher with smaller particles than with larger particles. This led to a higher impact on the thermal properties of clayey soils resulting in a lower temperature amplitude at the same water contents in clayey soils compared to sandy soils in this study (Fig. 2.1b, d).
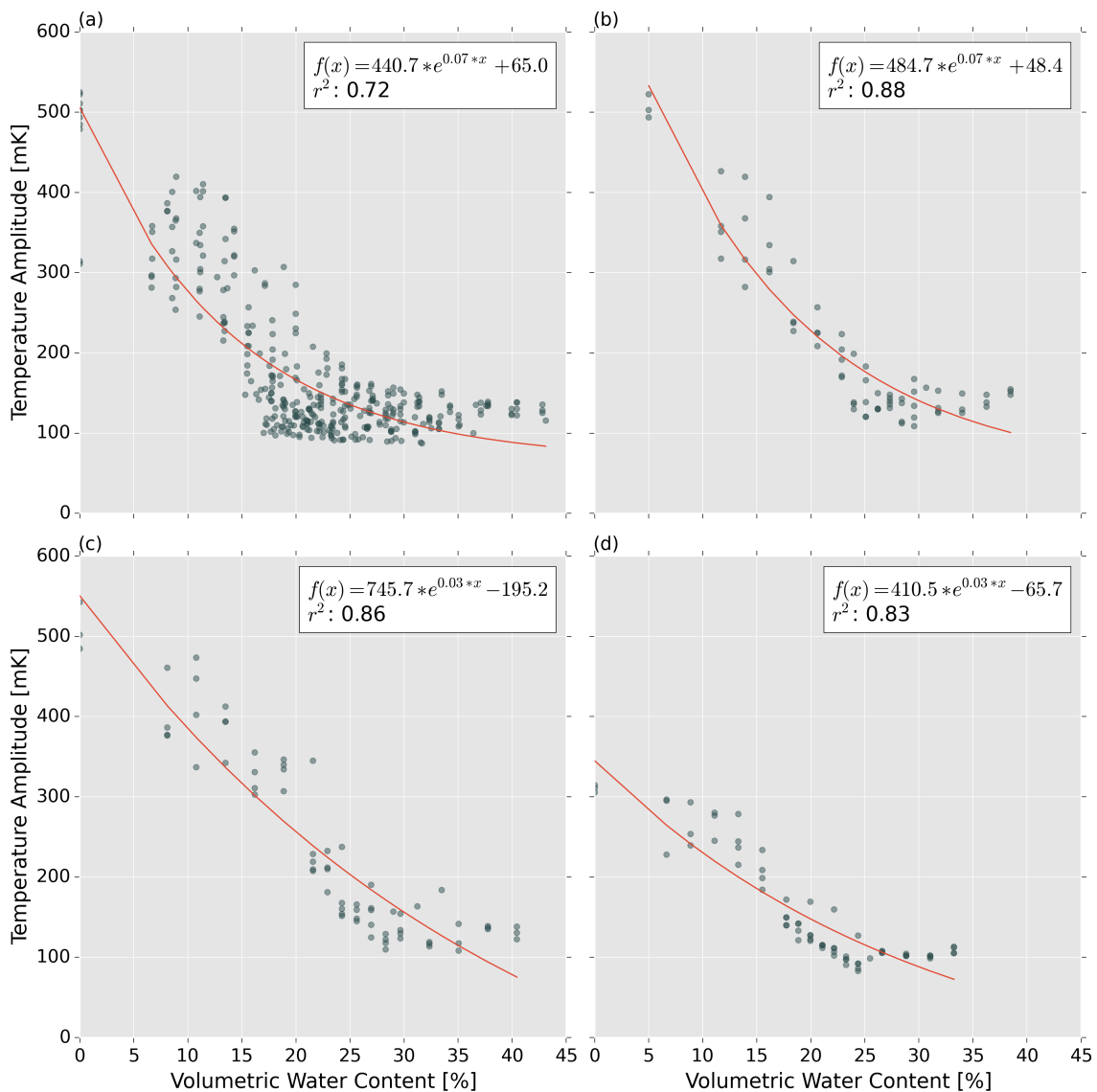


**Figure 2.1:** *The relationship of the mean temperature amplitude [mK] as function of the VWC [%]; (a) all soil samples, (b) soil sample A, (c) soil sample B, and (d) soil sample C. The red lines represent the fitted curves. The calibration functions with associated $R^2$ are depicted in the white boxes.*

However, 11 to 17% of the variance of the mean temperature amplitude values remained unexplained (Fig. 2.1b–d). We attribute this to the higher variability of soil moisture distribution at lower water contents so that the mean values of the temperature amplitude are less representative when the soil water content was low (Fig. 2.1b–d). It can be assumed that small amounts of water could not be mixed homogeneously into the soil samples resulting in inhomogeneous spatial distribution of soil moisture. For verification, Fig. 2.2 visualizes the spatial distribution of the temperature amplitude after rewetting to 15% (Fig. 2.2a) and 45% (Fig. 2.2d) WHC. According to both rewetting levels, histograms were plotted (Fig. 2.2b and e), quantifying the spatial variance of the temperature amplitude values. The distribution of the 15% WHC sample varied between 200 and 600 mK, while the 45% WHC sample varied at a lower range between 50 and 300 mK (Fig. 2.2b and e). Thus, higher variances in the temperature amplitude were observed for the drier 15% VWC soil sample, due to the inhomogeneous soil wetting. The rewetting procedure limited the prediction accuracy of the mean VWC at low water contents. Nevertheless, the relative differences in the spatial variation of temperature amplitude can predict the relative variations in the soil water content to some degree. Although active IRT has never been used to detect the spatial distribution of soil moisture, it has been used for moisture detection in building structures in civil engineering applications, e.g., during thermographic inspection (Grinzato et al., 2011; Ludwig et al., 2004; Wiggenhauser, 2002). Comparable to our results, Grinzato et al. (2011) concluded that active IRT is useful to describe the spatial distribution of moisture contents since lower surface temperatures were observed for unsaturated materials with increasing moisture contents. Antonucci et al. (2011) also confirmed these findings for moist soil samples.

The surface structure and density of the investigated soils also had to be considered when analyzing the spatial distribution of the temperature amplitude. Soil

areas with cavities within the soil structure are characterized by a higher reflectivity of incoming thermal radiation, and therefore more radiation gets absorbed. Consequently, the emitted thermal radiation is higher and the surface emissivity increases in such cavities and cumulates in near black-body radiation (Mollmann and Vollmer, 2007; Quinn, 1967; Usamentiaga et al., 2014). Since we used a fixed emissivity of 0.95 in this study, the temperature amplitude was overestimated in cavities. Moreover, soil areas with a high density are characterized by a lower thermal diffusivity (Abu-Hamdeh, 2003; Hain et al., 2009). These areas will show lower surface temperature amplitudes compared to lower dense soil areas, and consequently, soil moisture contents will be underestimated. To consider these effects concerning the spatial distribution of the temperature amplitudes, the phase angle was used as an approximation of soil surface structure and density, as described in section 2.2.2. Thus, the corresponding phase images (Fig. 2.2c and f) are visualized corresponding to the spatial distribution of the temperature amplitudes (Fig.2.2a and d) to find direct links between both images. For example, a semicircular structure in Fig. 2.2a and c (Position D/E 4/5), and a circular structure in Fig. 2.2d and f (Position D/E 1/2) were observed. Nevertheless, the phase angle cannot be used directly to correct the temperature amplitude, since they contain information about soil density, as well as information about soil structure, as detailed explained in section 2.2.2. Thus, the standard deviation was calculated for the phase images of Fig. 2.2c and f to assess the maximum error rate of the temperature amplitudes. The drier soil (Fig. 2.2c) revealed a lower standard deviation (6.2%) than the more moist soil (12.4%; Fig. 2.2f). The higher value of the more moist soil was the result of the aggregation of soil particles induced by water addition. This led to a higher structural diversity of the surface in comparison to the drier soil. Therefore, structurally richer soil surfaces are subject to higher insecurities in the spatial detection of soil moisture. However, the phase image can be taken into account to estimate these uncertainties.
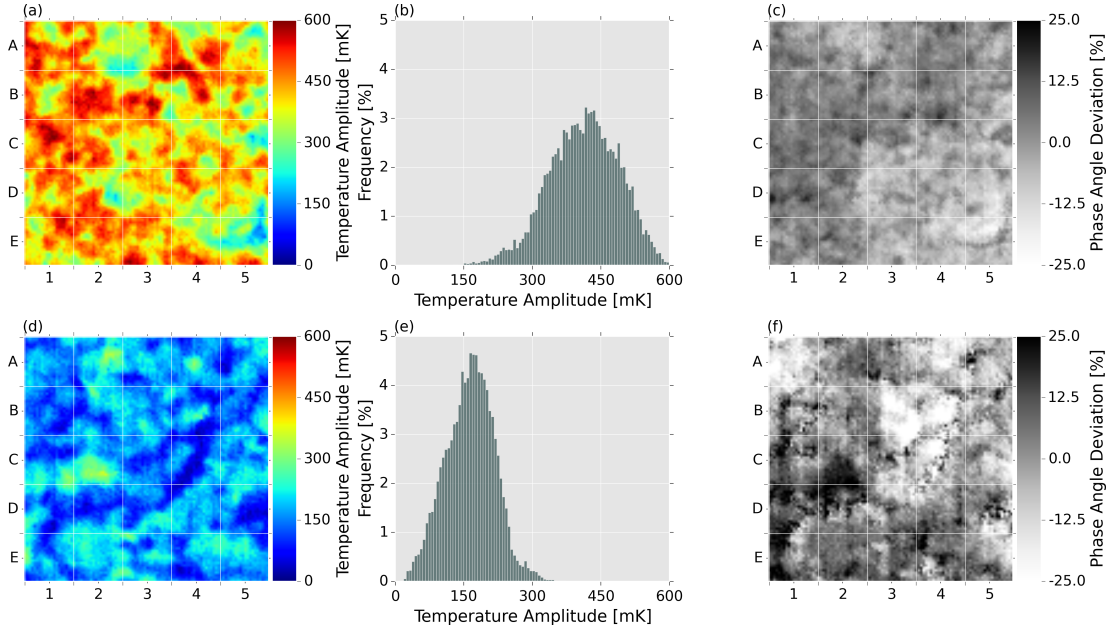
**Figure 2.2:** *Spatial variance of the temperature amplitude [mK] (a), (b) histogram of (a), (c) the percentage deviation of the phase image corresponding to (a) for 15% WHC. Spatial variance of the temperature amplitude [mK] (d), (e) histogram of (d), (f) the percentage deviation of the phase image corresponding to (d) for 45% WHC. The grid size of a, c, e, and f is 2.8 × 2.8cm.*

### 2.3.1.3   Spatial and temporal variability of surface moisture contents

Additionally, we analyzed the potential of active IRT for detecting temporal dynamics in spatial patterns of surface soil moisture, performing a continuous drying event (Experiment A2). Fig. 2.3a and d show the VWCs on the surface of soil A after 0 and 48 h of soil sample rewetting. The VWCs were calculated from the temperature amplitude values using the calibration function shown in Fig. 2.1b, c, and d. A general decrease of the spatial soil surface moisture during soil drying was detected. For verification, the differences between the time intervals ($\Delta$ 48/0h) were calculated for each image pixel >99% of the differences were negative indicating a drying of the soil surface. To evaluate the potential of active IRT for measuring spatio-temporal changes of soil moisture, the driest and wettest areas were extracted using the 5th and 95th percentile for both time steps (Fig. 2.3b and e). In general,

structural patterns of the driest and wettest areas remained unchanged, which could be explained by a uniform drying of the soil surface at stable ambient environmental conditions as in this experiment. Size and shape of individual structures were changing marginally, e.g., in position C-F 6, at which a wet belt was detected (Fig. 2.3a and c). The wet belt can be attributed to a depression by the phase image (Fig. 2.3c and f). After 48 h, the size of this wet belt increased (Fig. 2.3b and e) indicating slower drying-out processes compared to surrounding soil areas. We assumed that soil moisture was kept more stable in depressions or cavities because the influence of ambient conditions was lower than on elevations. In comparison to the amplitude images, the phase images remained more or less unaffected by soil drying and thus were useful for interpretation of the temperature amplitude images.
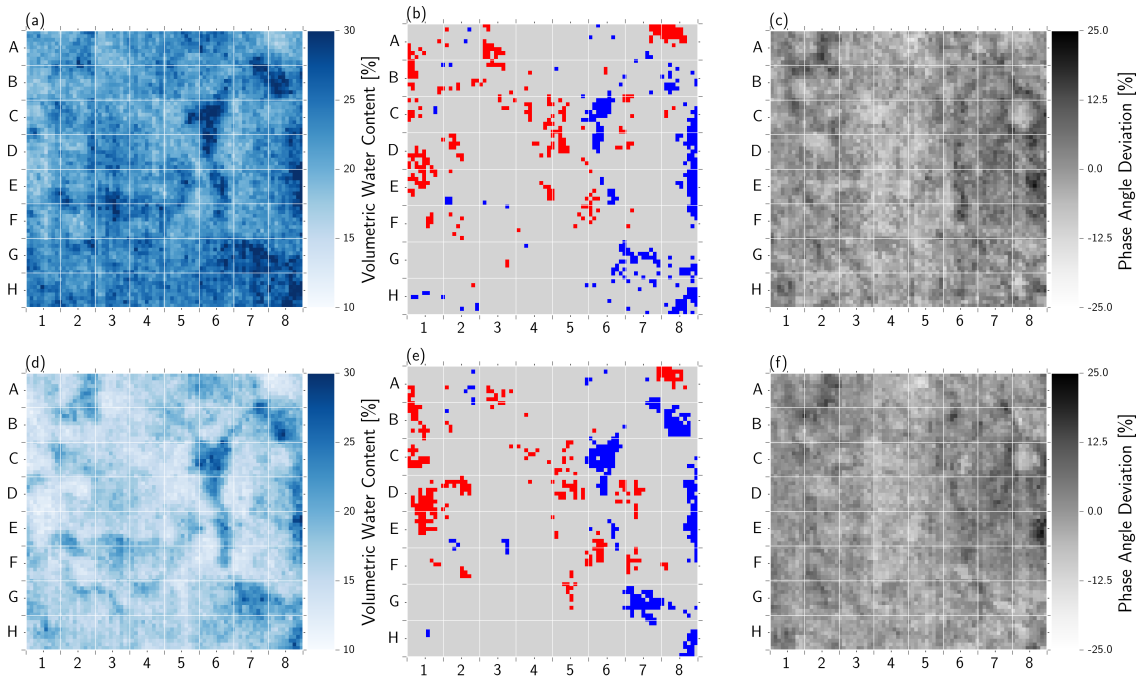


**Figure 2.3:** *Spatio-temporal patterns of soil surface drying for soil A; (a) calculated VWC [%] immediately after rewetting, (b) 5th (blue) and 95th (red) percentile of (a), (c) the percentage deviation of the phase image corresponding to (a), (d) calculated VWC [%] after 48 h, (e) 5th (blue) and 95th (red) percentile of (d), and (f) the percentage deviation of the phase image corresponding to (d). The grid size is 2.2 × 2.2 cm.*

## 2.3.2 Determination of soil microbial activity using passive infrared thermography (P)

### 2.3.2.1 Temporal course of mean surface temperatures

Fig. 2.4 shows the relative changes of the mean surface soil temperatures after rewetting of the sterile and non-sterile soil samples A (Fig. 2.4a), B (Fig. 2.4b), and C (Fig. 2.4c) within the first 12 h of incubation (Experiment P1). Immediately after rewetting, the mean surface temperature of the non-sterile samples increased by up to 0.5 K compared to the sterile samples, which showed no heat production. When testing these differences with two sample t-tests for each 1 min time interval, significant differences ($p < 0.05$) were only detected within the first 2 h of incubation. For soils A, B, and C, these comprised of 97%, 84%, and 99% of all time intervals. After 2 h of incubation, temperature differences between the sterile and non-sterile soil samples were no longer detectable and surface temperatures declined steadily in all samples. We attribute the initial heat pulse in the non-sterile samples to the so-called "Birch effect", first described by Birch (1958) as a pulse of microbial $CO_2$-release after rewetting dry soil samples. Thus, the observed thermal pulse of the non-sterile soils is likely associated with the rapid regrowth of the microbial population due to the high availability of easily available substrates from dead biomass resulting from drying (Birch, 1958; Kieft et al., 1987; Unger et al., 2010). This pulse of activity only lasts for a few hours because the labile substrates are rapidly depleted (Borken et al., 2003; Jones et al., 2005; Kuzyakov and Blagodatskaya, 2015). This is consistent with the duration of the observed thermal response thus showing that this pulse in metabolic activity produced enough heat to become detectable with passive IRT.

However, passive IRT can only detect the initial increased heat production from the growth of the microbial population and not the following energy production from basal respiration in the non-sterile samples compared to the sterile samples.
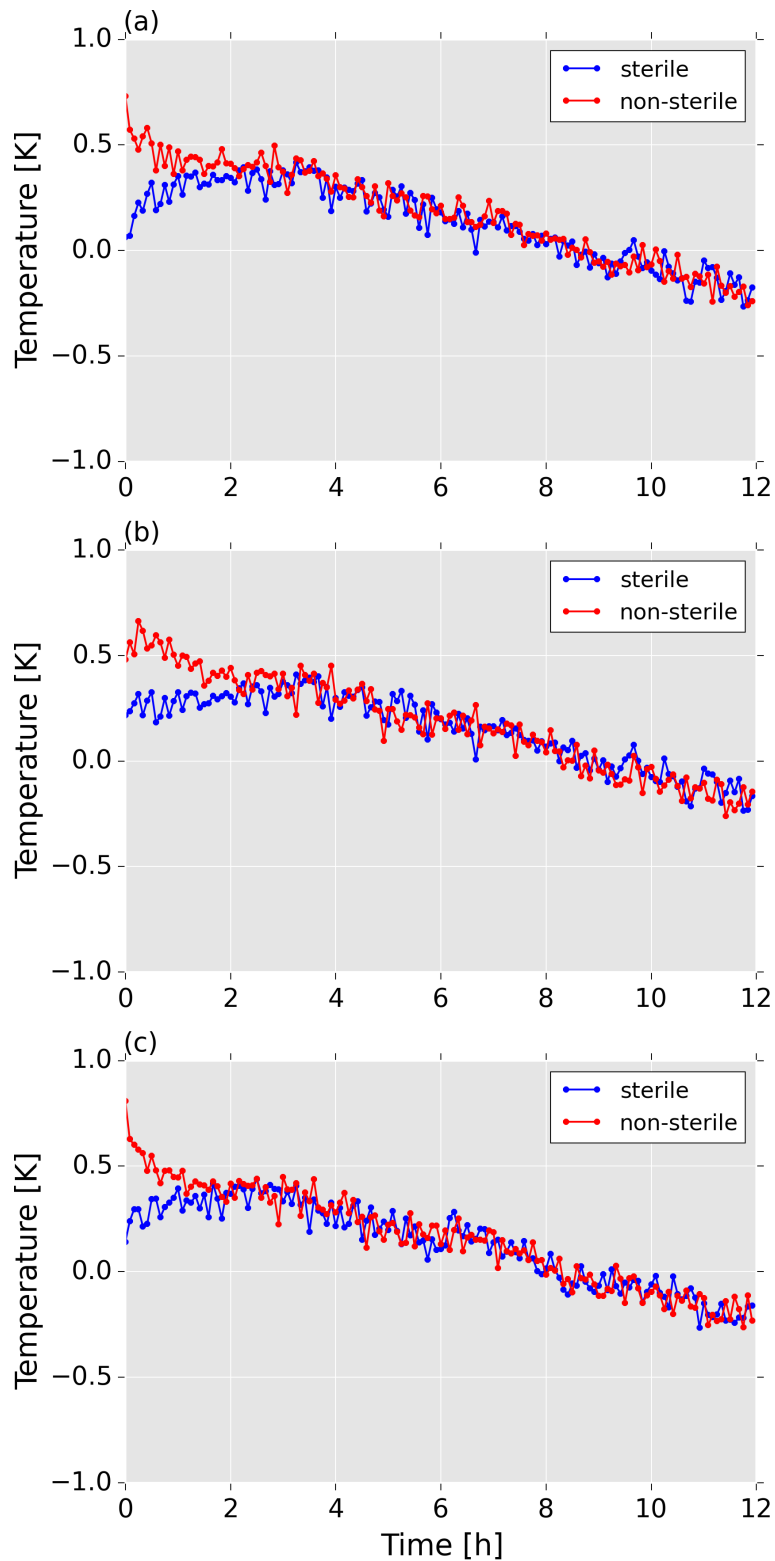
**Figure 2.4:** *Temporal course of the deviation of the mean surface temperature [K] of sterile as well as non-sterile soil surfaces after rewetting; (a) soil sample A, (b) soil sample B, and (c) soil sample C.*

Similarly, Kluge et al. (2013) detected substrate-induced heat evolution using passive IRT only for 20 h after adding glucose to soil samples. These results indicate that basal microbial respiration does not produce enough heat to become detectable with our IRT technique, possibly also due to small variations of ambient temperatures in the glove box. The gradual decrease of surface temperatures throughout the incubation period is attributed to evaporation as this induced cooling of the soil surface (Benasher et al., 1983; Han and Zhou, 2013; Kerridge et al., 2013). Differences in microbial activity between the three test soils were not reflected in their surface temperatures. Thus, the mean values of surface soil temperatures were not representative of their soil properties, but the spatial temperature variability could indicate differences in microbial activity by hot or cold spots. Therefore, the main advantage of the passive IRT method is that it allows monitoring at high spatial and temporal resolution of short-term events with greatly increased microbial activity such as the "Birch effect" (Fig. 2.4) or substrate induced mineralization processes (Barros et al., 1995; Kluge et al., 2013).

### 2.3.2.2 Spatial and temporal variability of surface temperatures

These spatio-temporal temperature dynamics of the non-sterile and sterile soil sample A are illustrated in Fig. 2.5 (Experiment P2). Immediately after rewetting, the surface temperature of the non-sterile soil showed rather high heterogeneity, ranging from 294.4 to 295.1 K, with a mean of 294.9 K (Fig. 2.5a). At the same time, the surface temperatures of the sterile sample ranged from 293.9 to 294.8 K (Fig. 2.5d), with a significantly lower mean value of 294.2 K compared to the non-sterile sample (Fig. 2.5d). Four hours later, the mean temperature in the non-sterile sample dropped to 294.5 K, which was not different from the sterile sample. Interestingly, the surface temperature of the non-sterile sample was more homogeneously distributed than at the beginning, ranging only from 294.5 to 294.7 K, with very few

spots >294.8K (Fig. 2.5b). The temporal temperature dynamics of the non-sterile sample along the transect marked in 2.5a and 2.5b is illustrated in Fig. 2.5c with a so-called Hovmöller diagram. Much of the cooling occurs within the first 2 h but with an irregular spatial distribution as seen in a longer lasting heat production within the upper part of the transect. The spatio-temporal heterogeneity of the surface temperature distribution can be discussed in the context of hot spots and hot moments (Kuzyakov and Blagodatskaya, 2015). Most soil microorganisms were in a dormant state (Joergensen et al., 2010; Kuzyakov and Blagodatskaya, 2015) since their activity is mainly limited by substrate availability (Hodge et al., 2000; Joergensen and Wichern, 2018). The limitations can be removed by feeding with fresh organic substrates resulting in an activation of dormant microorganisms (Joergensen and Wichern, 2018; Kuzyakov and Blagodatskaya, 2015) leading to the formation of hot moments which are time-limited enhanced microbial processes as compared to the average soil conditions (Kuzyakov and Blagodatskaya, 2015; McClain et al., 2003). Hot moments mainly occur in hot spots when high process rates occur over short sequences. Hot spots result from the non-uniform distribution of dead and easily available substrates (Blagodatskaya and Kuzyakov, 2013; Kuzyakov and Blagodatskaya, 2015; McClain et al., 2003). The highly variable temperature pattern on the surface of the non-sterile sample immediately after rewetting indicated these phenomena (Fig. 2.5a). For sterile samples, neither temporal variation nor spatial differentiation of the surface temperatures was expected. While the initial spatial temperature variability was indeed lower than in the non-sterile sample (Fig. 2.5d), an unexpected temperature increase by a mean value of 0.2 K occurred during the following 4 h, illustrated by both the overall surface temperature (Fig. 2.5e) as well as by the high-resolution temporal temperature dynamics along the transect (Fig. 2.5f). This phenomenon seemed to be likely due to non-sterile conditions in the glovebox resulting in microbial contamination and increasing microbial activation of the sterile samples over time.
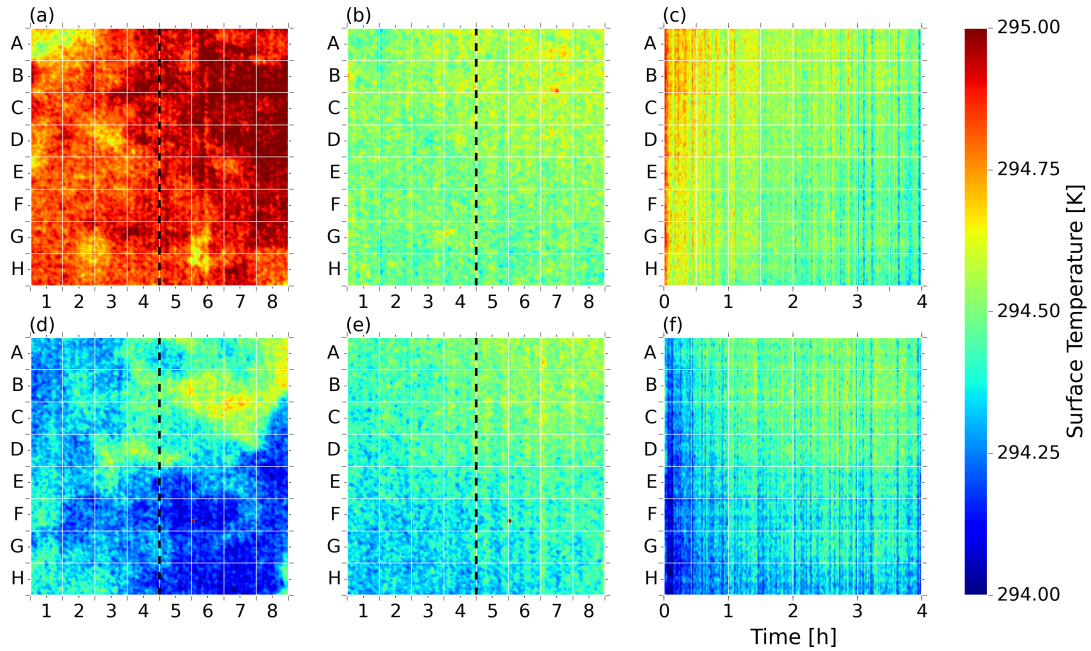
**Figure 2.5:** *Spatio-temporal dynamics of the surface temperature [K] for the non-sterile (top row) and sterile (bottom row) soil A: (a, d) surface temperature immediately after rewetting, (b, e) surface temperature after 4 h, (c, f) Hovmöller diagram taken from the transects (dashed line) in (a, b) and (d, e) during the first 4 h of incubation. The grid size is 5.5 × 5.5 cm.*

As observed from the gradual temperature decrease in all samples over time (Fig. 2.4), surface temperatures were also affected by evaporation and therefore by soil moisture. However, this cooling effect decreased with decreasing soil moisture (Kerridge et al., 2013). Additionally, emissivity varied with water content due to water films on the soil particles, which influenced the reflectivity and therefore the amount emitted infrared radiation (Mira et al., 2007). The effects of emissivity and evaporation rate changes were also subject to the temporal temperature variations of the non-sterile soil sample (Fig. 2.5c). In the beginning, when the heat production of the microbial activity was highest, described as the "Birch"-$CO_2$-pulse, the cooling by evaporation was also highest (Han and Zhou, 2013; Kerridge et al., 2013), leading to an underestimation of the initial microbial activity. Later on, heat production

decreased due to lower microbial activity, while at the same time, the emissivity change of the drying soil led to lower apparent surface temperatures (Mira et al., 2007), which might lead to an overestimation of heat production from microbial activity at the beginning compared to the consecutive measurements.

### 2.3.2.3 Combination of surface temperature, soil moisture, and surface structure

Besides C limitation, abiotic factors, such as soil moisture, are known to affect microbial activity as well as microbial process rates (Borken and Matzner, 2008; Kuzyakov and Blagodatskaya, 2015). Therefore, the inhomogeneity of soil surface temperatures has to be considered. In unsaturated soils, microbial activity increases with increasing water content (Rey et al., 2005; Tecon and Or, 2017) so that spatial variations in soil moisture can affect the spatial variability of microbial process rates. The influence of soil surface moisture on the spatial pattern of microbial activity was quantified in further incubation experiments using combined active and passive IRT approaches (Experiment P3). Fig. 2.6a shows the change in surface temperature distribution during the first 30min after rewetting and Fig. 2.6b the corresponding distribution of surface soil moisture 30min after rewetting. Interestingly, the areas of highest temperature decreases were partly linked to areas with higher water contents (i.e., Position G/H 1–8 in Fig. 2.6a and b). A linear regression analysis of surface temperature changes and VWC was conducted to quantify this relationship. About 35% of the surface temperature change variability is significantly ($p < 0.01$) explained by soil surface moisture. For precise interpretation of microbial activity patterns using passive IRT measurements, the soil moisture distribution, calculated from active IRT measurements, has to be considered.

Soil surface structure also influenced passive IRT measurements. For example, cavity structures and depressions were characterized by higher apparent surface tem-
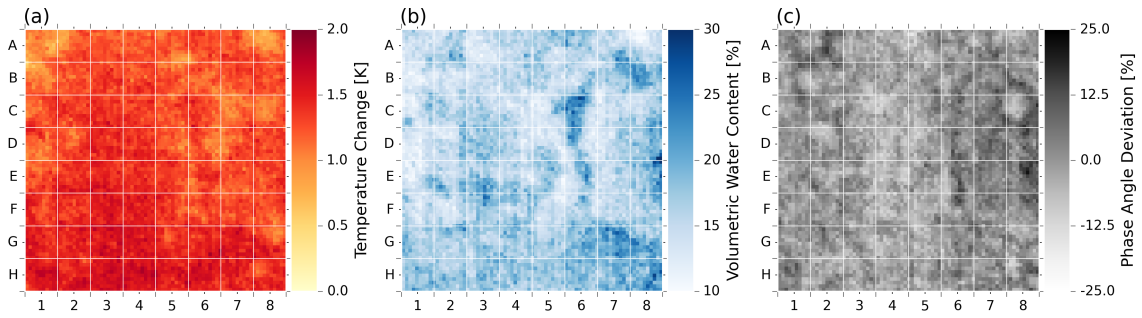
**Figure 2.6:** *Soil surface properties derived from passive and active IRT; (a) soil surface temperature change [K] during the first 30 min after rewetting, (b) the corresponding VWC [%], and (c) the percentage deviation of the mean phase angles corresponding to (a). The grid size is 2.2 × 2.2 cm.*

peratures. Incoming thermal radiation is reflected within cavities and depressions before the IRT sensor can detect the signal. Thus, more radiation gets absorbed and therefore emitted from these structures leading to higher emissivity (Mollmann and Vollmer, 2007; Quinn, 1967; Usamentiaga et al., 2014). Quinn (1967) analyzed the influence of cylindrical cavities on the emissivity and showed that the deeper a cavity, the higher the emissivity, cumulating in near black body radiation. For our study, this meant that using a fixed emissivity of 0.95 led to an overestimation of the surface temperature in cavities and depressions. Therefore, information about the surface structural properties could help in analyzing spatial surface temperatures patterns. Fig. 2.6c shows the phase image as an approximation of the surface soil structure and density in relation to the surface temperature pattern of soil A (Fig. 2.6a). Cavities in the surface structure can be detected, e.g., in Position A 1–2 in Fig. 2.6c. At the same position in Fig. 6a, an intermediate temperature change was detected, although a high temperature decrease was suspected due to the also high moisture content (Fig. 2.6b). In cavity structures, soil moisture was more stable (Fig. 2.3), and thus, microbial heat production could longer retain at a higher state (Kuzyakov and Blagodatskaya, 2015; Rey et al., 2005; Tecon and Or, 2017). This resulted in a lower temperature decrease. According to these findings, a more neutral surface structure in Fig. 2.5c at Position H 4 was characterized by

a higher temperature decrease at the same moisture content of 17.3% compared to 16.8% at Position A 1–2. Thus, the interpretation of passive IRT measurements can be improved by considering the active IRT measurements referring to the moisture contents and structural patterns.

## 2.4   Conclusions

In this study, we presented IRT as a promising technique to get temperature based information of the soil surface in a high spatial and temporal resolution. Active IRT proved to be a reliable method for measuring moisture content on soil surfaces with good accuracy. However, the calibration of soil moisture was only reliable at VWCs up to 30%, limited by the rewetting procedure. In addition, the relative residual errors for the separated soil calibrations were between 12 and 17% because soil texture influenced the thermal properties of soils so that a separate calibration of soil moisture for different soil samples is recommended for more precise results. Soil surface structure and density can affect the reflectivity of thermal radiation as well as the strength of soil drying. Thus, the phase image has to be considered for interpretation of soil surface moisture. The passive IRT technique enables the detection of increased microbial activity events as the "Birch effect" or substrate induced respiration. Temperature increases induced by microbial activity were detected up to 0.5 K at a camera accuracy at $\pm$ 20 mK. Basal respiration could not be measured due to influences of the surrounding ambient environment and evaporation. Especially spatial information about soil moisture content and soil surface structure are crucial for understanding various microbial processes, which were detectable with passive IRT.

Active and passive IRT approaches can be improved and validated to get more precise temperature based information. For example, the accuracy of spatial soil

surface moisture detection using active IRT can be validated by X-ray imaging. To quantify microbial activity on soil surfaces with passive IRT, the combination with 14C imaging or zymography seem to be very promising. Also, the detection of microbial activity in situ would be an interesting application for IRT techniques. However, before IRT can be tested in field applications, further studies should focus on the potential of IRT techniques to analyze undisturbed soil samples for soil moisture contents and soil microbial activity under laboratory conditions. It can be concluded that active and passive IRT, as non-contact techniques, are highly promising mapping tools for surface properties since they characterize intact soil structures on a microscale in a high spatial and temporal resolution. Moreover, these techniques can be used for real-time detection of three factors microbial activity, soil moisture, as well as soil structure, simultaneously.

# 3   Research Study II

**Hot movements on soil surfaces - Innovative insights into microbial dynamics using passive infrared thermography**

Co-Authors: Jannis Heil, Bernd Marschner, Britta Stumpe

Published in Geoderma (2021), 385: 114879 (accepted 28.11.2020)
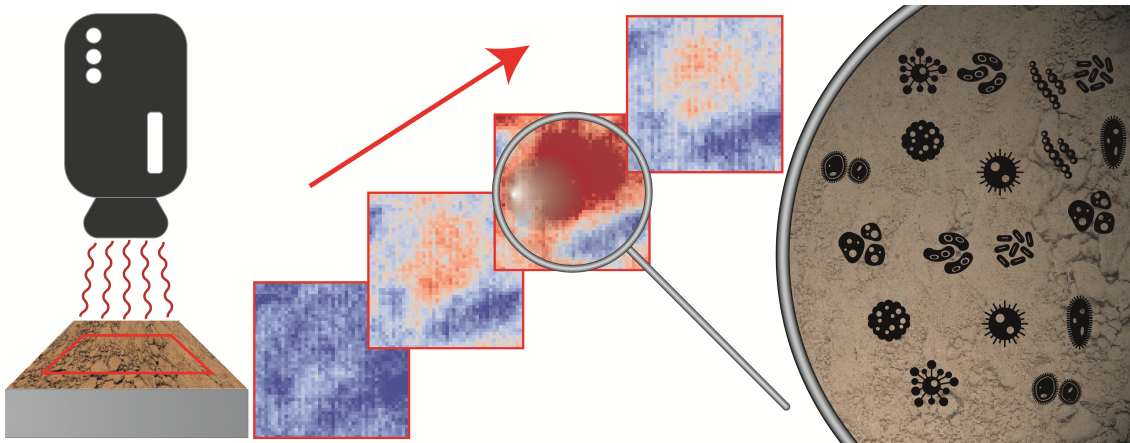
## 3.1 Introduction

In recent years, the spatial and temporal heterogeneity of soil microbial activity at the microscale has been acknowledged to be an important but often neglected aspect for understanding and quantifying microbial mediated soil processes, such as nutrient cycling or C turnover (Heitkötter and Marschner, 2018a; Kuzyakov and Blagodatskaya, 2015). Such microsites termed "hot spots" can develop due to locally improved environmental conditions, such as soil moisture or aeration and due to substrate inputs as in the rhizosphere (Kuzyakov and Blagodatskaya, 2015; Tecon and Or, 2017) or the drilosphere (Don et al., 2008). However, hot spots have also been detected in soil domains not visibly different from the surrounding bulk soil (Heitkötter and Marschner, 2018a). Apart from the spatial identification of such aggregated microbial colonies, their temporal dynamics may be of great relevance, when increased microbial activity is additionally limited to only short-term "hot moments", as it was termed by Kuzyakov and Blagodatskaya (2015). However, up to now, the dynamic nature of hot spots and hot moments was rarely analyzed in soils because only very few experimental approaches are available for determining soil microbial activity at a sufficiently high spatial and temporal resolution. Until now, the spatio-temporal detection of hot spots and/or hot moments has been determined with techniques like zymography, phosphor imaging, or planar optodes (Heitkötter and Marschner, 2018a; Pausch and Kuzyakov, 2011; Rubol et al., 2016).

Soil zymography allows determining enzyme activities on intact soil surfaces at a spatial resolution < 1 mm (Heitkötter and Marschner, 2018b; Kuzyakov and Blagodatskaya, 2015; Spohn et al., 2013). Although repeated measurements are possible, the minimum temporal resolution is about 30 min, due to the needed contact time of the substrate soaked gel with the soil surface (Spohn and Kuzyakov, 2014). Thus, short-term dynamics can only be mapped to a limited extent with a comparable long preparation time of the experimental procedure (Heitkötter and Marschner, 2018a).

Phosphor imaging of $\beta$-radiation has been used to identify spatial and temporal variations in $^{14}$C-activity from root exudation of labeled plants (Pausch and Kuzyakov, 2011; Spohn and Kuzyakov, 2013) or also from surface-applied $^{14}$C-glucose at a spatial resolution of about 0.1 mm (Heitkötter and Marschner, 2018a). With this technique, the mapping of temporal dynamics is only possible at a low resolution because the exposure time of the phosphor plates is relatively long ($>$ 3h up to 22 h) (Heitkötter and Marschner, 2018a; Pausch and Kuzyakov, 2011). Short-term dynamics can therefore not be determined but rather accumulated values over longer periods. This technique allows contactless detection of C consumption on the soil surface, but can only be used after addition of, e.g., $^{14}$C labeled substrates. The detection of $\beta$-radiation is additionally limited by its low energy, which is easily shielded by soil particles or aggregates (Heitkötter and Marschner, 2018a).

Lastly, planar optodes have been used to image $CO_2$ production or $O_2$ consumption at soil surfaces which are in contact with a membrane over several days, allowing a spatial resolution of up to 10 $\mu$m per pixel, depending on camera distance (Holst and Grunwald, 2001; Rubol et al., 2016). Although planar optodes allow continuous and highly resolved real-time measurements with a resolution $<$ 1 min, the accuracy is restricted by the measurement requirements. Contact and non-contact areas result in lateral oxygen diffusion affecting the accuracy of $O_2$ or $CO_2$ measurements (Askaer et al., 2010; Gansert and Blossfeld, 2008; Holst and Grunwald, 2001). Additionally, the samples must be water-saturated, which reduces the respiratory activity of microorganisms, which also affects the results and complicates the recording of microbial activity, especially in undisturbed soil samples (Barros et al., 1995; Skopp et al., 1990).

In contrast to these techniques, passive infrared thermography (IRT) allows detecting surface temperature changes induced by the energy released from microbial catabolism at high spatial and temporal resolution (Kluge et al., 2013; Schwarz et al., 2018), enabling the combined real-time evaluation of hot moments and hot

spots. This combination of phenomena is termed "hot movements" in this study. The advantage of the IRT technique is the non-invasive and non-contact approach for detecting hot moments on undisturbed soil sample surfaces at temporal resolutions of maximum 60 records per second and hot spots at spatial resolutions < 1 mm depending on camera distance.

Although the IRT approach has been applied for monitoring increased soil microbial activity after rewetting events (Schwarz et al., 2018) or measuring substrate-induced heat production (Kluge et al., 2013), no standardized methical procedure exists. The IRT technique is highly sensitive towards ambient environmental conditions, like changes in air temperature, which are reflected on moist soil surfaces or relative air humidity (Schwarz et al., 2018). The relative air humidity determines the intensity of soil drying (Schwarz et al., 2018), which thus influences the evaporative cooling and specific heat capacity of moist soil samples (Antonucci et al., 2011; Schwarz et al., 2018). These influences overlay temperature effects (> 0.03 K), which are triggered by microbial activity. Thus, there is a need for the development of a standardized method for comparing microbial activity levels in different studies and experiments. A standard IRT method can be a powerful and innovative tool for obtaining deeper insights into soil microbial processes at the microscale.

Consequently, the objective of the present study was to optimize the passive IRT technique regarding sensitivity and stability for the reliable detection of substrate-induced respiration at high spatial and temporal resolution on soil surfaces. We further developed the method by optimizing (i) the glucose application rates and techniques, (ii) incubation air humidity and temperature, and (iii) the data preprocessing procedure. For data validation, the microbial activity determined by IRT was compared to soil respiration determined with conventional $CO_2$ measurements. Finally, the optimized method was applied for mapping microbial hot spots and hot moments in so-called hot movements on soil surfaces.

## 3.2 Material and Methods

### 3.2.1 Soil samples

Two topsoil samples (0–20 cm) were collected from two sites in North Rhine-Westphalia (Germany). One soil sample was collected from an arable field in Witten and the other from a pasture near Kalkar. The soils were air-dried and sieved to < 2 mm after sampling. As shown in Table 3.1, both samples had a similar texture but differed in pH, soil organic carbon (SOC) contents, and microbial properties. Since the primary goal of this study was to develop a methodical approach and not to make a direct comparison between soils with different properties, only two soil samples varying in their characteristics were considered. With this first test series, possible sources of errors and limitations should be uncovered and discussed, leading to further methodological improvements.

### 3.2.2 Analytical techniques

#### 3.2.2.1 Infrared thermography

A high definition IRT camera (Variocam HD research, InfraTec, Dresden, Germany) with an image resolution of 1024 × 768 pixels was used to determine soil surface temperatures. The camera distance from the soil sample surfaces was 50 cm in all experiments, which resulted in a pixel resolution of 0.283 × 0.283 mm per pixel. Within the far-infrared spectral range of 7–14 $\mu$m, a temperature accuracy of ± 30 mK can be achieved with this camera. The emissivity of the soil surfaces was set to 0.95 in all experiments (Kluge et al., 2013; Schwarz et al., 2018). Although a maximum temporal resolution of 60 records per second could be achieved using passive IRT, it was set to one minute for all experiments.

**Table 3.1:** *Characteristics of the pasture and arable soil used for the incubation experiments.*

| Soil Sample | pH[a] | SOC[b] | WHC[c] | Sand[d] | Silt[d] | Clay[d] | $C_{mic}$[e] | Basal respiration[f] |
|---|---|---|---|---|---|---|---|---|
| | [-] | | | [%] | | | [ug g$^{-1}$] | [CO$_2$ mg g$^{-1}$ h$^{-1}$] |
| Pasture Soil | 5.9 | 1.7 | 46.3 | 13 | 82 | 5 | 5 | 0.11 |
| Arable Soil | 7.1 | 3.0 | 61.5 | 7 | 85 | 8 | 51 | 1.27 |

[a] 0.01 M CaCl2

[b] Vario EL Elementar Analyser (Elementar Analysesysteme GmbH, Hanau, Germany)

[c] After DIN EN ISO 11267 (2014-07)

[d] Analysette (Fritsch GmbH, Idar-Oberstein, Germany)

[e] after Anderson and Domsch (1978)

[f] Respicond (Nordgren Innovations AB, Bygdeå, Sweden)

### 3.2.2.2 Respirometry

To relate surface temperature to microbial activity, a Respicond System (Nordgren Innovations AB, Bygdeå, Sweden) was used to determine soil microbial respiration. For this purpose, incubation studies were conducted with 30 g soil samples placed into 250 mL vessels. The evolved $CO_2$ was trapped in KOH-solution placed inside the incubation vessel. By recording changes in electrical conductivity in the KOH-solution, the amount of $CO_2$ was determined hourly (Nordgren, 1988; Stumpe and Marschner, 2009). However, this method measures accumulated values over time for a specific soil volume and does not provide any information about spatial variations.

### 3.2.3 Incubation experiments

### 3.2.3.1 Incubation experiments for thermal imaging

Passive IRT is able to measure real-time surface temperatures of soils. Since the energy released during microbial catabolic activity results in temperature increase, the thermal contrast can be linked to spatial and temporal variations of microbial activity (Kluge et al., 2013; Schwarz et al., 2018). Thus, to detect microbial activity in high spatial and temporal resolution, incubation experiments for thermal imaging were performed using the passive IRT technique. For this, both soil samples were rewetted to 45% of their Water Holding Capacity (WHC), corresponding to the study of Schwarz et al. (2018), and pre-incubated for one week to avoid the "Birch"–$CO_2$-pulse (Birch, 1958; Schwarz et al., 2018). After pre-incubation, the equivalent of 12 g dry soil was filled into incubation vessels with a volume of 15.625 cm$^3$ and a surface of 2.5 × 2.5 cm. The ambient air temperature during the pre-incubation period and the experiments was about 20 °C in the laboratory and the incubation vessel. The monitoring of the surface temperature during incubation was carried out over a period of one week because the substrate-induced increase of

microbial activity or the so-called glucose effect lasts up to a maximum of five days (Anderson and Domsch, 1978; Stumpe and Marschner, 2009). For developing the method, the experiments were separated into three steps: (i) effect of glucose application, (ii) glucose application methods, and (iii) influence of ambient incubation conditions.

#### 3.2.3.1.1   Effect of glucose application

Passive IRT is not able to detect basal microbial activity (Schwarz et al., 2018), and, therefore, microbial activity was stimulated by the application of glucose (Kluge et al., 2013). In a first screening setup, the sensitivity of the passive IRT approach for the detection of substrate-induced respiration was evaluated by applying different glucose concentrations. Those were chosen on the basis of other studies, e.g., 140 $\mu$g glucose-C cm$^2$ (Heitkötter and Marschner, 2018b) or one weight percent of substrate mixture containing 80% glucose (Kluge et al., 2013). By recalculating the glucose mass of both studies to the sample size in this study, glucose levels of $\approx$0.24 mg glucose cm$^2$ and $\approx$0.96 mg glucose cm$^2$ were achieved. To evaluate the sensitivity of the method, we also considered intermediate steps as well as higher application rates. Therefore, the following nine glucose application rates were tested: 0.24, 0.48, 0.72, 0.96, 1.20, 1.44, 1.68, 1.92, and 2.16 mg cm$^2$ by preparing glucose solutions corresponding to the application of five drops of 10 $\mu$L cm$^2$ per treatment. For the control samples, only deionized water was added at the same amount. Three replicates of each treatment were used. The mean values of the replicates are presented in the results section, because all had the same initial conditions and comparable values. The temperature curves of the individual replicates with mean values can be found in the Appendix (Appendix Fig. A2.1).

After screening, three application rates (0.24, 0.96, and 1.68 mg cm$^2$) were selected for all further experiments to cover a range of concentrations and to induce different microbial response levels to evaluate the sensitivity of passive IRT.

### 3.2.3.1.2 Glucose application methods

To develop an IRT method for disturbed as well as for undisturbed soil samples, glucose solution was pipetted (G$_P$) on the surface of potentially undisturbed soil samples and, on the other hand, mixed into disturbed soil sample (G$_M$).

For G$_P$, the glucose solution was pipetted on the soil surface with 10 $\mu$L each on five spatially separated spots since a homogeneous application of glucose on the surface was technically not possible. The drops were placed in four corners and into the center of the surface, avoiding overlaps of the drops to cover most of the surface area of the soil sample. Thus, added glucose is expressed in mg per cm$^2$, taking the complete surface area of 6.25 cm$^2$ into account. Since the diffusion into depth is unknown, the concentration is only an estimate.

In contrast to G$_P$, G$_M$ allows a nearly homogeneous distribution of the glucose in the soil sample and on the soil sample surface. Using G$_M$, 1 mL of glucose solutions (1.4, 7.0, and 14.0 mg $g^1$) was carefully stirred in the pre-incubated soil samples to maintain soil aggregates. Three replicates were used for every treatment. The addition of glucose is given in mg per g, as this application method refers to the total soil volume and not only to the surface. For the controls, deionized water was used to consider the impact of enhanced soil moisture on microbial activity.

### 3.2.3.1.3   Influence of ambient incubation condition

The effect of environmental influence factors should be avoided or minimized as much as possible to develop a reliable IRT method for the detection of microbial activity since surface temperature is highly sensitive towards ambient environmental conditions (Schwarz et al., 2018). Thus, the following conditions and influence factors were taken into account in our experiments: Relative air humidity and air temperature.

**3.2.3.1.3.1 Relative air humidity**

Controlling the relative air humidity is necessary since soil samples lose moisture at low relative air humidity due to increased evaporation. Relative air humidity of < 100% will result in soil drying, which affects the soil surface temperature, e.g., due to evaporating cooling processes. This effect would depress a thermal increase from increased microbial activity. In addition, soil drying will result in emissivity changes (Axelsson, 1988) and decreased microbial activity (Barros et al., 1995). Soil drying cannot be fully corrected mathematically, because not only do the physical soil properties change, but microbial activity is also affected. While changes in the relative water content of soils can be determined by active infrared thermography and then used as a correction factor for the physical soil properties (Schwarz et al., 2018), moisture-dependent changes in microbial activity cannot be accounted for. In order to test this, experiments under different ambient humidity levels were carried out.

The incubation experiments were conducted in three approaches: at ambient laboratory conditions (ALC), at ALC with samples covered by an IR-transparent polypropylene foil (PPF), and uncovered samples placed in a gas-tight glovebox with controlled air humidity conditions (CHC). During all three approaches, relative air humidity was monitored inside and outside the glovebox at 1-minute temporal reso-

lution using wireless data loggers (M-Log5W-HUMIDITY, Geoprecision, Ettlingen, Germany). For the ALC approach, the relative humidity was about 35% during the experiments. In the PPF approach, the air space of 0.625 cm$^3$ between the soil sample surface and PP foil had a microclimate with a relative humidity of about 100%, avoiding evaporation from the soil sample. This approach has already been used by Kluge et al. (2013).

For the CHC approach, incubation experiments were performed in a gas-tight glovebox. The glovebox was made of a stainless steel body and plexiglass windows. Inside the box, the relative humidity was adjusted to over 80% by using two methods: using a water-filled bowl (resulting in about 80% relative humidity) or a saturated salt solution (Rockland, 1960; Young, 1967) combined with a ventilation system. Saturated salt solutions have the ability to adjust a level of relative humidity in a closed system depending on the salt. Further information is given in Young (1967). We used a sodium chloride solution resulting in a relative humidity of about 85% and potassium chloride resulting in a relative humidity of about 95%.

### 3.2.3.1.3.2 Air temperature

As the surface temperature of wet soil samples is sensitive to variations in air temperature (Schwarz et al., 2018), the air temperature was monitored in all humidity approaches minutely by wireless data loggers (M-Log5W-HUMIDITY). The loggers were placed inside and outside the glovebox to capture the differences and variations in air temperature. Thus, the variations in the measured surface temperatures were corrected for the course of the air temperature to eliminate, e.g., diurnal cycles. Although all experiments were conducted under laboratory conditions, a diurnal cycle in air temperature could not be avoided completely.

### 3.2.3.1.4   Data preprocessing

Conducting the experiments in a closed system enabled minimization of the influencing environmental factors. Since those could not be removed entirely, processing of the raw data was necessary to minimize small temperature effects and to increase thermal contrasts for the sensitivity of the IRT identification of microbial activity. As slight temperature increases could be detected, high microbial response rates were measurable without preprocessing (Kluge et al., 2013; Schwarz et al., 2018).

As a first step, outliers were corrected from the time series by using the 5% and 95% quantiles to eliminate measurement errors. Second, a low pass filter was applied to reduce the noise of the raw thermal time series and to get more comparable variances, as shown by Grudzielanek and Cermak (2015). In the third step, the temperature time series were linearly detrended (Antonucci et al., 2011) to correct for soil drying, which would result in a temperature increase over time (Schwarz et al., 2018). The camera accuracy of $\pm$ 30 mK and surface structural patterns might produce scattering effects that result in sloping and shifting of the starting point of the thermal time series (Schwarz et al., 2018; Usamentiaga et al., 2014), which need to be corrected. Thus, in a fourth step, an offset correction was applied to fit the start points of each time series to each other. In a final step, the temperature of the control samples was subtracted from the temperatures of the glucose treated samples to remove ambient environmental temperature changes. Another advantage of subtracting was that only differences in the temperature trends were considered and the data focused on thermal contrasts (Kluge et al., 2013).

All surface temperature evaluations were performed after preprocessing. In order to evaluate the soil surface temperature, mean values were calculated over the soil surfaces for each treatment, and the temporal courses were compared to each other qualitatively. In addition, thermograms were used from the start time and the

time of the highest temperature increase induced by microbial activity to assess the spatial patterns of temperature change.

### 3.2.3.2 Respirometry incubation experiments

Incubation experiments using a respirometer were performed to validate the measurements of the surface temperature by passive IRT. According to the other experiments, the soil samples (30 g per vessel) were pre-incubated for one week at 20 °C to create equal conditions compared to the IRT experiments. After pre-incubation, glucose was added at application rates corresponding to those of the IRT experiments ($G_M$). The incubation experiments were carried out over a period of one week.

For qualitative evaluation and validation of the IRT measurements, the time-dependent course of the substrate-induced soil respiration was compared with the temporal changes of the mean temperature on the soil surfaces. For a quantitative evaluation and validation, the accumulated energy release was calculated for both the IRT and the respirometry incubation experiments.

For the calculation of the thermal energy release measured by passive IRT, the integral of the mean temperature curve was calculated and inserted into the formula for thermal energy, where $Q$ [J min] is the amount of thermal energy release as a function of time $t$ [h], $m$ is mass [kg], and $c$ is specific heat capacity [J/(g * K)]:

$$\int_0^t Q(t) = m \times c \times \int_0^t T(t) \tag{3.1}$$

We assumed a uniform specific heat capacity ($c$) for the moist soil of 2000 $J \times kg^{-1}K^{-1}$ (Abu-Hamdeh, 2003). In terms of simplification, small-scale differ-

ences, as variations in texture, density, or soil moisture, on the soil surface could not be considered. Thus, Eq. (3.1) was used as an approximation to the current thermal energy release.

On basis of the respiration curves ($Q_R$ [kJ]), the energy release was calculated by using the accumulated $CO_2$, which is related to the caloric equivalent of 20.2 kJ/l (Critter et al., 1994) using the following equation:

$$Q_R = \frac{\sum_0^t R(t)}{1960mg} \times 20.2kJ \tag{3.2}$$

Here, 1960 mg refers to the density of $CO_2$ and $R$ is the mineralized amount of $CO_2$ [mg] at each time step. The energy releases calculated for the temperature curves and the respiration rates can be compared to each other. Additionally, the energy was calculated per gram soil in order to compare the energy release $Q(t)$ of the mean surface temperature of 12 g soil to the accumulated energy release $Q_R$, referring to 30 g soil.

In a further step, we calculated the pixelwise energy release of the surface temperature for each thermogram, referring to the calculation of Q(t) using Eq. (3.1). With this approach, spatio-temporal dependencies, such as microbial hot spots, can be detected.

### 3.2.3.3 The potential of hot movement identification on soil surface using IRT

In order to identify and characterize microbial hot movements, the combination of hot spots and hot moments, on the soil sample surface, the surface temperature of the incubated and substrate-induced soil samples were examined using time-lapses.

For this purpose, both soil samples were incubated under the optimal incubation conditions. After soil sample pre-incubation, the highest application rates of glucose (1.68 mg cm$^{-2}$ for pipetting and 14 mg g$^1$ for mixing) were pipetted (G$_P$) or mixed (G$_M$) into the soil samples. Afterwards, thermal images were preprocessed as described above (section 3.2.3.1.4) and switched into an image sequence with a temporal resolution of 15 min. These time-lapses visualized spatio-temporal patterns, i.d., microbial hot spots, in combination with hot moments. Additionally, periods of maximum activity in space and time were quantitatively assessed and compared to the average soil conditions.

### 3.2.4    Software

The thermal images were converted and exported using IRBIS3 professional (InfraTec). The data preprocessing, calculations, and image creation were done using Python 3.7.

## 3.3    Results and discussion

### 3.3.1    Incubation experiments for thermal imaging

#### 3.3.1.1    Effect of glucose application

Fig. 3.1 shows the effects of different glucose application rates on the mean soil surface temperature during the first 30 h of incubation of the pasture soil (G$_P$). After about 8 h, mean $\Delta T$ increased on all soil surfaces until a temperature peak was achieved after 15 to 20 h, depending on glucose application rate. Additionally, the temperature increase was larger and the duration of the peak lasted longer with increasing glucose application. The highest temperature increase of 0.15 K was reached with a glucose application of 1.68 mg cm$^2$ after about 20 h. The lowest temperature increase of 0.05 K after about 15 h was detected for the glucose addition of 0.24 mg cm$^2$. After reaching the peak, the surface temperature decreased,

indicating declining microbial activity. The intensity and duration of the thermal signal were related to the amount of applied substrate. At the three highest glucose application rates, the temperature effect was not completed after 30 h of incubation. The data after 30 h was not available due to a measurement gap. Nevertheless, other experiments in this study showed that the temperature always leveled down to zero, so reliable measurements could be assumed here as well. Interestingly, $\Delta T$ of the samples with low glucose application rates decreased to below 0 K after about 25 h of incubation. The replicates showed similar temperature curves without significant deviations in mean values or standard deviation (paired t-test, p > 0.05, Appendix Fig. A2.1).
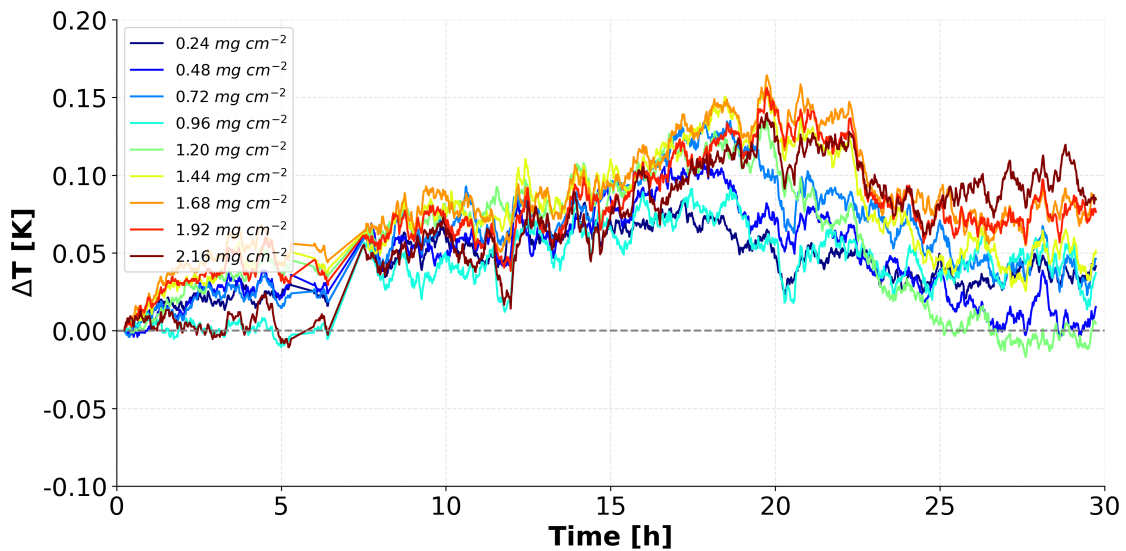


**Figure 3.1:** *Mean $\Delta T$ [K] of the pasture soil after application of nine glucose concentrations ($G_P$) under controlled humidity conditions using water.*

The temperature increase over time can be explained by the substrate-induced increase in microbial activity. Jones and Murphy (2007) showed in their study on microbial response to glucose addition to soils that the initial increase of respiration and, thus, microbial activation already occurs at least half an hour after substrate addition. Further, Anderson and Domsch (1973) showed that the response intensity

depends on the amount of added substrate. The progressive time lag of the highest microbial response with increasing glucose addition has already been shown in various studies (Anderson and Domsch, 1986; Griffiths et al., 1999; Reischke et al., 2014). The rates of labile C input affect microbial and fungal growth rates significantly (Blagodatskaya and Kuzyakov, 2013; Griffiths et al., 1999). The increasing amount of substrate input has an impact on the resulting microbial community. Thus, community structure changes consistently with increasing substrate addition, which affects the microbial response rates and duration (Griffiths et al., 1999). The temperature decrease below 0 of mean $\Delta T$ was possibly an artifact from the offset correction by which the initial thermal response was eliminated.

To identify the reliability of this technique, the relationship between glucose application and the corresponding maximum temperature increase was modeled with linear regression. This resulted in a significant relationship ($^*$p $< 0.05$) with an $R^2$ of 0.84 (Appendix Fig. A2.2). Despite the high explaining variance, the linear regression did not reflect the slightly lower temperature peak at glucose applications above 1.68 mg cm$^2$ (Fig. 3.1). This corresponds to observations made by Beare et al. (1990), who found that microbial activity response increased with higher amounts of added glucose but was suppressed at high concentrations. Likely, the high glucose additions caused anaerobic conditions in the soil due to rapid oxygen depletion and/or through pore-clogging, which might lower the heat production (Barros et al., 1995; Vor et al., 2002). Another reason could be suppressed microbial growth by nitrogen limitation at high glucose application rates. As known, response rates to substrate addition by microorganisms depend on the amount of added glucose and the available nutrients such as nitrogen (Blagodatskaya et al., 2007). Adding glucose combined with nitrogen to soil samples resulted in significantly higher respiration rates (Blagodatskaya et al., 2007; Tian et al., 2016). If only glucose is added, nitrogen limitation may occur so that no further microbial growth can take place, and thus might also lead to lower temperature increases for very high glucose concentrations.

Still, those results showed that the IRT technique reflected total microbial activity in soil samples within a certain range of added amounts of glucose reliably. Therefore, three glucose concentrations were selected for all following experiments. To cover a range of concentrations and to provoke different microbial response levels without risking anaerobic conditions, the glucose application rates of 0.24, 0.96, and 1.68 mg cm$^2$ were chosen.

### 3.3.1.2 Glucose application methods

Fig. 3.2 shows the course of $\Delta T$ of the two glucose application methods mixing ($G_M$) and pipetting ($G_P$) at the highest glucose application rate for both soils. In both soils, the temperature effect was significantly greater when glucose was pipetted on the surfaces compared to mixing it into the soil (paired t-test, $^*p < 0.05$). This effect was more pronounced for the pasture soil with a maximum $\Delta T$ for $G_P$ of 0.51 K and $G_M$ of only 0.25 K. Differences for the arable soil were smaller, but the thermal peak in $G_P$ was broader than in $G_M$.

Mixing the glucose solution into the soil samples diluted the substrate concentration over the whole soil volume, thus concentrations at the surface were lower compared to glucose application with a pipette. Since five drops of glucose solution were pipetted on the soil surfaces, a spatially selective substrate enrichment was induced, resulting in a higher local temperature increases at the soil surface. During the experiments, the pipetting procedure was not changed in order to maintain uniform conditions during the experiments for the method development and the comparability of the results. For further IRT studies, this method can be improved by using a spray system, which provides the possibility to apply liquids, like glucose solutions, evenly on surfaces (Heitkötter and Marschner, 2018a; Stoeckli et al., 2014). Such a spray system would enable to analyze the spatio-temporal microbial activity on undisturbed soil samples surfaces using passive IRT.
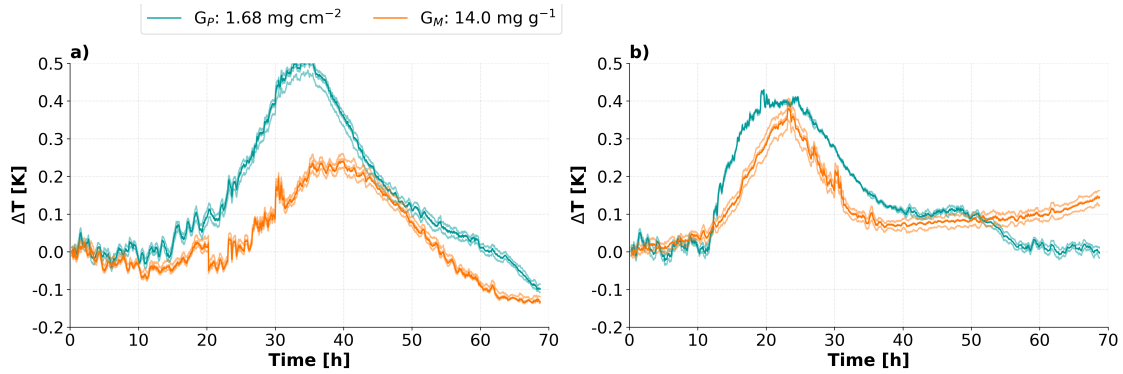
**Figure 3.2:** *Temporal course of $\Delta T$ of the three replicates (light colors) and their mean values (bold) of pasture soil (a), and arable soil (b), after glucose pipetting procedure ($G_P$, 1.68 mg $cm^2$), and glucose mixing procedure ($G_M$, 14.0 mg $g^1$) at CHC.*

#### 3.3.1.3   Influence of ambient incubation conditions

**Relative air humidity**

Fig. 3.3 shows the temporal course of $\Delta T$ for the pasture soil after glucose application ($G_P$) at 1.68 mg $cm^2$ in four experimental setups with varying relative air humidity. In the left column, $\Delta T$ of the experiments PPF and CHC are depicted for the first 70 h after glucose application. The results of the ALC experiment are not shown because the soil had already dried out before the glucose peak occurred.

In the PPF experiment, in which an IRT transparent PP-foil covered the soil sample, $\Delta T$ increased slightly up to a maximum of 0.04 K after 20 h of incubation and decreased afterward, with a steady noise (Fig. 3.3a). The neglectable surface temperature increase (paired t-test, p > 0.05) suggested that the evaporation of the water from the soil increased the relative humidity to 100% in the small air space between the soil surface and PP-film and caused condensation on the PP-film, thus shielding IR rays from detection. Although Kluge et al. (2013) used a similar experimental setup in their study, it could not be replicated here. Likely, perforation of the covering foil could help with ventilation so that the microclimate is counteracted. Another possibility would be to choose a larger airspace between soil surfaces

and the foil cover since we used only 1 mm distance a microclimate with condensing conditions formed very quickly.

In the CHC experiment, in which the humidity inside the glovebox was adjusted to about 80%, a more intense but not significant (paired t- test, $p > 0.05$) increase of $\Delta T$ up to 0.08 K was detectable after 36 h (Fig. 3.3b). The increase started after about 20 h and continued until 50 h after substrate addition. The associated thermograms show that there was a general rise in temperature on the entire soil surface. Due to the comparably low relative humidity of 80%, it can be assumed that evaporation occurred on the whole soil surface and thus superimposed the effect of glucose, resulting in an underestimated temperature increase on the entire soil surface.

In Fig. 3.3c and 3.3d, the results of the CHC experiment using a saturated salt solution are presented. In Fig. 3.3c, an increase of $\Delta T$ started 10 h after glucose application up to a maximum of 0.14 K after 32 h (paired t-test, $^*p < 0.05$) using an adjusted relative humidity of 85% (sodium chloride). With an adjusted relative humidity of 95% (potassium chloride), the most pronounced increase of $\Delta T$ occurred with up to 0.51 K after 37 h incubation time (Fig. 3.3d; paired t-test, $^*p < 0.05$).

The efficiency of this setup is also reflected in the corresponding thermograms (Fig. 3.3d). At the peak of $\Delta T$, the temperature increased highly inhomogeneously on the soil surface, with areas of hardly any difference compared to the control and areas with up to 0.7 K increase. This was clearly related to the non-uniform punctual application of the glucose solution on the soil surface. Apparently, the relative humidity level of about 95% prevented soil drying and evaporation with the associated thermal interferences of the biological heat production. Thus, an overlay caused by these physical processes could be minimized for the determination of microbial activity.
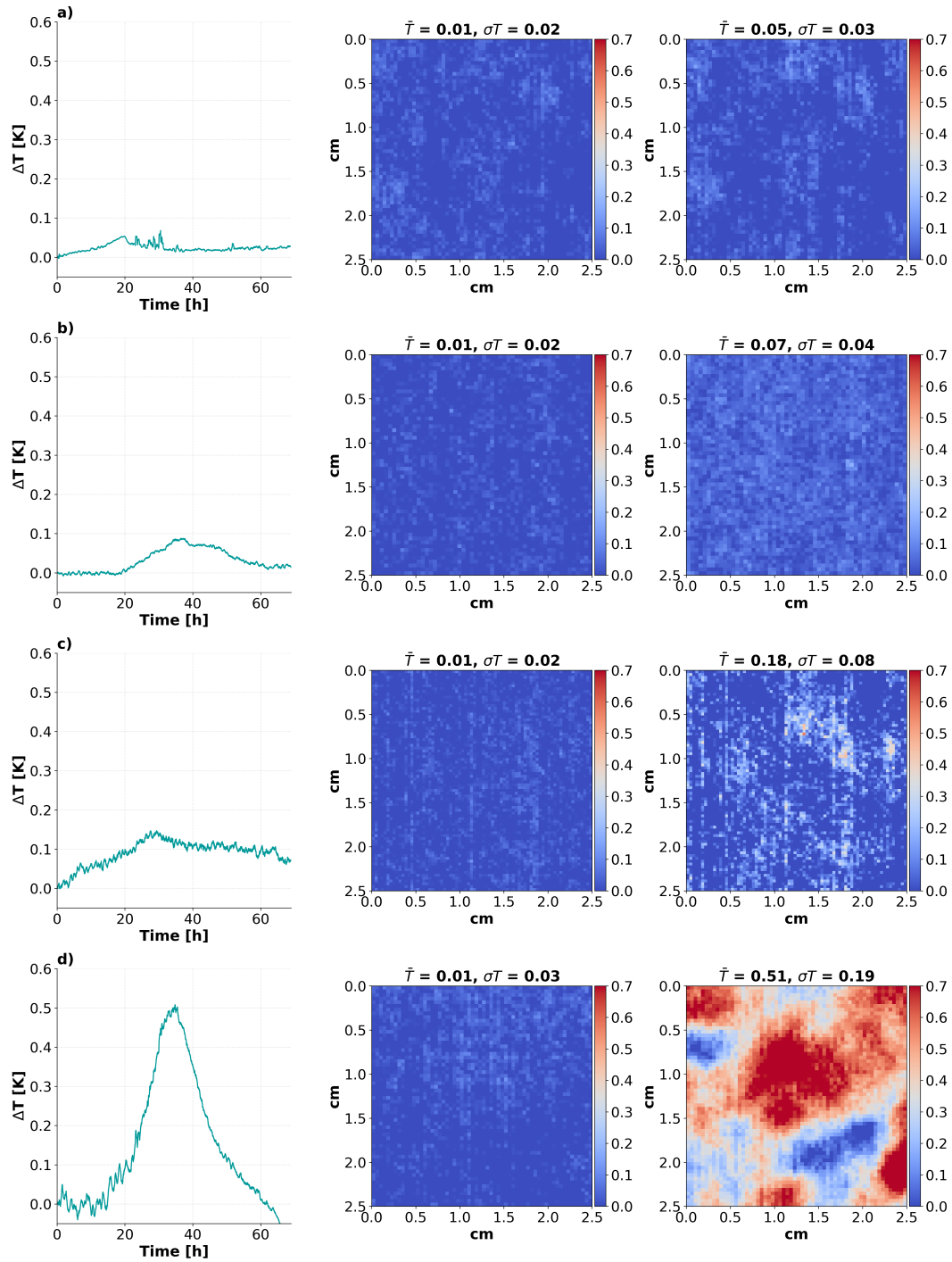
**Figure 3.3:** *Effects of air humidity control measures on soil surface temperatures of the pasture soil after glucose addition (1.68 mg cm 2). The left column shows the temporal course of ΔT [K] in the four experimental setups: polypropylene foil (PPF) (a), controlled humidity conditions (CHC) using water (b), sodium chloride (c), and potassium chloride (d). Corresponding to the experimental setups, in the middle column, the initial thermograms of each experiment and in the right column, the thermograms of the time of highest temperature increase are presented, with mean values (T) and SD (σ T) depicted above each panel.*

These results clearly showed that the ambient relative humidity is a highly important interference factor for the identification of microbial activity using passive IRT. Thus, the relative humidity should be kept constant at close to 100% to minimize soil dehydration and to be able to identify a maximum temperature effect by microbial activity on soil surfaces. Such restrictions must also be considered in other approaches for the detection of microbial activity. Looking at the example of respirometry or isothermal microcalorimetry, the samples have to be kept as evenly moist and at constant temperatures as possible (Barros et al., 2011; Herrmann et al., 2014; Vor et al., 2002).

**Air temperature**

Fig. 3.4 shows the mean temperature course of the rewetted pasture soil ($G_P$, control) in combination with the temperature course of the ambient air using the experimental setup CHC (sodium chloride). Two important factors can be observed: the daily fluctuations of the air temperature and cooling effects by evaporation processes. The air temperature in the glovebox fluctuated between 20.8 and 21.3 °C in a more or less regular 24-hour rhythm. This diurnal cycle was conveyed to the mean soil surface temperature, with a slight time lag. Thus, the surface temperature clearly reflected the ambient temperature, as already shown by Kluge et al. (2013). Therefore, small surface temperature changes are overlaid and underestimated by this effect.

The mean soil surface temperature showed a mean temperature difference of about 0.04 K to the air temperature (Fig. 3.4), which was attributed to evaporative cooling. Due to the cooling effect of the moist soil, which evaporates when the air humidity is not fully saturated, the soil surface temperature is always below the air temperature (Barreira and Almeida, 2015; Grinzato et al., 1998). Our results showed that the ambient air temperature greatly affected soil surface temperatures,

as already discussed by Schwarz et al. (2018). However, different from the effects of the relative humidity, these temperature effects can be mathematically corrected by, e.g., calculating $\Delta T$ described in the data preprocessing.
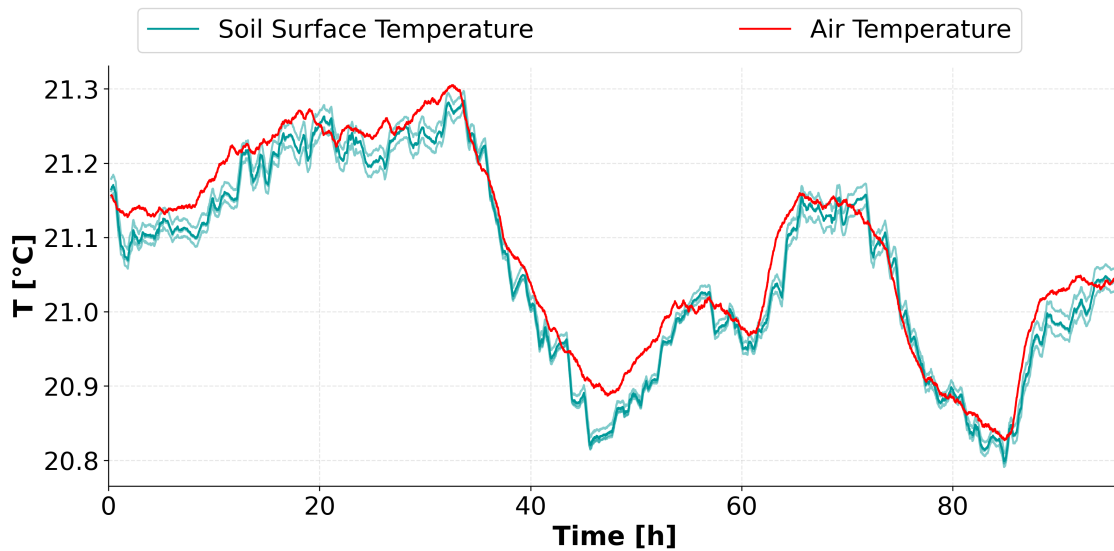


**Figure 3.4:** *Temporal course of the mean soil surface temperature [°C] of the three replicates (light green) and their mean values (bold green) and the air temperature [°C].*

### 3.3.1.4 Data processing

Fig. 3.5 shows the mean temperature courses for the raw thermal data and the time series after preprocessing procedure. The mean temperature of the treated sample was higher than that of the control sample (Fig. 3.5a). The course of $\Delta T$ showed a peak after about 20 h, which was likely caused by substrate increased microbial activity (Kluge et al., 2013). In addition, there was a second slow increase in $\Delta T$ after about 50 h. The corresponding histogram (Fig. 3.5c) shows a multimodal distribution of $\Delta T$, which is left skewed. The lowest values of $\Delta T$ were all above 0.0, indicating a general overestimation of the peak.

In general, large fluctuations caused by variations in the ambient air temperature dominated the temperature courses (Fig. 3.5a). Nevertheless, measurement

errors were found in the time series. Large outliers have to be considered, but also small effects as the scattering in the surface temperature caused, e.g., by camera noise, which was a result of the camera accuracy of $\pm$ 30mK. In Fig. 3.5a, a general increase in the surface temperature was detected, which might be a result of soil drying over time. However, slow soil drying processes could not be avoided technically. In the experimental setup CHC, high relative humidity with a maximum of 95% was achieved. Nevertheless, as far as the relative humidity is not fully saturated at 100%, soil drying processes will occur and can influence the temperature course of $\Delta T$. Soil drying results in a temperature increase, as emissivity increases with decreasing soil moisture (Axelsson, 1988). The emissivity in this study was assumed to be a constant of 0.95, which led to an apparent temperature increase. Additionally, the evaporative cooling also decreases with decreasing soil moisture (Kerridge et al., 2013; Schwarz et al., 2018), so that there is no additional cooling effect that counteracts the apparent rise in temperature. This further increases the temperature effect.

Due to possible inhomogeneous starting conditions of the samples, a temperature trend in $\Delta T$ could also occur. Still, $\Delta T$ showed a higher temperature increase in the glucose treatment over time, indicating different temporal trends between glucose treated and the control samples, probably caused by differences in soil drying. Most likely, evaporation was reduced by the relatively high glucose concentration leading to an increased osmotic potential or salinity of the soil solution (Al-Shammiri, 2002) and the associated cooling effect. Further, the mean difference of both samples was about 0.2 K (Fig. 3.5a), which can be an artifact from the pretreatment of the soil samples induced by, e.g., inhomogeneous soil rewetting before pre-incubation, but also by scattering effects induced by the camera noise or structural patterns of the soil sample. Finally, the large fluctuations caused by variations in the ambient air temperature were apparent. Although the experiments were conducted under

laboratory conditions, diurnal variations in air temperature could not be avoided completely.
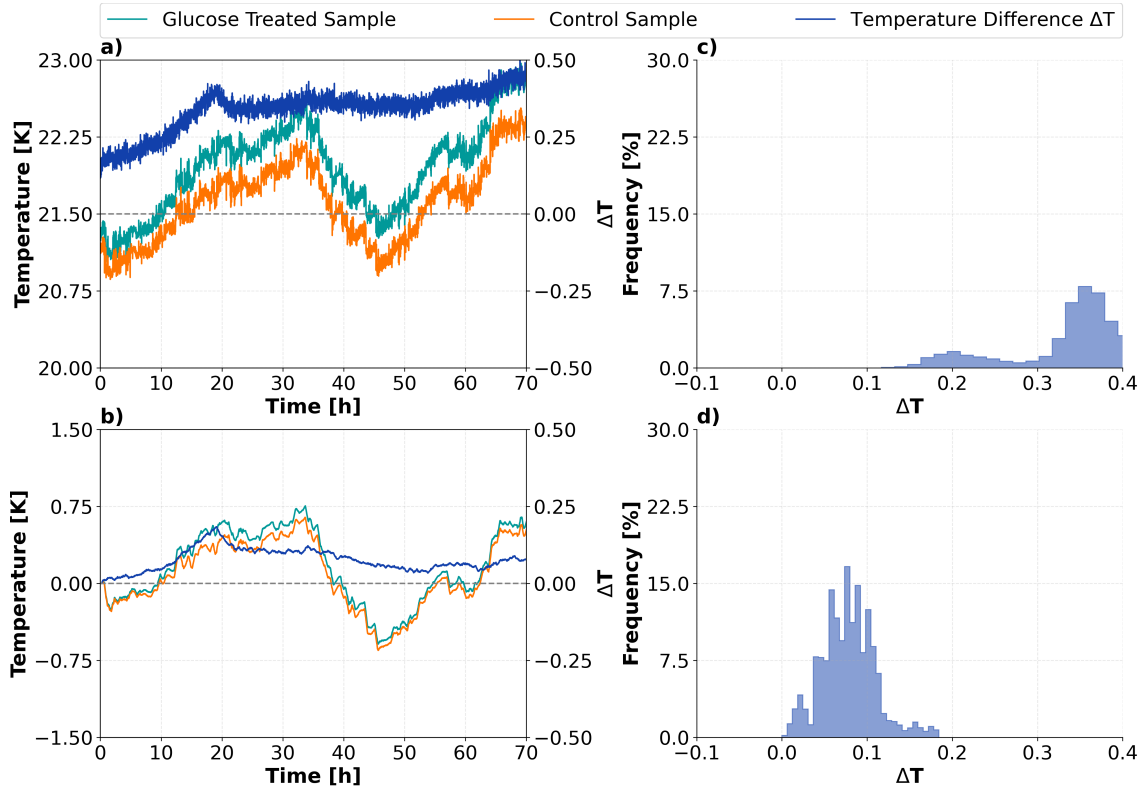


**Figure 3.5:** *In the left column, the mean surface temperature [K] at CHC of the control and the glucose (1.68 mg cm$^{-2}$) treated arable soil ($G_P$), and the corresponding $\Delta T$ are shown as raw data (a) and after mathematical preprocessing procedure (b). In the right column, the corresponding histograms of T are demonstrated (c and d).*

To avoid those errors, the data was preprocessed. As first step, outliers were corrected from the time series by using the 5% and 95% quantile to reduce major deviations due to measurement errors. Small effects, which were superimposed by the noise of the camera, were highlighted by applying a low pass filter to minimize noise as described by Grudzielanek and Cermak (2015). Temperature trends in $\Delta T$ by soil drying and changes in evaporation were corrected by a linear detrending of the time series. The shift in mean $\Delta T$ of 0.2 K was corrected by subtracting the offset of the start points from the time series.

The corrected time series of surface temperatures with $\Delta T$ after preprocessing are presented in Fig. 3.5b. The described errors were corrected as far as possible and the temperature peak of $\Delta T$ was strengthened. After this correction, even small effects caused by microbial activity were detectable using passive IRT as the external factors have been corrected for. Nevertheless, some limitations due to the processing must be considered. An offset correction is conducted to equate the start conditions and, thus, to pronounce the peak in $\Delta T$ caused by microbial activity. However, this correction may lead to a possible underestimation of the peak of $\Delta T$. The application of water and glucose solution to the soil samples and the subsequent placement under the camera was accompanied by a time offset of half an hour. Within this time, an initial glucose-induced temperature increase may already occur, which is eliminated by this correction. Variations in the temperature trends of glucose treated and untreated soil samples may also occur by differences in microbial activity and may not exclusively be a result of increasing the osmotic potential or salinity of the soil solution. The correction ignored this effect. However, with the same treatment of the soil samples and the same preprocessing of the time series, the same error can be assumed for all samples and, thus, the data were reliably prepared and can be used for comparative analysis. Finally, $\Delta T$ was adjusted through this preprocessing procedure so that temperature increases induced by glucose are pronounced (Fig. 3.5b). Thus, all following data series were subjected to this procedure. $\Delta T$ was used to focus directly on the glucose effect on the soil surface temperature. In addition, the histograms show that an approximation to a normal distribution of the data is achieved by the preprocessing (Fig. 3.5d) and, thus, the data is also better suited for further statistical analysis.

To sum up, good results can be obtained even with less strict protocols due to the effective mathematical preprocessing procedure of the raw data. The most important factor is to keep the soil moist, as it is also the case for other measuring

methods, such as for zymography (Spohn et al., 2013). This, of course, complicates the application of the technique, e.g., in field experiments, but this technique has a very high potential to map spatio-temporal changes of microbial activity and especially energy fluxes in undisturbed soils.

### 3.3.2 Respirometry incubation experiments

In order to evaluate the passive IRT measurements regarding their applicability for the detection of substrate-induced microbial activity, IRT measurements were compared to soil respiration. In Fig. 3.6, the courses of the respiration rates are plotted together with the mean $\Delta T$ ($G_M$) for the first 70 h of incubation after glucose application for both soils and with three glucose application rates. Generally, the temporal course, as well as the shape of $\Delta T$ and the soil respiration curves, are quite similar. At the lowest glucose application, the thermal signal for the pasture soil seemed to be more sensitive than the $CO_2$-detection. For the medium glucose concentrations (Fig. 3.6b & e), the respiration peaks were a few h later than those of $\Delta T$. Nevertheless, for the highest glucose concentration, the peaks were more or less overlapping (Fig. 3.6c & f). The time of the maximum peak of $\Delta T$ was similar to the results of Kluge et al. (2013), who detected a maximum temperature increase of 0.35 K after about 39 h. In addition, the authors also compared surface temperature with respiration rates. At a clearly lower respiration rate of 0.36 mg $g^{-1}$ $h^{-1}$, they were able to measure a comparably high temperature increase.

In addition, the results showed that the peak heights of $\Delta T$ and the respiration rates were related to the applied glucose concentration (see Table 3.2, Fig. 3.6). Interestingly, the thermal peak from the different glucose application rates reflected the different substrate availabilities better than the $CO_2$ peak in both soils. While doubling the glucose additions from 7 and 14 mg $g^{-1}$, peak heights for $CO_2$ increased by 23 and 10% only for the pasture and arable soil, respectively, the $\Delta T$

peak heights almost double corresponding to glucose increase (Table 3.2). Similarly, the fivefold increase in glucose application rates from 1.4 mg g$^{-1}$ to 7.0 mg g$^{-1}$ was better reflected in the peak height of $\Delta T$ than that of $CO_2$ (Table 3.2).
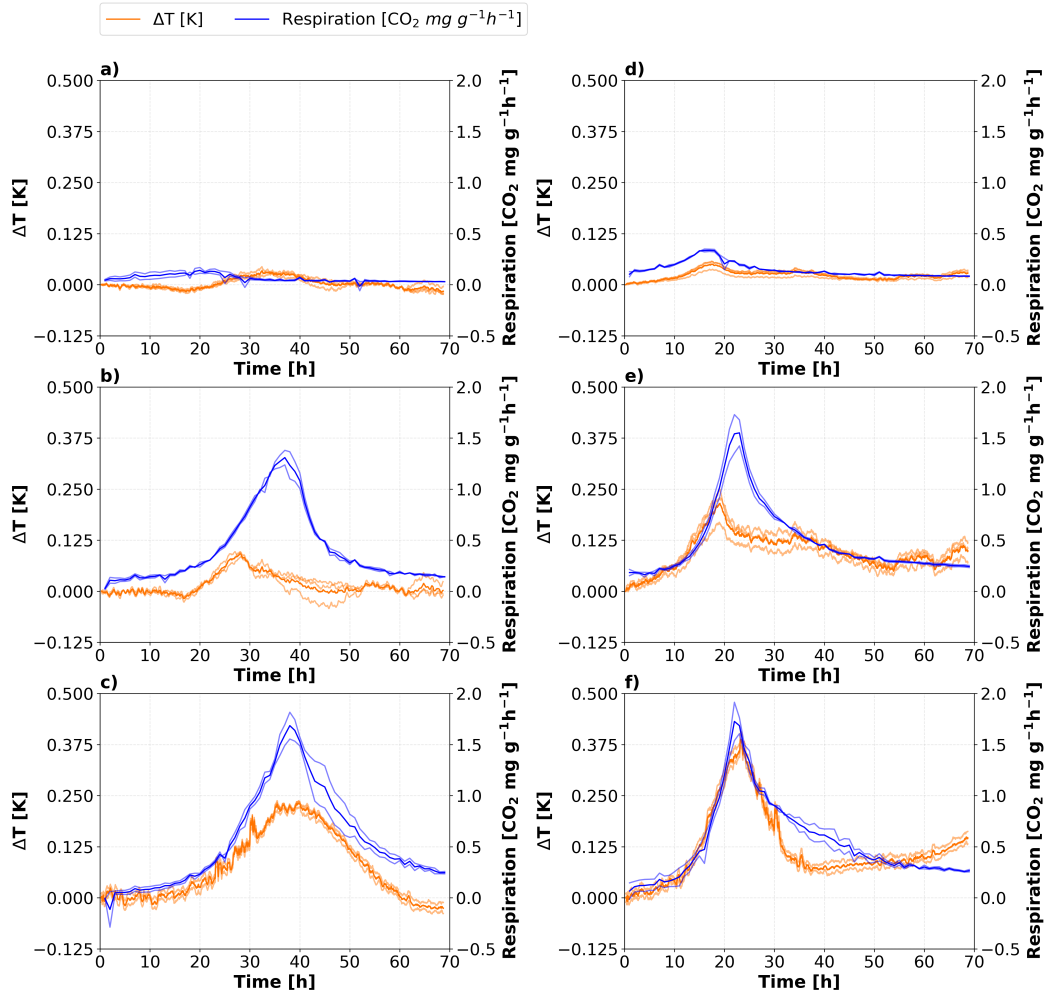


**Figure 3.6:** *Temporal course of mean $\Delta T$ [K] of the replicates (light orange) and their mean values (bold orange) at CHC and respiration rates [$CO_2$ mg g$^{-1}$ h$^{-1}$] of the replicates (light blue) and their mean values (bold blue) for pasture soil (a–c) and arable soil (d–f) for three mixed glucose concentrations ($G_M$): 1.4 mg g$^{-1}$ (a, d), 7.0 mg g$^{-1}$ (b, e), and 14 mg g$^{-1}$ (c, f).*

A direct comparison of the two different soil microbial activity parameters is possible by calculating the energy release from the soil surfaces based on the mean surface temperature (Eq. (1)) and the respiration rates (Eq. (2)). For both parameters, the energy release increased at higher glucose application rates.

When comparing the energy release between IRT and respirometry, similar values were determined for both samples (Table 3.2). For the pasture soil, the match between IRT and respirometry energy values was much better than for the arable soil, for which the calculated energy release based on $CO_2$ production was always much lower than calculated from IRT, especially at the two higher concentrations (Table 3.2). These deviations were probably a result of the different reference values. While the respirometry refers to the entire soil volume, IRT is based on the soil surfaces only. Additionally, respirometry records accumulated values over a specific time and not the actual respiration rate at a particular time, as with thermography (Kluge et al., 2013; Schwarz et al., 2018). Further, substrate utilization or $CO_2$ release might have an impact on the measured values for respirometry, since there could be a limitation within the soil matrix compared to the surface, e.g., by $O_2$ depletion in finer pores at high respiration rates or a lag in $CO_2$ diffusion from lower parts of the sample (Angert et al., 2015). In contrast, heat is conducted to the surface via soil particles (Abu-Hamdeh and Reeder, 2000; Critter et al., 2001), which is detectable for the IRT camera. However, the methodological limitations probably had a greater influence on the comparability of the data than the fact that there are chemical factors that significantly influence the system. Still, the increases in heat and $CO_2$ release occurred more or less simultaneously so that the heat flux can clearly be attributed to soil microbial activity. The linear relation- ship between glucose application and thermal energy release also showed that IRT is a sensitive and reliable method for recording microbial activity at soil surfaces (Table 3.2).

**Table 3.2:** *Peak heights of $\Delta T$ [K] and the respiration rate [$CO_2$ mg g$^{-1}$ h$^{-1}$], and corresponding cumulative energy release calculated using Eqs. (1) and (2) for both soil samples using one glucose application method ($G_M$).*

| Soil Sample | Glucose Concentration $G_M$ [mg g$^{-1}$] | Maximum Peak | | Cumulative Energy Release | |
|---|---|---|---|---|---|
| | | $\Delta T$ [K] | Soil Respiration [$CO_2$ mg g$^{-1}$ h$^{-1}$] | $\Delta T$ [J min] | Soil Respiration [J] |
| Pasture Soil | 1.4 | 0.02 | 0.16 | 37.73 | 44.59 |
| | 7.0 | 0.09 | 1.31 | 206.50 | 287.88 |
| | 14.0 | 0.24 | 1.68 | 470.12 | 395.85 |
| Arable Soil | 1.4 | 0.05 | 0.27 | 138.99 | 106.44 |
| | 7.0 | 0.23 | 1.55 | 490.93 | 346.64 |
| | 14.0 | 0.38 | 1.72 | 736.59 | 385.44 |

### 3.3.3 The potential of hot movements identification on soil surface using IRT

Previous results showed that IRT offers the opportunity for determining spatial as well as temporal dynamics of microbial activities on soil surfaces. Thus, the spatio-temporal patterns of temperature changes are evaluated in the following. Fig. 3.7 shows the spatial distribution of cumulative energy release from the surface of both soils calculated with Eq. (1). Among the four energy maps, the pasture soil with glucose surface application ($G_P$) showed the highest heat production with a mean of 1.35 kJ with a standard deviation of 0.44 kJ and a maximum of 2.73 kJ for the whole surface (Fig. 3.7a). The pattern of the five drops applied to the soil surface is clearly visible at the corners and the center on the soil surface indicated by partially higher energy releases. The drops at the corners are partly outside the image section because the edges of the sample were cut off to avoid interfering thermal effects from the margins. Due to diffusion, the droplet size had increased, so that not the whole effect can be seen at the corners. In the arable soil ($G_P$), this pattern was not recognizable (Fig. 3.7c), possibly due to a more homogeneous distribution of glucose on the surface because of the surface structure. Here, the mean energy release was 0.89 kJ and the standard deviation was 0.34 kJ, with a maximum of 1.94 kJ.

The maximum thermal energy release from the pasture soil was higher than from the arable soil ($G_P$, Fig. 3.7a and c), although the microbial biomass content and basal respiration of the pasture soil were initially much lower than that of the arable soil (Table 3.1). Apparently, microorganisms in the pasture soil utilized the added glucose to a greater extent for energy production (catabolism), indicating the presence of a microbial community that is strongly limited by substrate availability in this slightly acidic and SOC-poor soil (Blagodatskaya and Kuzyakov, 2013; Blagodatskaya and Anderson, 1998; Kuzyakov and Blagodatskaya, 2015). The arable soil

originated from an organically managed field, thus, the inherent substrate availability was potentially higher. The lower thermal response may also be due to a more efficient diffusion of glucose solution into soil domains below the surface. Glucose infiltration might also be a reason for the energy release differences since both soil samples vary in SOC content and water holding capacity. The arable soil could absorb more water due to higher SOC contents (Franzluebbers, 2002; Rawls et al., 2003). Thus, more glucose solution might remain at the surface and affect the temperature production by microorganisms.

When mixing glucose into the soil sample ($G_M$), the thermal signals of the two soils were more similar but not as homogeneously distributed as expected (Fig. 3.7b and d). Indeed, very distinct hot spots with an energy release of about 2.5 kJ min$^1$ occurred on the surface of both samples, which were very different from the mean thermal signals of 0.34 kJ min$^1$ with a standard deviation of 0.51 kJ and 0.63 kJ min$^1$ with a standard deviation of 0.45 kJ for the pasture and arable soils, respectively. Those results clearly showed that a homogeneous distribution of the glucose in the soil samples could not be achieved with our mixing procedure since the results in section 3.3.2 showed that the mean surface temperature was a reliable measure for total microbial activity.

Nevertheless, the mapped spatial patterns showed that IRT is able to detect and visualize microbial hot spots in a very strict sense. Generally, hot spots are considered to be soil volumes, which are characterized by higher mineralization rates compared to the conditions in the mean bulk soil (Kuzyakov and Blagodatskaya, 2015; Schwarz et al., 2018). With our approach, hot spots can actually be identified as areas with high thermal energy release at the soil surface (Fig. 3.7).
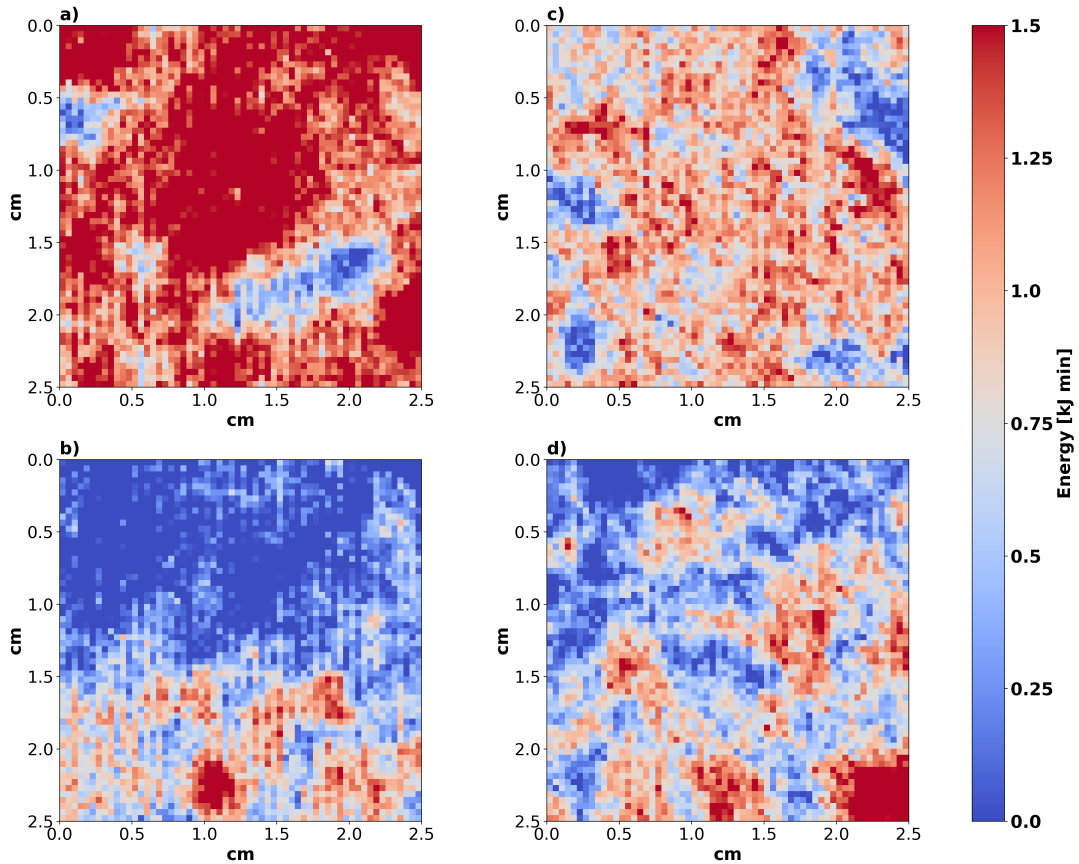
**Figure 3.7:** *Cumulative thermal energy release [J min] from the surfaces of pasture soil (a, b), and arable soil (c, d) using two glucose application methods $G_P$ (a, c), and $G_M$ (b, d) for the concentration of 1.68 mg $cm^2$ ($G_P$), and 14.0 mg $g^1$ ($G_M$) at CHC.*

In this investigation, we artificially created hot spots by glucose application that were unevenly distributed across the sample surfaces. Working with disturbed samples, no natural hot spots were expected, as the natural aggregate structure of the soil had been destroyed (Kuzyakov and Blagodatskaya, 2015; Ruamps et al., 2011). However, the results indicated that substrate-induced mineralization differences could be detected by IRT, which could therefore be applied to undisturbed soil samples, similar to the approach of Heitkötter and Marschner (2018b)), who determined hot spots of enzyme activities on undisturbed soil samples using zymography. They also showed that the distribution of the microbial hot spots drastically changed after adding substrate evenly on soil surfaces.

In addition to the spatial perspective, IRT also allows recording the temporal dimension. This temporal dimension is an important perspective for the concept of hot moments. Such hot moments are short-term events of increased mineralization rates after removing limitations by, e.g., adding substrate to soil samples (Kuzyakov and Blagodatskaya, 2015; Schwarz et al., 2018). Thus, they consider the temporal change of microbial activity in the soil. Until now, the temporal perspective was mostly considered by monitoring mean values on soil surfaces (Kluge et al., 2013) or accumulated values from a bulk soil sample, even if spatial information is available (Pausch and Kuzyakov, 2011; Spohn and Kuzyakov, 2014). In Fig. 3.7, the temporal perspective is considered as an accumulated energy release value, but the temporal dynamics are not represented here. A first approach to a spatio-temporal analysis of microbial activity can be found in the study by Schwarz et al. (2018), where a Hovmöller diagram was used to observe the change in microbial activity along a transect on the soil surface over time. However, this approach neglects much information on soil processes in the spatial domain, as it does not capture the full size of potential hot spots. So far, the spatio-temporal dynamics of microbial activity parameters could not be determined.

Here, IRT offers a unique opportunity for recording changes in microbial activity parameters spatially over time by imaging the time-lapse of $\Delta T$ for a 70 h incubation period (Video 3.8). It is interesting to see that different sized and shaped hot spots appear and disappear as hot moments at various locations and time periods.

For the pasture soil ($G_P$), a temperature increase starting after about 20 h incubation and lasting until 55 h was recorded (a). A maximum increase of up to 1.1 K occurred after 35.5 h (Video 3.8a), whereas the temporal mean values had their peak after 37 h with only 0.51 K (Fig. 3.3a). When glucose was mixed into the pasture soil ($G_M$), only a small area was characterized by heating (Video 3.8b). This began

after about 8 h incubation time and lasted comparatively long until about 60 h. In this sample, the temperature increase was primarily limited to the lower third of the surface, whereas the rest remained at the initial level.



**Figure 3.8:** *Video. [Link: http://gofile.me/4xIyV/uMDXTbcog]*
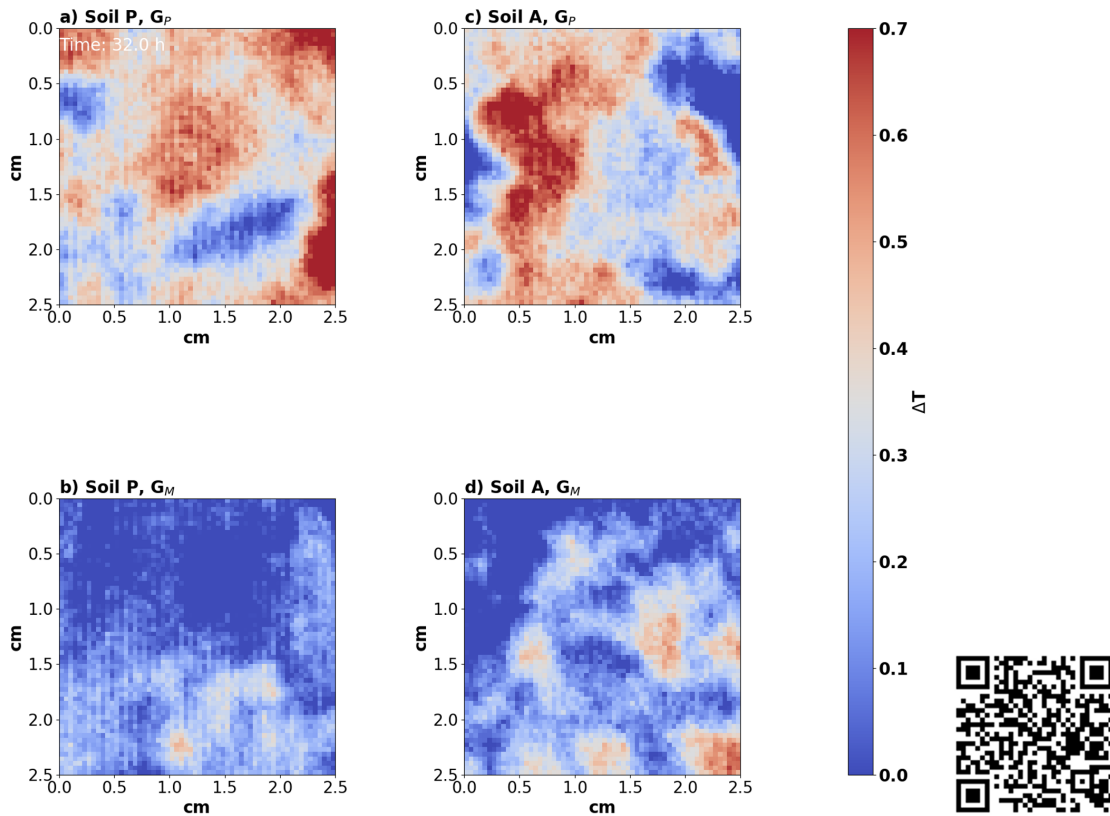
For the arable soil (Video 3.8c and d), temporal shifts in the thermal signals were also detected. When glucose was mixed into the arable soil using the $G_M$ approach, the temperature started to increase after 15 h (Video 3.8d), while for the samples using the $G_P$ approach, the initial temperature effect was detected only after 25 h. For both samples, the initial temperature level was again reached after about 50 h. Here, it can be seen that there were deviations from the time of the highest $\Delta T$ comparing mean values to the spatial values. For the arable soil $G_P$, the highest

mean temperature occurred after 19 h with a maximum increase up to 0.43 K (Fig. 3.3b), but locally the highest thermal signal of 0.9 K was recorded after 33 h (Video 3.8c). Similarly, the maximum response of mean T was reached for $G_M$ after 21 h with 0.38 K (Fig. 3.3b), but on the spatial perspective, 1.0 K was reached after 26.5 h (Video 3.8d).

In addition, there were also inhomogeneities regarding spatio-temporal temperature developments, so that the hot moments and hot spots within a sample not only differed in location but also in start and end times. They showed an apparent movement of the location characterized by higher temperatures over time. We therefore called it "hot movement". This clearly showed that neither a purely temporal nor a purely spatial view is sufficient to evaluate those dynamics. However, a combined view, e.g., time-lapses, gives the most accurate information on the temporal and spatial variability of hot spots and hot moments of microbial activity.

## 3.4 Conclusions

This study showed that after method optimization, microbial activity stimulated by glucose addition could be assessed on soil surfaces using passive IRT at a high spatial ($< 1$ mm) and temporal ($< 1$ min) resolution. Depending on the glucose application rate, the increased microbial activity produced a mean soil surface temperature increase of up to 0.5 K and an absolute soil surface temperature increase of up to 1 K per pixel at a camera accuracy of $\pm$ 30 mK.

After optimizing the methodological approach, the following factors were identified as crucial for reliable measurements with passive IRT:

- Data preprocessing procedure using data smoothing, detrending, and offset correction is highly important for the calculation of statistically significant

$\Delta T$. Thus, we recommend using a standardized data preprocessing procedure when dealing with thermal soil data.

- The intensity and duration of the thermal signal were related to the amount of applied substrate ($R^2 = 0.84$, $^*p < 0.05$). From this, we can conclude that IRT is sensitive towards varying microbial response levels.

- Homogeneous glucose application to the bulk soil results in a homogeneous distributed thermal response that corresponds well with total soil respiration rates. Thus, this procedure is only recommended when hot moments should be monitored in disturbed soil samples at high temporal resolution.

- Pipetting glucose on the soil surfaces produces artificial hot spots on soil surfaces, with significantly higher local temperature profiles. It is therefore suggested to use a homogeneous glucose lamination procedure to monitor hot spots on potentially undisturbed soil surfaces at high temporal and spatial resolution.

- For a reliable determination of microbial activity with passive IRT, relative humidity needs to be stabilized above 95%, air temperature needs to be monitored for mathematical correction, and the experimental environment should not contain any highly reflective surfaces to minimize diffuse reflectances on the soil surface.

Thus, after experimental and mathematical optimization, the detection of microbial hot spots and hot moments on soil surfaces using IRT has the potential to be non-invasive as well as contact-free approach. Additionally, the high temporal and spatial resolution makes this approach highly attractive, since this enables the simultaneous study of hot spots and hot moments in so-called "hot movements".

Nevertheless, many boundary conditions need to be controlled for obtaining accurate results. Considering the fact that established laboratory methods, which deal with the detection of microbial activity, have similar restrictions, a general application of IRT to detect microbial activity is conceivable. In our current studies, the spatio-temporal variability of microbial activity in undisturbed samples taken from different vertical profiles is investigated. Glucose is applied uniformly to the soil sample surface to avoid artificial hot spots. This allows equal conditions on the entire soil surface as a prerequisite for detecting hot movements.

With the help of such extensions of the measurement setup, the rhizosphere could also be examined more closely. As known, microbial activity increases in the rhizosphere in the proximity of dead or living roots. Hot spots of those strongly depend on carbon inputs such as rhizodeposits and root detritus (Spohn and Kuzyakov, 2014). Since we were able to measure increased microbial activity and changes over time using an IRT-camera, it strongly suggests that even diurnal variations in activity and root exudation can be detected. This would enhance our understanding of the controls and dynamics of soil microbial processes at the millimeter to centimeter scale.

Furthermore, our IRT approach offers the possibility to record energy fluxes at soil-atmosphere interfaces at high temporal and spatial resolution and relating this to soil microstructures and associated interactions of living and non-living soil components on a process level or regarding carbon and energy use efficiency. Since microbial activity is linked to thermodynamic soil processes, IRT can contribute to a more systematic understanding of microbially induced energy fluxes from a high spatial and temporal perspective.

# 4   Research Study III

**High-resolution mapping of surface heat evolution combined with other imaging approaches for analyzing spatial heterogeneity and temporal dynamics of microbial hot spots and hot moments in undisturbed soil samples**

Co-Authors: Theresa Reinersmann, Jannis Heil, Bernd Marschner, Britta Stumpe

Submitted to Geoderma on 26.06.2021
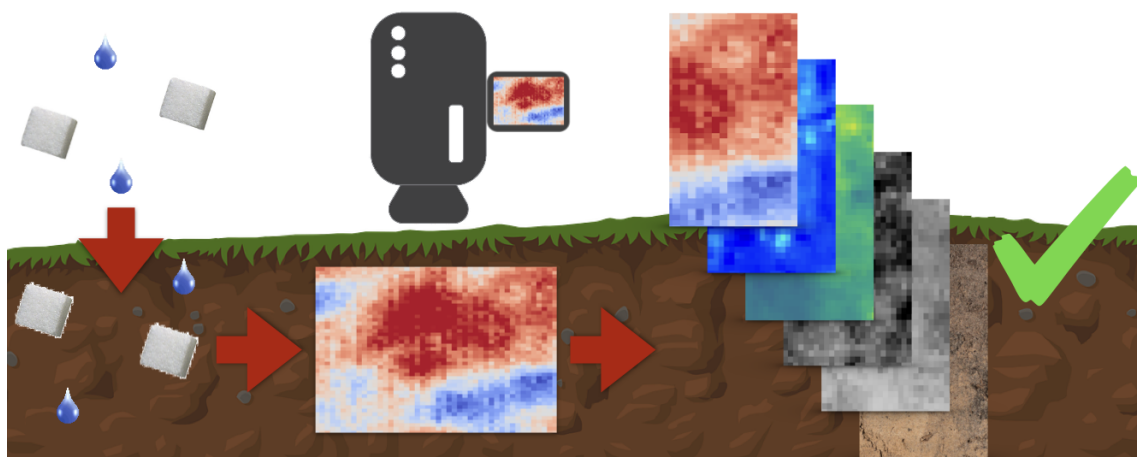
## 4.1   Introduction

Soil microbial activity is one of the major drivers for metabolization processes and the carbon (C) cycle in the pedosphere (Bölscher et al., 2016; Schimel and Schaeffer, 2012). Thereby, organic matter is converted into other forms of energy by using the energy in organic compounds. The metabolic energy generated by energy-dense organic matter degradation processes is accompanied by a corresponding heat release from the soil surface (Chakrawal et al., 2020; Drotz et al., 2010; Liang et al., 2017). Thus, thermodynamic processes by metabolic activity in soils were researched intensively in the past decades (Barros et al., 2007; Critter et al., 2001; Ljungholm et al., 1979; Sparling, 1981). Until now, the systemic understanding of catabolic heat production and soil functional microbial diversity is missing. The technical challenges in analyzing metabolization processes in their spatial and temporal complexity and dynamic, especially in undisturbed soil samples, were not untangled so far.

However, considering undisturbed soil samples in their natural complexity, it comes to light that the soil matrix is highly structured and a complex growth medium for microorganisms. Thus, soil microbial activity cannot be found homogeneously distributed in the soil matrix, but in distinct hot spots which are characterized by high concentrations of microorganisms in regions of high substrate availability (Heitkötter and Marschner, 2018a; Kuzyakov and Blagodatskaya, 2015; Nunan et al., 2003).

While hot spots exhibit elevated process and microbial activities, especially temporally in hot moments, on the microscale, there is considerable variation in the microbial structure (Kuzyakov and Blagodatskaya, 2015; Nunan et al., 2003). Capturing microbial hot spots and hot moments has become an increasing focus with innovative techniques since microbial activity is subject to large dynamics and is not evenly distributed in the soil (Heitkötter and Marschner, 2018a; Kuzyakov and

Blagodatskaya, 2015; Schwarz et al., 2021). In particular, the detection of these in temporal and spatial perspectives is with conventional measurement techniques, such as calorimetry, only strongly limited possible since these techniques refer to bulk soil samples. Here, the measured heat release from soil surface cannot be associated with distinct hot spots (Kluge et al., 2013; Kuzyakov and Blagodatskaya, 2015; Sparling, 1981). Soil heat production measurements as a proxy for soil microbial activity have gained increasing attention as there is the possibility to determine the energy conversions in the soil matrix (Chakrawal et al., 2020).

Passive infrared thermography (IRT) has proved its usefulness as a measurement technique for mapping spatio-temporal dynamics of microbial activity in hot spots and hot moments since heat evolves through metabolic processes, which is detectable in substrate-induced approaches (Kluge et al., 2013; Schwarz et al., 2021). Passive IRT enables the high-resolution detection of heat development in soils at a spatial resolution of $< 1$ mm and a temporal resolution of $< 1$ min. (Schwarz et al., 2021, 2018). In recent studies, the passive IRT approach was developed considering the influences of the ambient conditions (Schwarz et al., 2021), but also including internal effects by soil physical properties (Schwarz et al., 2018). Both the spatial and temporal patterns of hot spots and hot moments have not been elucidated and described in detail, although these are linked to structural and functional microbial diversity, heat flux, and the spatial distribution of soil organic carbon (SOC). While passive IRT is now revised in the context of soil investigations to detect microbial activity, there is still a lack of knowledge on how to interpret the measured surface temperature to contextualize it in catabolic heat production. This knowledge gap can be filled in combination with other mapping techniques.

A variety of technical approaches allow for the combination of temporal and spatial information regarding soil microbiological properties that can fill this knowl-

edge gap, especially in undisturbed soil samples on the mm-scale. In this context, techniques such as photography or zymography are promising mapping tools to map spatial soil properties (Heil et al., 2020; Heitkötter and Marschner, 2018a,b).

Photography has been successfully applied to map surface color parameters and link them to SOC and further soil properties like iron or soil moisture (Heil et al., 2020; Viscarra Rossel et al., 2008; Zanetti et al., 2015). Heil et al. (2020) showed that using the color space CIELa$^*$b$^*$, SOC could be reliably predicted with an R$^2$ of 0.94 using a multiple linear regression model in dependence on soil treatment. Since SOC contents are linked to the availability of easily degradable substrates for microorganisms, higher basal microbial activity is expected in regions of high SOC contents (Anderson, 2003). Thus, fundamental changes in temperature due to varying microbial activity could be predicted via the content of SOC. Therefore, soil color parameters should be considered for spatial characterization of undisturbed soil samples with an inhomogeneous SOC distribution.

Soil zymography is an established mapping tool for spatial soil microbial activity parameters under consideration of a variety of soil enzymes, e.g., $\beta$-glucosidase, acid phosphatase, or chitinase (Heitkötter and Marschner, 2018a,b; Spohn et al., 2013). Since heat development is connected to C turnover in soils (Barros et al., 2016; Critter et al., 1994), mapping $\beta$-glucosidase enables the spatial validation from a microbiological perspective because it offers the opportunity to record the activated enzymes by the turnover of C in the soil (Heitkötter et al., 2017; Zhang et al., 2020). Thus, this technique is promising as a validation of passive IRT in the sense that differences in the turnover of C can be detected on soil surfaces, which also release heat during catabolic processes (Chakrawal et al., 2020; Heitkötter and Marschner, 2018a; Zhang et al., 2020).

Further, active IRT was also applied for mapping soil surface moisture contents in different development approaches (Antonucci et al., 2011; Axelsson, 1988; Schwarz et al., 2018) but was also used for surface structure detection by Schwarz et al. (2018). As moisture changes the specific heat capacity of soil material, active heating of moist samples enables the detection of relative differences in the distribution of soil moisture contents. Schwarz et al. (2018) had shown that volumetric water contents could be explained up to 88% using active IRT. Since soil moisture determines the heat production by microbial activity (Baldrian et al., 2010; Barros et al., 1995), the spatial distribution of soil moisture needs to be considered for the further analysis of soil surface heat production.

To our knowledge, no published studies are combining such technical approaches for deeper insights into the metabolic characterization of microbial hot spots. Thus, this study aims to explain the surface heat production on undisturbed soil sample surface measured by passive IRT in a sequential recording. On the one hand, the results should show the possibilities of spatio-temporal intersection of soil property data sets. On the other hand, they should contribute to a deeper understanding of microbial heat generation.

Thus, we investigated the potential of spatial surface soil property mapping under consideration of zymography, photography, but also passive and active IRT to determine spatio-temporal microbial activity patterns and get further deeper insights into the connection between surface soil properties and heat development. For this, glucose and water treated undisturbed sub- and topsoil samples were used to cover the microbial diversity in soils. In addition, we treated the soil samples as homogeneously as possible, especially when glucose was applied, to create equal soil conditions to avoid distinct artificial hot spots. As Schwarz et al. (2021), the experiments were conducted in a stable ambient environment to avoid interfering signals during the thermal acquisition of the soil surface temperatures.

In the first part of the study, the temporal and spatial patterns of heat development on soil surfaces after evenly glucose application concerning substrate-induced stimulation of microorganisms are spatially and temporally characterized regarding hot spots and hot moments. The temporal characteristics of the hot moments are first worked out mathematically. On this basis, the spatial dependencies are analyzed using geostatistical methods. The second part of the study focuses on the spatial surface soil properties mapping techniques superimposed on the thermal passive IRT images. For this purpose, active IRT, photography and zymography were used to determine soil moisture contents, surface color parameters as proxy for SOC contents, and initial $\beta$-glucosidase activity, respectively. Multiple regression analyses were applied to find explanatory variables of the heat development on undisturbed soil surfaces. Since regression analyses were not able not handle the temporal variability of temperature evolution, in a third part hierarchical k-means cluster analyses were used. These analyses based on the sequential thermal images referring to the hot moments in order to highlight spatio-temporal heat development characteristics on the soil sample surfaces. The clustered thermograms, in combination with the corresponding surface properties, namely active IRT images, surface color parameters, and initial $\beta$-glucosidase activity, were statistically analyzed to establish contextual references to each other.

## 4.2 Material and methods

### 4.2.1 Soil sampling

For this study, two pairs of undisturbed top- and subsoil samples were collected from two forest sites in Germany from the depths listed in Table 4.1. One pair was taken from the "Grinderwald" beech forest near Hannover (Lower Saxony, Germany). This site is part of a long-term monitoring program within the SUBSOM research unit

(Heinze et al., 2018) and characterized by a Dystric Cambisol (WRB) from quaternary glacial till which is sandy with some loamy bands. The other pair was taken from the "Kalwes" beech forest in Bochum (North-Rhine Westphalia, Germany) stocks on a Dystric Luvisol (WRB) from quaternary loess with a very homogeneous loamy texture in the top 50 cm. A custom-made steel box with sharpened edges (127.76 × 85.48 mm) was pressed into the soil matrix and carefully removed for obtaining vertical raw undisturbed samples for sample collection. After collection, the samples were wrapped in cling film to prevent drying and stored at -20 °C for about four weeks.

### 4.2.2 Analytical techniques

#### 4.2.2.1 Determination of microbial activity using passive IRT

Passive IRT was used to get spatial information about thermal soil surface properties that are highly associated with substrate-induced microbial activity, as described by Schwarz et al. (2018). Briefly, a high definition IRT camera (Variocam HD research, InfraTec, Dresden, Germany) with an image resolution of 1024 × 768 pixels was used to obtain thermal images of the undisturbed soil surfaces. The camera distance to the soil sample surfaces was set to 30 cm, resulting in a pixel resolution of 0.17 mm. The IRT camera detected the spectral range in the far infrared of 7-14 $\mu$m with a temperature accuracy of $\pm$ 30 mK. In all experimental designs, an overall emissivity of 0.95 [-] was assumed for the soil surfaces (Kluge et al., 2013; Schwarz et al., 2021, 2018).

Passive IRT detects the outgoing long-wave radiation from soil surfaces in a temporal resolution of up to 60 Hz. Thus, using substrate-induced respiration techniques, temporal and spatial temperature changes can be attributed to microbial hot spots and hot moments, as described by Schwarz et al. (2021).

**Table 4.1:** *Characteristics of the sampling sites and the soil samples used for the incubation experiments.*

| Sampling site | Soil type | Texture | Vegetation | Depth | | | Name | pH | SOC | Bulk density | Water content | Water loss |
|---|---|---|---|---|---|---|---|---|---|---|---|---|
| | | | | | | | | | % | g m$^{-3}$ | % | % |
| Grinderwald | Dystric | Loam | Fagus | Topsoil ($T$) | 10 - 23 cm | | G$_T$ | 3.5 | 1.2 | 1.18 | 13.59 | -11.96 |
| (G) | Cambisol | Sand | Sylvatica L. | Subsoil ($S$) | 30 - 43 cm | | G$_S$ | 4.2 | 0.2 | 1.24 | 22.57 | -18.41 |
| Kalwes | Luvisol | Silt | Luzulo- | Topsoil ($T$) | 13 - 26 cm | | K$_T$ | 3.4 | 1.3 | 1.23 | 10.25 | -9.30 |
| (K) | | | Fagetum | Subsoil ($S$) | 35 - 48 cm | | K$_S$ | 3.7 | 0.4 | 1.35 | 27.01 | -21.27 |

The passive IRT images were preprocessed according to Schwarz et al. (2021), where a sequence of mathematical correction methods was applied. First, a low-pass filter was used to reduce the scatter of the data originating from the camera's noise. A detrending of the time series was then made to remove any temperature increases resulting from the drying of the soil surface. Finally, an offset correction was applied to standardize the starting points of the time series.

### 4.2.2.2 Determination of soil surface moisture and structure using active IRT

Active IRT techniques were used to detect soil surface moisture content and soil surface structure, according to Schwarz et al. (2018). A halogen spotlight (1,500 W) was used as an external heat source to induce a clear thermal contrast on the object surfaces. The spotlight was placed at a distance of 30 cm from the object surface, and active IRT was conducted in lock-in mode. The halogen spotlight was illuminated with a lock-in frequency of 0.5 Hz and a 30 Hz frame rate. The thermal response of the soil surfaces was recorded during the heating and transient cooling phase.

Active IRT uses the measured temperature profile of the heating and cooling phase to obtain the temperature amplitudes and phase angles (Ranjit et al., 2015; Schwarz et al., 2018). The temperature amplitude refers to soil moisture contents since the specific heat capacity of soil samples is determined by water contents. A high temperature amplitude indicates dry soil and, due to the buffering of water, a low temperature amplitude indicates moist soil (Schwarz et al., 2018). The phase angle approximates the surface structure. Due to the change in the reaction rate with different soil properties, statements can be made about the density, roughness of the surface or cavities. High variances in the phase image indicate high structural differences in the surfaces or bulk density (Bristow, 1998; Schwarz et al., 2018; Usamentiaga et al., 2014). Further information is given by Schwarz et al. (2018).

### 4.2.2.3   Determination of surface $\beta$-glucosidase using zymography

For obtaining an additional spatially resolved microbial activity parameter from the soil sample surface, the activity of the enzyme *beta*-glucosidase was using soil zymography according to Spohn and Kuzyakov (2014), and Heitkötter and Marschner (2018a). Briefly, polyamide membranes (Sartorius Stedim, Göttingen, Germany) were soaked in a 12 mM fluorescent 4-Methylumbelliferyl-$\beta$-D-Glucopyranoside (MUF) solution, which were placed on 1 mm thick agarose gels (1% agarose) and incubated for 1 h at 25°C on top of the soil samples. After incubation, photographs of the now fluorescent membranes were taken in a gel documentation system (Biostep GmbH, Burkhardtsdorf, Germany) under epi-UV lighting at 365 nm using a Canon EOS-700D with an image resolution of 2592 × 1728 pixels. The camera was fitted with a fixed focal lens ($f/1.8$) and a 420 nm filter. To gather information on autofluorescence, 1 mm thick agarose gel on a steel plate was covered with a MUF soaked membrane and further treated matching to the soil samples and their respective membranes.

Image processing was done similar to Heitkötter and Marschner (2018a), with georeferencing, subtraction of autofluorescence, reducing image noise via a Gaussian blur algorithm, and pixelwise conversion of gray values to enzyme activities with the help of a calibration line. The $\beta$-glucosidase activity values were extracted from the enzyme images using Fiji ImageJ, as described by Heitkötter and Marschner (2018a) and Schindelin et al. (2012).

### 4.2.2.4   SOC distribution accessed using surface color parameters

To have an indicator for the spatial distribution of SOC on the undisturbed soil surfaces, RGB information gained by digital photographs had been used accordingly to Heil et al. (2020). A Canon EOS 5DS digital single-lens reflex (DSLR) camera

(Canon Inc., Tokyo, Japan) with a pixel resolution of 8688 × 5792 pixels equipped with a Canon EF 50 mm $f$/1.8 STM (Canon Inc.) prime lens was used. The camera setup, lighting, and data handling were adopted from Heil et al. (2020). For the photographs, moist soil samples were used so that the contrasts would be prominent for further evaluating the surface properties. The RGB colors are extracted from the photographs and transferred to CieLa*b* color space using the custom function by Heil et al. (2020) based on the equation given in Viscarra Rossel et al. (2006). Heil et al. (2020) already showed that SOC can be predicted very well using the CieLa*b* color space. The achromatic vector L showed the highest correlation to SOC, and using multiple regression analysis, also good predictions of SOC contents were obtained combining L, a*, and b* values. Therefore, all three raw color values were used in this study to get an approximation of the surface SOC contents.

### 4.2.3 Soil sample incubation setup and procedure

The soil samples were taken from the freezer for each series of incubation experiments. The samples were thawed for five days, still wrapped in cling film to avoid soil drying. Immediately before the experiments started, the samples were removed from the cling film, and the excess soil extending over the steel box's edges was carefully cut off with a spatula, resulting in a fresh flat undisturbed sample surface.

After soil preparation, $\beta$-glucosidase activity was determined by zymography using the procedure described in section 4.2.2.3. After zymography, the fresh weight of the sample was recorded with a conventional balance as an approximation to soil moisture contents.

Following this, the entire surface was sprayed with water (5 $\mu$l cm$^{-2}$) to increase soil moisture homogeneously. Then, one vertical half of the sample surface

was sprayed with 5 $\mu$l cm$^{-2}$ glucose solution at 140 $\mu$g C cm$^{-2}$ (Heitkötter and Marschner, 2018a) to encourage substrate induced microbial activity increase. As a control, the same amount of water (5 $\mu$l cm$^{-2}$) was applied to the other vertical side of the soil sample. The control and the glucose solution were applied with a spray system (iMatrix Spray instrument, tardo GmbH, Subingen, Switzerland) for the uniform application of liquids (Stoeckli et al., 2014).

Then, the undisturbed soil samples were passed to active IRT imaging, which was used to get the initial moisture of the undisturbed soil surface as described in section 4.2.2.2. For this purpose, the samples were then placed in styrofoam box, which is integrated into the IRT measurement setup used for active and passive IRT.

Immediately after active IRT imaging, soil surface temperature monitoring with IRT started and continued for 5 days at a temporal resolution of 10 min, as described in section 4.2.2.1 so that about 720 recordings of each soil sample were made. For the passive IRT approach, the styrofoam box was closed, and a thermally insulated room was created at a constant ambient temperature of 21 °C and 85% relative humidity during soil incubation, according to Schwarz et al. (2021) since passive IRT is sensitive to ambient environmental condition changes (Schwarz et al., 2021, 2018). The box had a precisely fitting recess for the camera lens on the top to create a closed climatic system. The temperature and relative humidity inside the box were continuously recorded using wireless data loggers (M-Log5W-HUMIDITY, Geoprecision, Ettlingen, Germany). During thermal imaging, the styrofoam box was not opened to maintain an undisturbed system so that the surface temperatures of the soil samples would be as unaffected as possible.

Directly after incubation, samples were weighed again to record water loss and then left to air-dry for dry weight determination.

As a last step, digital photographs were taken according to the setup described in section 4.2.2.4. For this purpose, the air-dried undisturbed samples were uniformly rewetted using the spray system (iMatrix Spray) for a uniform application of 30 $\mu$L cm$^{-2}$ of water to increase the color contrast for a more accurate evaluation of the surface properties.
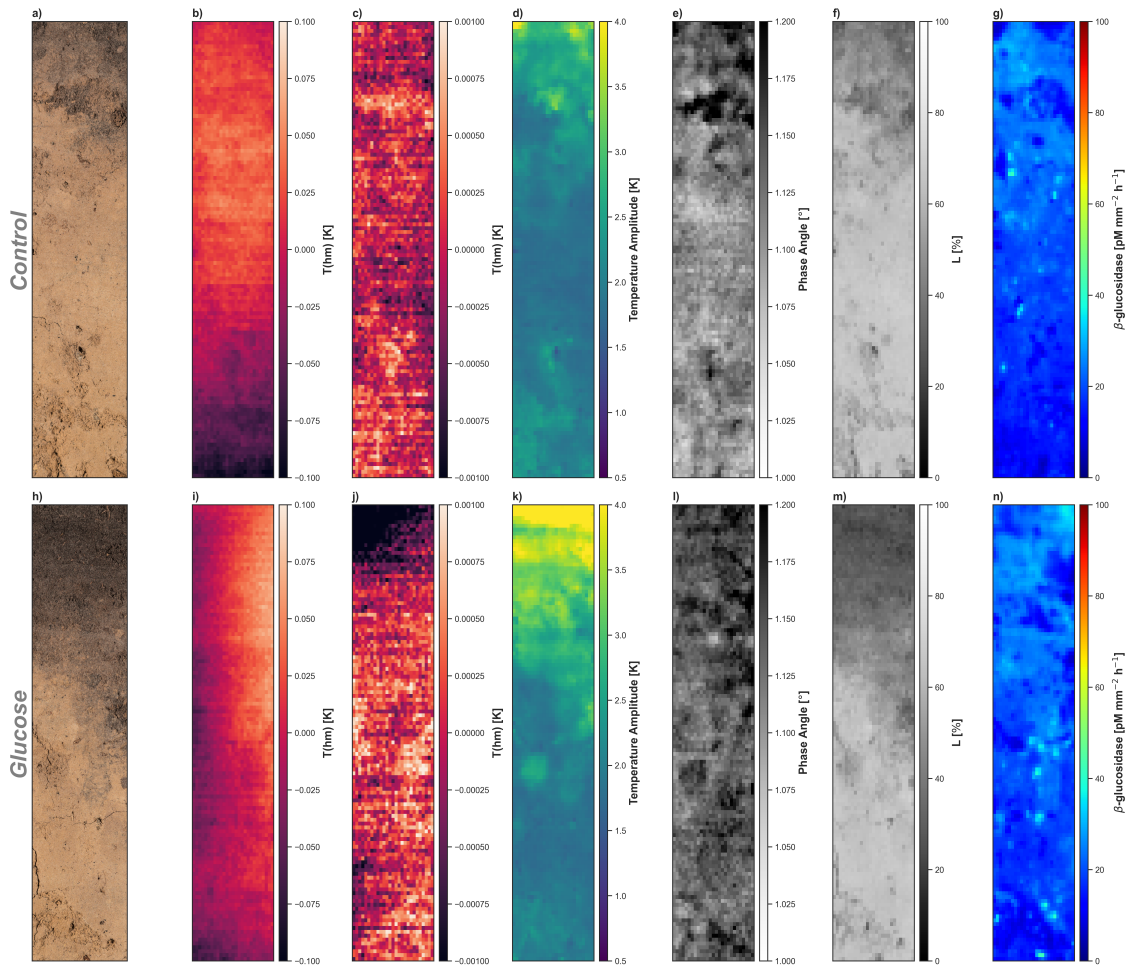


**Figure 4.1:** *Spatial characteristics of surface soil properties for soil sample $K_T$ considering RGB image (a, and h), $T(hm)$ (b, and i), pixelwise variance of $T$ referring to the hot moment (c, and j), temperature amplitude (d, and k), phase angle (e, and l), surface color parameter L (f and m), as well as initial $\beta$-glucosidase activity (g and n) with control samples in the upper row and glucose-treated samples in the lower row.*

### 4.2.4   Georeferencing and scaling of the data

All spatial data sets have to be superimposed and spatially adjusted by moving the sample from the gel documentation system during zymography into the closed IRT system; there was a displacement of the sample in the images. For this purpose, the georeferencing tool of QGIS (Version 3.16 Hannover, 2020 QGIS Development Team) was used. Zymography and surface color parameter images were placed on top of the IRT images since passive and active IRT were recorded without moving the sample, and thus, these images are an optimal database. Fixed points in the database were searched for, such as the corner points of the steel box. The entire images were scaled and rotated according to the database automatically based on the selected points. Afterwards, all soil surface images were cut out in longitudinal cross-sections separately for water application and glucose application to get distinct data sets. All further analyzes of the data were performed using Python 3.8.

The preprocessed thermal images were then reduced by a factor of 25 from a resolution of $590 \times 136$ pixels to $118 \times 27$ pixels in order to reduce the two-dimensional image noise resulting from the camera accuracy, but also to facilitate the following calculations. At a $25\times$ reduction, the image noise was corrected visually satisfactorily, and the duration of the calculations using Python were reduced sufficiently. The downscaling was done using weighted averages of the values to be scaled ($Y_{scale}$) from the raw thermal image size to the new thermal image grid, calculated in the following equation based on Odgers et al. (2012):

$$Y_{scale} = \frac{1}{n} \sum_{i,j=1}^{n} w_{i,j} Y_{i,j} \tag{4.1}$$

$Y_{(i,j)}$ is the given value and $w_{(i,j)}$ the areal proportion of each pixel of values to be scaled to the passive IRT grid. $n$ is the number of pixels that lie within one

IRT pixel. The calculation is performed for each pixel of the IRT grid.

After all data had been collected, there was a variety of spatial datasets. $\beta$-glucosidase activity and CIELa*b* images had a different spatial resolution than passive and active IRT images. The spatial resolution of the $\beta$-glucosidase activity images ($1101 \times 241$ pixels) as well as L, a*, and b* images ($4248 \times 992$ pixels) were also larger than the new IRT grid of $118 \times 27$ pixels. Thus, they were downscaled using equation 4.1.

The scaled data sets of all measurement techniques are shown as an example for the Kalwes soil in Fig. 4.1.

### 4.2.5 Mathematical quantification and delineation of hot moments and hot spots

#### 4.2.5.1 Temporal delimitations characterization of hot moments

To delineate the start and endpoint of the glucose-induced increases in surface temperature dynamics (hot moments), the thermal time series of each undisturbed surface was subjected to a series of mathematical extraction steps. First, the temperature differences ($\Delta T$) of the time series of the surface temperature ($T$) of glucose-treated and water-treated samples were calculated, according to Schwarz et al. (2021). These difference curves can be used to determine the intensity of the temperature increase because of glucose induced increased microbial activity.

For a detailed hot moment characterization, the exact start and endpoints of increased surface temperature induced by microbial activity were captured. Therefore, the second derivative of $\Delta T$ was determined. For this, a curve fitting of $\Delta T$ must first be made. The following Gaussian function was used as the best approximation

of the course of $\Delta T$, where $\boldsymbol{\mu}$ is the mean and $\sigma^2$ the variance of the time series:

$$\varphi_{\boldsymbol{\mu},\sigma}(x) = \frac{1}{\sqrt{2\pi\sigma^2}} \times e^{-\frac{(x-\boldsymbol{\mu})^2}{2\sigma^2}} \tag{4.2}$$

From these fitted functions, the second derivatives were calculated, since it describes the turning points of the first derivative as local maxima. Before and after the peak, these local maxima describe the start and endpoints of the hot moment. These time points were used to characterize the temporal component of increased microbial activity from glucose application. When $\Delta T$ is greatest, this point is also determined as the time of maximum microbial activity. Based on the pixelwise calculation of these temporal parameters, the means and standard deviations of the time points and the entire period were calculated to characterize the soil samples with respect to their glucose-induced temporal variations in surface temperature.

### 4.2.5.2   Spatial relationship and characterization of hot spots

To characterize the hot spot distribution during the hot moment period, the mean temperature values referring to the hot moment $(T(hm))$ were calculated for each pixel of the thermal data grid. These thermograms have been calculated for each undisturbed soil sample separately for the spatial glucose and water application.

Geostatistical analyzes were performed to describe the spatial relationships of surface temperature development regarding the inner pixel distance (Nunan et al., 2003). The semivariance was calculated for mean $T(hm)$ using the Gaussian model due to the minor prediction error when used to analyze soil properties (Obroślak and Dorozhynskyy, 2017; Slaets et al., 2021). With the calculation of the semivariance,

spatial correlations of the measured values over the distance can be described via the sill, range, and nugget effect. They give information about the total variability in the dataset (sill), the average distance over which a variable is spatially auto-correlated (range), and the irregular distribution of values at very small distances (nugget effect) (Boeddinghaus et al., 2015; Grundmann and Debouzie, 2000; Nunan et al., 2003).

### 4.2.6 Analysis of soil surface temperature and further soil properties

#### 4.2.6.1 Relating soil properties pixelwise to surface temperature

For finding explanatory variables for the surface temperature development of the hot moments, stepwise forward regression analyzes were performed with the mean $T(hm)$ as the dependent variable. Pixelwise information gained from the active IRT (temperature amplitude, and phase angle), zymography ($\beta$-glucosidase activity), photography (surface color parameters L, a*, and b*) were used as independent variables. All parameters were standardized with a mean 0 and variance 1 for obtaining standardized $\beta$-coefficients. This approach was applied to each glucose-treated soil sample separately (4), and to all glucose-treated samples (1), resulting in 5 regression equations. For each regression analysis, the $R^2$ is determined as the quality parameter of the prediction.

#### 4.2.6.2 Cluster analysis of hot moments and hot spots

As a last step, for a more detailed analysis of the spatio-temporal temperature dynamic, a cluster analysis was performed for dividing the data set into groups of similar thermal characteristics. The k-means algorithm was used as one of the most commonly used methods for complex data sets (Altdorff and Dietrich, 2012; Heil et al., 2019). For this purpose, the temperature curves T referring to the hot

moment ($\Delta T(hm)$) were used. The type of hot spot is determined, which is characterized by the temperature course.

Initially, the Shapiro Wilk and Levene tests confirmed the residual normality and the homogeneity of variance between treatments (Heitkötter and Marschner, 2018b; Herrmann et al., 2014; Zhang et al., 2017). Therefore, $T(hm)$ was standardized with a mean 0 and variance 1 (Ye and Wright, 2010), and the hierarchical k-means cluster analysis was then performed to compare the soil microbiological attributes in glucose-treated samples. In order to find the optimal number of clusters, the partition coefficient ($C_P$) and the partition entropy ($E_P$) were used (Heil et al., 2019; Martz et al., 2019). The number of clusters reaches its optimum when $E_P$ is maximized, representing the maximum variance within one class, and $C_P$ is minimized, referring to the minimum variance in between the cluster groups (Heil et al., 2019; Viscarra Rossel et al., 2016).

The cluster groups of the thermal data were spatially assigned to the further data sets of active thermography (temperature amplitude and phase angle), zymography ($\beta$-glucosidase activity), and photography (surface color parameters L, a*, and b*) to verify whether the thermally differentiated clusters also differed significantly in their parameters. For this purpose, an ANOVA was calculated between the cluster groups within each data set, followed by Tukey's HSD test (Bölscher et al., 2017; McDowell et al., 2006). In this way, the individual cluster groups are characterized in terms of their soil properties.

## 4.3 Results and discussion

### 4.3.1 Mathematical quantification and delineation of hot moments and hot spots

#### 4.3.1.1 Temporal delimitations characterization of hot moments

Fig. 4.2 shows the effects of glucose and water application on the mean surface temperature ($T$) during the incubation of the four soil samples and the respective air temperature. $T$ of each sample showed similar courses independent of the incubation series (Fig. 4.2a, b, c, and d). In the first hours, the $T$ increased in all samples, regardless of soil type and treatment, because of the temperature adaptation to the ambient conditions inside the closed styrofoam box, until a plateau is reached after about 8 to 15 h. From this point on, temperature curves differentiated depending on their treatment. The mean $T$ of the glucose-treated samples increased above the level of the water-treated samples. After about 70 h, $T$ of the glucose-treated samples decreased again to the same temperature level as the water-treated samples. The trends in the time series were characterized by increasing (Fig. 4.1b), stagnating (Fig. 4.2c and 2d), or decreasing $T$ (Fig. 4.2a) since those were products of the respective ambient conditions. Increasing surface temperatures over time indicated that the air temperature was also increasing and vice versa. This assumption was confirmed with the data loggers' temperature curves (Fig. 4.2a, b, c, and d).

Fig. 4.2 (e f, g, and h) shows the mean temperature differences ($\Delta T$) to focus on the temperature alteration characteristics between the glucose and water amended soil surfaces. $\Delta T$ was unaffected by the temperature trends of the air temperature. Since a clear peak could be observed in each $\Delta T$ curve, the application of glucose accounted for a temperature effect on the surfaces of the soil samples. After about 8 h to 15 h, the mean $\Delta T$ increased on all soil surfaces until a temperature peak was achieved after 35 to 45 h with an afterward decrease.
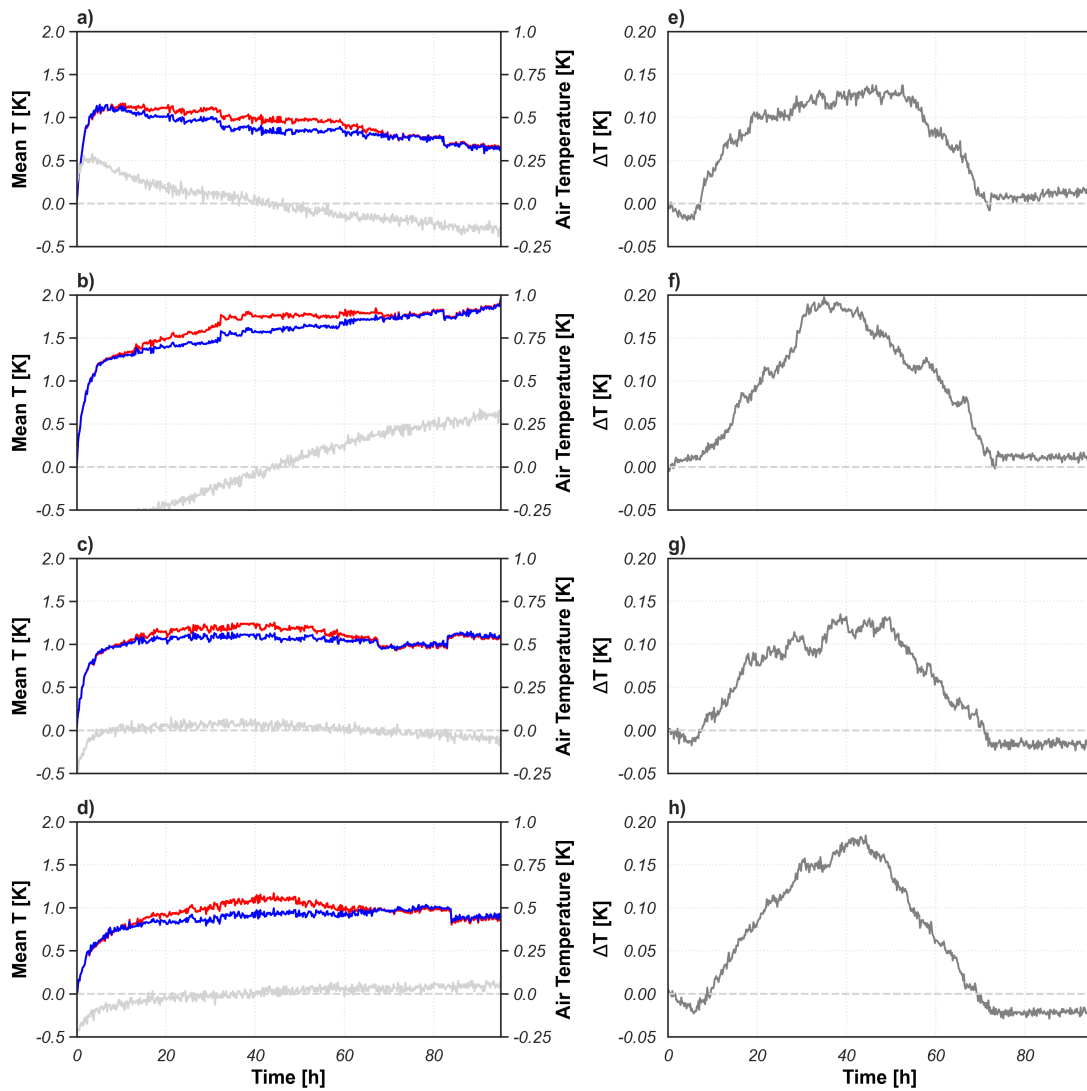
**Figure 4.2:** *Temporal mean surface temperature (T) of soil sample $G_T$ (a, and e), $G_S$ (b, and f), $K_T$ (c, and g), and $K_S$ (d, and h) referring to the incubation period after glucose application. The left column shows the courses of the mean temperature of the glucose-treated samples (red line), the control sample (blue line), and the air temperature measured by the data loggers (gray line). The right column shows the temperature difference ($\Delta T$) between glucose-treated and control samples of the corresponding sample on the right side.*

Between the Grinderwald and Kalwes soils, there were only a few differences regarding the course of $\Delta T$ after the hot moment's end at about 70 h (Fig. 4.2e, f, g, and h). The negative $\Delta T$ of soil K is striking (Fig. 4.2g and h) since the temper-

ature dropped to a lower level here. This could be due to potential measurement errors, as $T$ showed erratic changes after 70 to 80 h (Fig. 4.2c and d), which might also affect $\Delta T$. It could also be an artifact of the preprocessing and the camera accuracy of $\pm$ 30 mK.

For a more detailed characterization of the temporal and temperature characteristics of the hot moment, Table 4.2 shows the concise time points referring to the hot moment and the associated mean $\Delta T$. The general duration of the hot moment of soil G was longer with 63.5 h for $G_T$ and 57.8 h for $G_S$ compared to soil K with 54.0 h for $K_T$ and 48.2 h for $K_S$. $G_S$ remained significantly warmer for almost 10 h compared to the KS but with similar temperature increase. The hot moment start time for soil K was also significantly later, at over 11 h, compared to less than 11 h for soil G. However, no particular differences could be observed in the mean $\Delta T$ values.

The differences between soils G and K might result from differences in SOC contents. While soil $K_T$ has 1.3% SOC, soil GT has only 1.2% (Table 4.1). Jílková et al. (2021) have also shown that soils with lower SOC contents had a more prominent microbial growth effect by adding labile C to the soil, compared to high-SOC soils. The addition of easily available C, such as glucose, rapidly overcomes this limiting effect by low SOC-contents and ensures an increase in microbial growth rates, which might lead to greater effects, especially with stronger substrate limitations (Heitkötter et al., 2017; Heitkötter and Marschner, 2018a; Jílková et al., 2021). This might also result in a delay in the glucose effect in soil K that lasted for a shorter period (Table 4.2). Regarding the fact that lower SOC contents characterized $G_S$ compared to $K_S$ (Table 4.1), it can be assumed that a stronger substrate limitation prevailed here, which may cause the longer duration of the hot moment of $G_S$ due to the higher catabolic activity.

**Table 4.2:** *Time and temperature characteristics of the hot moment of each soil sample.*

| Soil sample | Time | | | Hot moment $\Delta T(hm)$ | Start hot moment $\Delta T(start)$ | Max $\Delta T(max)$ | End hot moment $\Delta T(end)$ |
|:---:|:---:|:---:|:---:|:---:|:---:|:---:|:---:|
| | Start [h] | Max [h] | Duration [h] | | | | |
| $G_T$ | 8.0 | 45.8 | 63.5 | 0.09 | 0.02 | 0.14 | 0.11 |
| $G_S$ | 11.0 | 35.0 | 57.8 | 0.12 | 0.03 | 0.20 | 0.13 |
| $K_T$ | 11.8 | 38.7 | 54.0 | 0.09 | 0.03 | 0.14 | 0.09 |
| $K_S$ | 15.0 | 44.3 | 48.2 | 0.12 | 0.05 | 0.18 | 0.10 |

When comparing the course of $\Delta T$ for top- and subsoils (Fig. 4.2e, f, g, and h), apparent differences in T could be highlighted. The peak heights differed depending on the soil depth, as a maximum peak was achieved after 35 to 45 h of about 0.14 K in the topsoils (Fig. 4.2b and f) and up to 0.2 K in the subsoils (Fig. 4.2d and h). After about 70 h, $\Delta T$ decreased to its initial level in all soil samples. The shape of $\Delta T$ differed depending on soil depth, since the courses of the subsoil samples GS and KS were characterized by a clearer temperature peak, compared to the topsoil samples $G_T$ and $K_T$, characterized by flattened curves. Table 4.2 also shows that the hot moment duration was longer lasting for the topsoils ($G_T$ & $K_T$). However, a higher mean $\Delta T(hm)$ was recorded for the subsoil samples than the corresponding topsoils.

The course of $\Delta T$ can be attributed to increased microbial activity due to metabolization processes in the soil, which causes a release of heat energy (Chakrawal et al., 2020; Kluge et al., 2013; Schwarz et al., 2021). $\Delta T$ increased until a peak of maximum microbial growth is reached at $\Delta T(max)$. Subsequently, $\Delta T$ decreased again with declining microbial growth as the amount of released heat energy is reduced. This could be attributed to an initial growth of the microbial population by adding easily available substrates to the soil matrix, and an afterward decline in microbial growth rate when the substrate has been completely consumed (Blagodatskaya and Kuzyakov, 2013; Blagodatskaya et al., 2007).

The thermal signal's intensity and duration were also connected to soil depth since top-, and subsoil samples had similar effects in height and duration of temperature rise of $\Delta T$ after glucose and water application, respectively. The topsoils, $G_T$ and $K_T$, were characterized by a longer heating duration, and the subsoils, $G_S$ and $K_S$, by a more intense increase of $\Delta T(max)$ which could also be associated with the more substantial substrate limitation in the subsoil (Heitkötter and Marschner, 2018a; Kuzyakov and Blagodatskaya, 2015). The availability of easily available sub-

strates in the soil is crucial for microbial growth. In soil regions that are highly substrate-limited, microorganisms are in a dormant state (Joergensen and Wichern, 2018; Kuzyakov and Blagodatskaya, 2015). Activation of these microorganisms is coupled to overcoming substrate limitation by adding fresh, easily available substrate to the soil (Blagodatskaya and Kuzyakov, 2013; Heitkötter and Marschner, 2018a). Due to the stronger limitation in the subsoil, more microorganisms are stimulated to grow than in the topsoil, where the basal activity is already higher due to higher substrate availability resulting in a slower microbial growth compared to the subsoil. The faster and more extensive the growth, the greater was the temperature effect that could be observed (Fierer et al., 2003; Griffiths et al., 1999; Heitkötter and Marschner, 2018b). This caused the flattened temperature profile in the topsoils compared to the clear peak in the subsoils (Fig. 4.2). Another influencing factor may be the slightly stronger acidity of soil $K_T$ compared to $G_T$ (Table 4.1), which is accompanied by also lower mean $\Delta T(max)$ (Table 4.2). Aciego Pietri and Brookes (2009) investigated substrate addition to soils of different pH. The results showed that the lower the pH, the lower the microbial activity after substrate addition. These findings correspond well to the results shown in Table 4.2.

### 4.3.1.2 Spatial relationship and characterization of hot spots

The spatial distribution of mean $T$ referring to the hot moment ($T(hm)$) is shown in Fig. 4.1 for topsoil $K_T$ (Fig. 4.1b) and subsoil $K_S$ (Fig. 4.1n), respectively. $K_S$ was characterized by a vertical temperature gradient with decreasing temperature with soil depth (Fig. 4.1b). Small-scale areas with slightly elevated or slightly lower $T(hm)$ could also be visually identified but are of secondary importance for the distribution compared to the temperature gradient. $K_T$ is characterized by a horizontal temperature gradient (Fig. 4.1n). $T(hm)$ increased from left to right with predominantly higher $T(hm)$ in the upper region of the soil profile section. Again,

small-scale patterns were of secondary importance. The other soils were also characterized by large-scale gradients in $T(hm)$ rather than showing small-scale spatial temperature variations (Appendix Fig. A3.2).
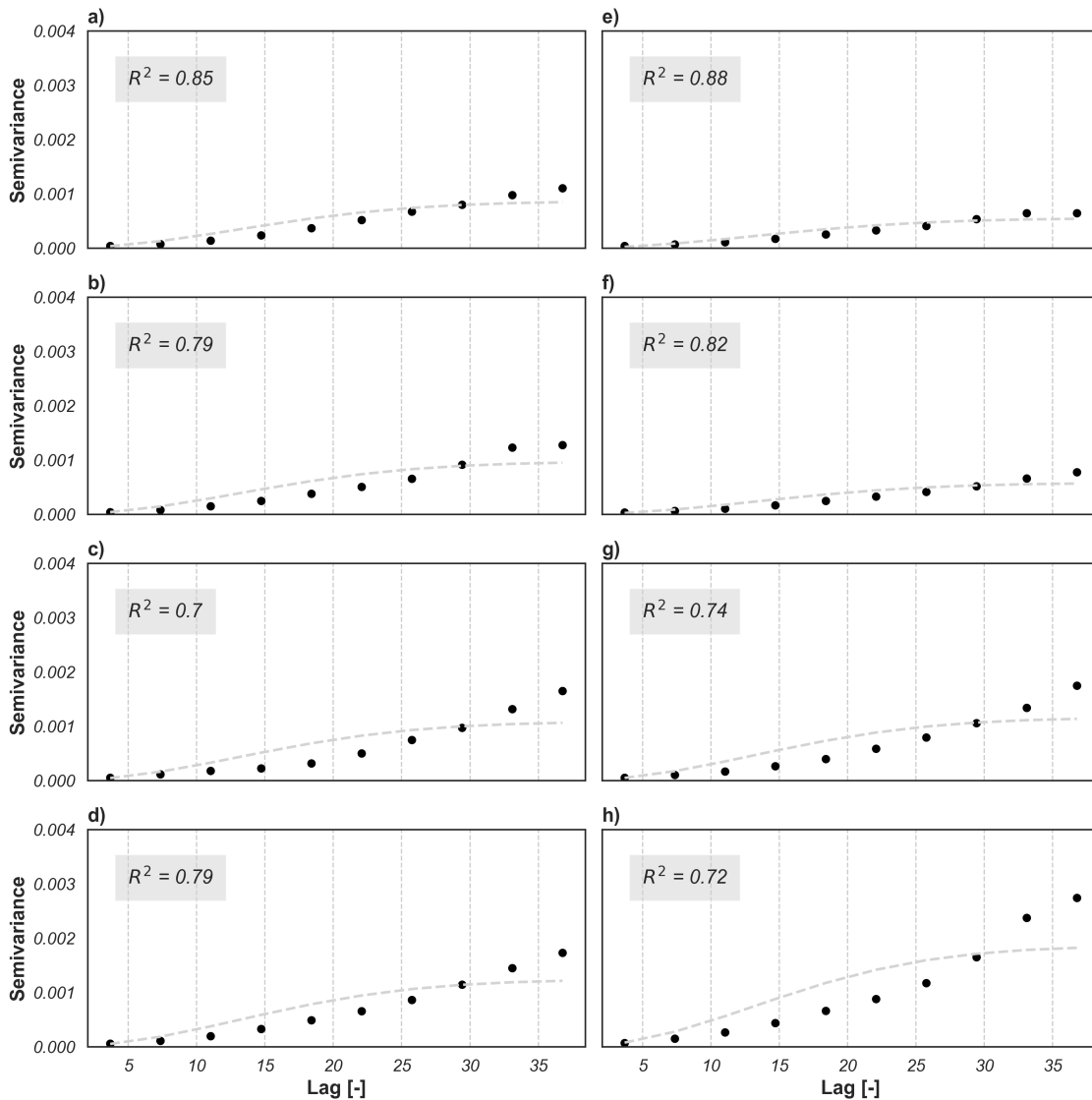


**Figure 4.3:** *Semivariance of mean $T(hm)$ using the Gaussian model for soil samples $G_T$ (a, and e), $G_S$ (b, and f), $K_T$ (c, and g), and $K_S$ (d, and h) up to a lag distance of 35 (about 6 mm). The right column refers to the control samples and the left column to the glucose-treated samples.*

The distribution of $T(hm)$ is described and evaluated in more detail using geostatic analysis in Fig. 4.2. The semivariance increased consistently in all samples, but no plateau was reached. The prediction quality of the Gaussian model was very good ($R^2$ up to 0.9), but due to not reaching the sill, the prediction was limited with increasing distance. When comparing the two soils, it can be seen that soil G had flatter semivariance curves (Fig. 4.3a and b) compared to soil K (Fig. 4.3c and d). Soil G exhibited a semivariance up to 0.0015 at a lag distance of 35 (Fig. 4.3b), but it did not reach the sill in any sample. Flatter slopes of the fit were found in the glucose-treated samples $G_T^+$ (Fig. 4.3e) and $G_S^+$ (Fig. 4.3f). For soil K, significantly higher semivariances with a distance of 35 could be assessed with values up to 0.0035 in the variant $K_S^+$ (Fig. 4.3h).

Soil K exhibited higher semivariances with increasing lag distance, which might result from the more prominent variability in SOC content (Table 4.1). The SOC content had a demonstrable effect on active microorganisms, contributing to the temperature changes on the soil surface (Schwarz et al., 2021). In particular, areas characterized by a stronger substrate limitation, such as the SOC-poorer areas in the lower part of the soil K, benefited from the glucose application (Blagodatskaya and Kuzyakov, 2013; Jílková et al., 2021). From higher spatial variability of soil K compared to soil G (Fig. 4.1a and k, Appendix Fig. A3.1), a larger variance of temperature was expected (Appendix Fig. A3.3), which was reflected in increasing semivariances with increasing lag distance (Fig. 4.3c, d, g, and h).

When differentiating the semivariances by soil depth, no striking differences could be identified. In soil G, the differences were not differentiated by soil depth but by treatment (Fig. 4.3a, b, e, and f). In soil K, however, a significantly higher semivariance was detected in the glucose-treated subsoil sample ($K_S^+$, Fig. 4.3h) compared to the water-treated sample ($K_S^-$, Fig. 4.3d), which only showed a semivariance

of 0.002. It can be assumed that the variability of surface characteristics was of the same magnitude. The more significant increase in semivariance of soil $K_S^+$ can probably be attributed to the activation of dormant microorganisms by glucose application (Blagodatskaya and Kuzyakov, 2013; Heitkötter and Marschner, 2018a). The activation did not lead to the highest mean $T(max)$ (Table 4.2), but was characterized by a greater spatial variability, which could be confirmed based on the spatial variance of $T(hm)$ (Fig. 4.1m).

No sill was reached in all soils and treatments so that an increasing semivariance could be assumed over the lag distance of 35, a distance of nearly 6 mm. The range reflects the average distance over which a variable is spatially autocorrelated (Boeddinghaus et al., 2015; Grundmann and Debouzie, 2000; Nunan et al., 2003); thus, there was autocorrelation of the data with increasing distance. The nugget effect resulted in values around 0 in all variants so that there was no or only a minimal dependence in spatial terms with increasing distance (Cambardella et al., 1994; Zhang et al., 2017). This showed that the selected soil sections from each soil profile were not representative of the depth section they were taken from.

Microbial activity takes place on a smaller scale, thus, smaller sections with a larger image resolution would have to be chosen, similar to Nunan et al. (2003), who used thin sections on a scale up to 1 mm. This would allow a more focused view of microbial activity and allow spatial dependencies to be highlighted. When looking at the cm-scale with IRT, processes and soil properties on a larger scale are considered, such as large-scale SOC distribution, water content, soil pH, or even ambient conditions, which has an influence here (Aciego Pietri and Brookes, 2009; Barros et al., 1995; Blagodatskaya et al., 2007; Schwarz et al., 2021).

Small-scale variabilities could be highlighted when considering the soil surface and its variance in the hot moment (Fig. 4.1c and m). Since microbial activity is

recorded on a very small scale in the range from µm to mm (Kuzyakov and Blago-
datskaya, 2015), it was not of relevance for this study. The large-scale gradients
of $T$ overlaid the small-scale effects of microbial activity so that the semivariance
could not be used to represent their spatial dependencies. Therefore, the influence of
the individual surface properties, which relate to both microbiological and physical
properties, should be considered in order to make more accurate statements.

### 4.3.2 Analysis of soil surface temperature and further soil properties

#### 4.3.2.1 Relating soil properties pixelwise to surface temperature

An overview of the spatial mean surface properties with their corresponding coeffi-
cients of variation (CV) is shown in Table 4.3. The values are referring to the tem-
perature amplitude (Appendix A3.4), phase angle (Appendix A3.5), surface color
parameters L, a*, and b* (Appendix A3.6, A3.7, and A3.8, respectively), and $\beta$-
glucosidase activity (Appendix A3.9). The mean values showed the values differed
in terms of soil type and depth, but in terms of treatment with glucose or control,
properties were very similar when the respective CVs are considered. Only soil KS
showed significant differences in temperature amplitude and the L color parameter
between the two sections of the sample. Interestingly, the higher soil moisture con-
tent (= low temperature amplitude) of $K_S^+$ is associated with high L values, which
indicate lower SOC contents.

Since all parameters describing the physical properties of the soil samples initially
showed no differences between the control and glucose treatment sides, any changes
in heat release in response to the glucose application must be related to increased
microbial metabolic activity. Since these heat release patterns are distributed het-
erogeneously on the sample surface, their controlling factors will be analyzed in more
detail using the stepwise backward regressions.

**Table 4.3:** *Characterization of the soil surfaces using spatial mean properties (ø) and corresponding variation coefficient (CV) of temperature amplitude [K], phase angle [°], surface color parameters (L, a\*, and b\*) [%], and $\beta$-glucosidase activity [pM mm$^{-2}$ h$^{-1}$].*

| Soil sample | Active IRT | | | | Surface color parameters | | | | | | Zymography | |
| | Temperatur amplitude [K] | | Phase angle [°] | | L | | a* | | b* | | $\beta$-glucosidase activity [pM mm$^{-2}$ h$^{-1}$] | |
| | ø | CV | ø | CV | ø | CV | ø | CV | ø | CV | ø | CV |
|---|---|---|---|---|---|---|---|---|---|---|---|---|
| $G_T^-$ | 1.75 | 0.05 | 1.13 | 0.03 | 58.32 | 0.11 | 11.08 | 0.10 | 23.09 | 0.17 | 14.29 | 0.46 |
| $G_T^+$ | 1.77 | 0.05 | 1.12 | 0.03 | 56.55 | 0.13 | 10.85 | 0.09 | 21.87 | 0.20 | 19.55 | 0.35 |
| $G_S^-$ | 2.13 | 0.08 | 1.08 | 0.02 | 63.74 | 0.07 | 11.40 | 0.14 | 31.46 | 0.08 | 7.20 | 0.20 |
| $G_S^+$ | 2.19 | 0.07 | 1.07 | 0.02 | 62.40 | 0.06 | 11.81 | 0.08 | 31.98 | 0.06 | 7.72 | 0.26 |
| $K_T^-$ | 2.11 | 0.17 | 1.12 | 0.03 | 58.51 | 0.16 | 10.65 | 0.17 | 23.19 | 0.25 | 19.20 | 0.26 |
| $K_T^+$ | 2.47 | 0.30 | 1.14 | 0.02 | 50.89 | 0.30 | 9.02 | 0.29 | 19.02 | 0.41 | 20.27 | 0.26 |
| $K_S^-$ | 2.19 | 0.11 | 1.07 | 0.03 | 55.23 | 0.12 | 10.67 | 0.12 | 24.07 | 0.16 | 18.00 | 0.44 |
| $K_S^+$ | 1.76 | 0.09 | 1.08 | 0.02 | 64.27 | 0.07 | 11.07 | 0.06 | 26.89 | 0.08 | 19.92 | 0.30 |

As shown in Table 4.4, the prediction quality of the regression models for the measured $T(hm)$ showed by the $R^2$ was highest (0.71 and 0.70) for the Grinderwald topsoil ($G_T^+$) and subsoils ($G_S^+$). In contrast, much lower prediction accuracies of only 44% were got for both Kalwes soil samples, $K_T^+$ and $K_S^+$. When considering all glucose-treated soil samples, the associated regression model reached an $R^2$ of 0.33, thus clearly showing that the factors controlling the glucose-induced temperature increases were quite distinct between the soil samples. The strengths of the influence of the individual independent variables on $T(hm)$ were considered separately for each soil sample in the following.

The temperature amplitude obtained from active IRT describes the soil surface moisture contents, with high values related to a low soil surface moisture content and vice versa (Schwarz et al., 2018)(Schwarz et al., 2018). As shown in Table 4.4, the standardized $\beta$-coefficients were negative for all samples, indicating that $T(hm)$ was positively related to soil moisture content. Apparently, higher soil moisture contents contributed to increased $T(hm)$ and thus increased microbial growth rates (Barnard et al., 2013; Barros et al., 1995; Rey et al., 2005). Similarly, Barros et al. (1995) found a positive correlation between soil moisture contents and heat production. In our samples, the greatest influence of the temperature amplitude was found for $G_S^+$ with a standardized $\beta$-coefficient of -0.79 and the lowest of -0.06 for $K_S^+$, which may be attributed to the rather high moisture content of this sample (Table 4.3).

The phase angle describes surface structural richness, with high values standing for lower densities and cavities (Ranjit et al., 2015; Schwarz et al., 2018). The standardized $\beta$-coefficients showed negative and positive influences of the phase angle on $T(hm)$ (Table 4.4). The strongest contribution of this parameter to explain $T(hm)$ was found for the topsoils $G_T^+$ with a $\beta$-coefficient of -0.65, followed by a value of 0.20 for $K_T^+$, indicating an opposing influence in these two samples. If this is due to textural (sand vs. silt) or structural differences between the two samples is not known.

**Table 4.4:** *Regression analysis of surface parameters for predicting $T(hm)$ of the glucose-treated soil samples $G_T^+$, $G_S^+$, $K_T^+$, and $K_S^+$, as well as all glucose-treated samples combined (+) with each the standardized $\beta$-coefficients.*

| Soil sample | $R^2$ | Active IRT | | Soil color parameters | | | Zymography |
|:---:|:---:|:---:|:---:|:---:|:---:|:---:|:---:|
| | | Temperature amplitude | Phase angle | L | a* | b* | $\beta$-glucosidase activity |
| $G_T^+$ | 0.71 | -0.26 | -0.65 | -0.31 | 0.37 | -0.99 | *n.s.* |
| $G_S^+$ | 0.70 | -0.79 | 0.12 | -0.05 | 0.18 | 0.14 | 0.17 |
| $K_T1+$ | 0.44 | -0.32 | 0.20 | 1.11 | 0.85 | -0.55 | *n.s* |
| $K_S^+$ | 0.44 | -0.06 | -0.11 | 0.51 | 0.32 | -0.47 | 0.12 |
| + | 0.33 | -0.30 | 0.06 | -0.12 | 0.47 | -0.34 | 0.14 |

The soil color parameters L, a*, and b* were derived from the photographs, and each refer to different color values. The color value L described the brightness, where high values indicated bright areas, a* represents the gradient from -100 red to +100 green, and b* describes the gradient from -100 blue to +100 yellow (Heil et al., 2020; Khan et al., 2009; Viscarra Rossel et al., 2006). The value L is negatively related to the SOC content of the soil (Heil et al., 2020). In Table 4.4, negative $\beta$-coefficients were found for both Grinderwald soils, $G_T^+$ (-0.31) and $G_S^+$ (-0.05), thus indicating that SOC positively contributed to the observed temperature increases. Since microorganisms are closely associated with SOC as their primary source of substrates (Barros et al., 2011; Chakrawal et al., 2020; Zhou et al., 2021), the observed relationship indicates that glucose is metabolized most at such sites of higher microbial densities. However, for the Kalwes samples $K_T^+$ and $K_S^+$, the L parameter contributes with positive $\beta$-coefficients (1.11 and 0.51) to both regression models (Table 4.4). Thus, the glucose-induced temperature increases appear to be negatively related to SOC content. One could expect this to occur if SOC-associated microorganisms are not substrate limited and therefore do not respond to additional substrate or their growth response is limited by the availability of other nutrients, such as N (Blagodatskaya et al., 2007; Kuzyakov and Blagodatskaya, 2015). In consequence, sites with lower SOC content would be less nutrient-depleted and therefore more responsive to substrate additions, as also observed with enzymatic reactions to glucose additions (Heitkötter and Marschner, 2018a).

The green color value a* can be interpreted as an inverse indicator of iron oxide contents since a high proportion of red tones indicates a high iron oxide content while green tones are associated with microbially induced reducing conditions (Schwertmann, 1993). In Table 4.4, the $\beta$-coefficients of a* showed throughout positive values ranging from 0.18 to 0.85. Such positive $\beta$-coefficients for a* show that $T(hm)$ decreases with increasing iron oxide contents. This relationship, therefore, indicates that the microbial utilization of glucose for growth is limited in the presence of iron oxides, possibly due to their high sorption capacity for enzymes and SOC, especially

in acidic soils (Gu et al., 1994; Saidy et al., 2013; Yan et al., 2010). Similar results were obtained by Heil et al. (2020) who found a positive relationship between red tones and SOC content, so that the combination of L and a* in multiple linear regression analyses provided excellent predictability of SOC, with R2 up to 0.90.

The color value b* refers to blue and yellow tones on the soil surface and therefore is also inversely related to iron oxides and SOC (Heil et al., 2020; Viscarra Rossel et al., 2006). In Table 4.4, the $\beta$-coefficients showed a generally negative impact on the measured $T(hm)$ with values ranging between -0.47 to -0.99, except for $G_S^+$ with a $\beta$-coefficient of 0.14. These negative $\beta$-coefficients, therefore, indicate that $T(hm)$ is generally positively related to SOC content.

$\beta$-glucosidase activity is a measure for the microbial potential to degrade cellulose into glucose compounds and thus provide energy for microbial activity (Chen et al., 2014; Sinsabaugh et al., 2008; Zhang et al., 2020). In general, $\beta$-glucosidase activity is closely linked to organic matter contents (Sinsabaugh and Follstad Shah, 2011; Sinsabaugh et al., 2008). While for the topsoils $K_T^+$ and $G_T^+$, no significant contribution to the regression could be observed, positive $\beta$-coefficients with 0.17 and 0.12 were determined for the subsoils $G_S^+$ and $K_S+$, respectively (Table 4.4). These positive $\beta$-coefficients indicate that a high initial $\beta$-glucosidase activity resulted in an increase in measured $T(hm)$. Thus, areas with the initially high provision of energy as a contribution for microbial activity were confirmed to have, during the incubation experiments, higher increases in the surface temperature, independently from subsequent glucose application (Salgado et al., 2018; Zhang et al., 2020). As Zhang et al. (2020) had discussed, a high enzyme activity increased the substrate use efficiency, which led to a higher heat production by microbial activity.

The results of these regression analyses show that the spatially resolved mean heat production during the hot moments $T(hm)$ can, at least partly, be explained by

other soil surface properties. However, the contribution of these properties strongly varies between the samples and the predictability of $T(hm)$ for the Kalwes soils $K_T^+$ and $K_S^+$ was very poor. Since the observed hot moments not only differed in the magnitude of $T(hm)$ but also in their temporal temperature dynamics, this data is additionally considered in the following cluster analysis.

### 4.3.2.2 Cluster analysis of hot moments and hot spots

The temperature development $T(hm)$ was classified in spatio-temporal terms using the hierarchical k-means cluster algorithm with an optimal number of four groups. In Fig. 4.4, the spatial $T(hm)$ for the glucose-treated samples is shown (Fig. 4.4a - 4.4d) with the corresponding distribution of the assigned surface clusters of each pixel to the four cluster groups (Fig. 4.4e – 4.4h). The clusters were formed based on the temporal course of the heat evolution from the pixels in order to differentiate between groups of similar temperature curves. In a next step, each cluster is further characterized by its mean temperature amplitude, phase angle, surface color parameters (L, a*, and b*), and $\beta$-glucosidase activity (Table 4.5).

The cluster assignment was mainly dominated by cluster differences in $T(hm)$ since the mean $T(hm)$ of the clusters is increasing from cluster 1 to cluster 4. These differences were significant within each soil sample (ANOVA, *p $<$ 0.05), showing that the absolute temperature and not the temperature time course dominate the pixel grouping. The assumption is obvious that the overall temporal courses did not play an important role because they were co-determined by the ambient air temperature and therefore showed very strong similarities, as can also be seen in Fig. 4.2 based on the logger data (gray lines). Corresponding to the increasing mean $T(hm)$, from cluster 1 to 4, the mean temperature amplitudes in the clusters decreased, except in sample $K_T^+$ (Table 4.5). Significant differences between the cluster groups could be found for all samples, except for $K_S^+$, where the mean temperature amplitudes did not differ with values between 1.74 to 1.79 K.
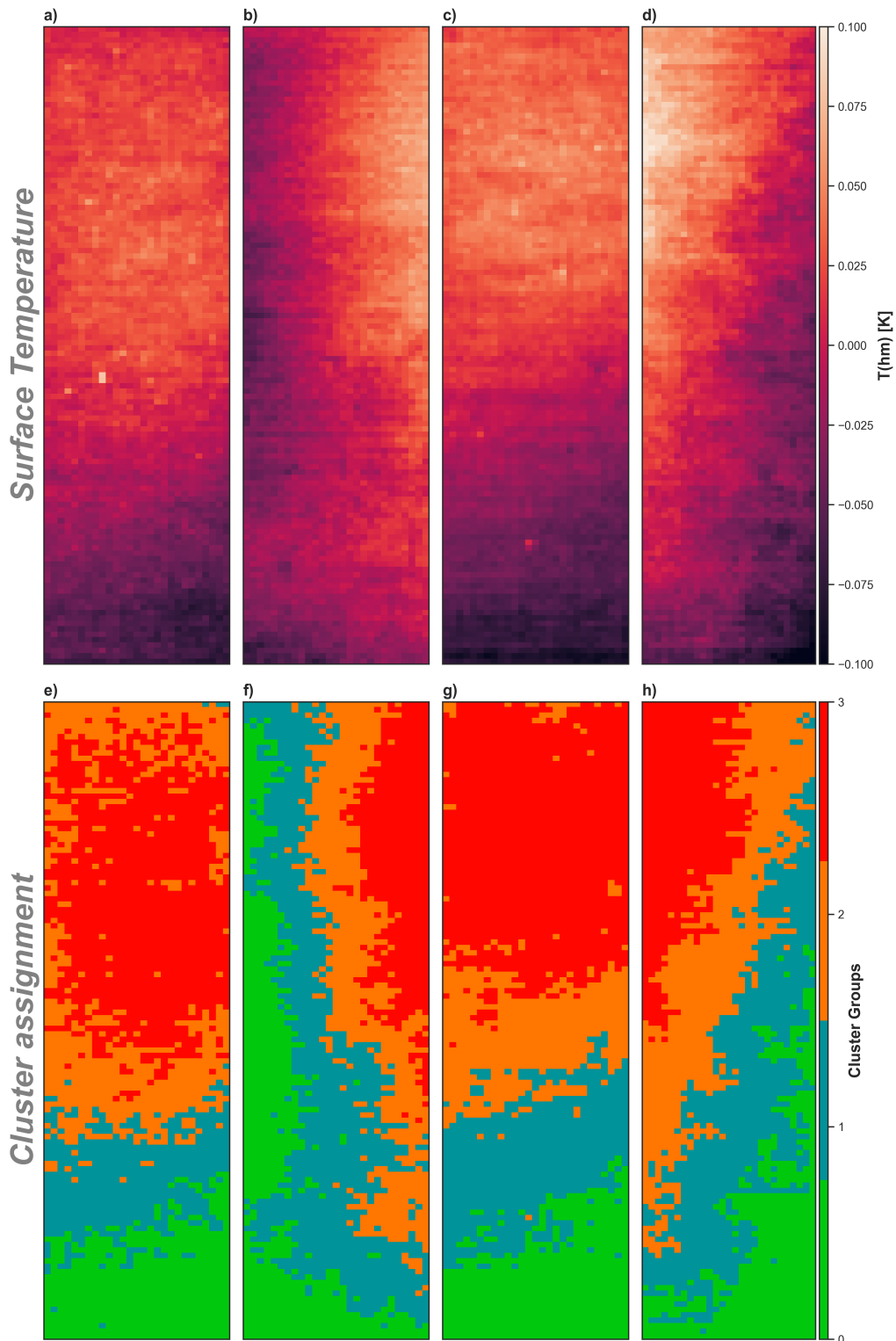
**Figure 4.4:** *Surface temperature $T(hm)$ for soil samples $G_T^+$ (a), $K_T^+$ (b), $G_S^+$ (c), and $K_S+$ (d) with the corresponding hierarchical k-means cluster group assignments for samples $G_T^+$ (e), $K_T^+$ (f), $G_S^+$ (g), and $K_S^+$ (h).*

Since low temperature amplitudes indicate higher soil moisture (Antonucci et al., 2011; Schwarz et al., 2018), higher mean $T(hm)$ of a cluster are associated with initially higher soil moisture. This shows that microbial activity is somewhat moisture limited, as it is generally assumed that microbial activity will increase until the soil is saturated with water (Baldrian et al., 2010; Barros et al., 1995; Brockett et al., 2012). Another possible reason could be that the diffusion of the dissolved glucose to the consumers is promoted in soil regions where more pores are filled with water.

Interestingly, $K_T^+$ showed a contrasting relationship, with increasing temperature amplitudes from 2.19 to 3.02 K with increasing $T(hm)$ from cluster 1 to cluster 4. This sample showed the highest values for the mean temperature amplitudes of the clusters. Since high temperature amplitudes mean low soil moisture contents, the evolution of $T(hm)$ might result from suppressed microbial activity at lower soil moisture contents. As Barros et al. (1995) showed, there is a high correlation between soil moisture contents and heat development induced by microbial activity. In addition, the darker soil was characterized by a higher emissivity and, thus, could also absorb more thermal radiation when heated by an active signal (Mira et al., 2007; Usamentiaga et al., 2014). This could amplify the described temperature effect.

The mean phase angles of each cluster group differed only slightly within one soil sample, with significant differences only for soil $K_T^+$ with values ranging from 1.13° to 1.16°, increasing with increasing $T(hm)$ (Table 4.5). Great differences in the phase angles could also be detected for topsoil $G_T^+$ with values ranging from 1.11° to 1.15° with partly significant differences but with decreasing values with increasing $T(hm)$.

**Table 4.5:** *Temporal pixelwise cluster groups assigned to mean $T(hm)$ and the corresponding mean soil surface properties of each cluster group. Different letters indicate significant differences in between the cluster groups within one soil sample (ANOVA, Tukey's HSD post hoc test (*p < 0.05)).*

| | | Passive IRT | Active IRT | | Surface color parameters | | | Zymography |
| | | Mean $T(hm)$ [K] | Temperatur Amplitude [K] | Phase Angle [°] | L [%] | a* [%] | b* [%] | $\beta$-glucosidase activity [pM mm$^{-2}$ h$^{-1}$] |
|---|---|---|---|---|---|---|---|---|
| $G_T^+$ | k 1 | $0.86^a$ | $1.84^a$ | $1.15^a$ | $63.22^a$ | $10.70^a$ | $25.40^a$ | $15.76^a$ |
| | k 2 | $0.90^b$ | $1.77^b$ | $1.15^a$ | $62.38^a$ | $11.14^c$ | $25.00^a$ | $16.26^a$ |
| | k 3 | $0.93^c$ | $1.78^b$ | $1.12^b$ | $54.52^b$ | $10.74^b$ | $20.93^b$ | $20.53^b$ |
| | k 4 | $0.95^d$ | $1.74^c$ | $1.11^c$ | $52.62^c$ | $10.86^b$ | $19.70^c$ | $21.87^c$ |
| $G_S^+$ | k 1 | $1.57^a$ | $2.43^a$ | $1.06^a$ | $64.90^a$ | $10.85^a$ | $31.21^a$ | $7.11^a$ |
| | k 2 | $1.61^b$ | $2.27^b$ | $1.06^b$ | $62.09^b$ | $11.82^b$ | $32.07^b$ | $6.97^a$ |
| | k 3 | $1.64^c$ | $2.19^c$ | $1.06^b$ | $62.44^b$ | $11.75^b$ | $31.91^b$ | $8.05^b$ |
| | k 4 | $1.67^d$ | $2.06^d$ | $1.09^c$ | $61.48^c$ | $12.23^c$ | $32.29^c$ | $8.20^b$ |

Continued on next page

| | | Passive IRT | Active IRT | | Surface color parameters | | | Zymography |
|---|---|---|---|---|---|---|---|---|
| | | Mean $T(hm)$ [K] | Temperatur Amplitude [K] | Phase Angle [°] | L [%] | a* [%] | b* [%] | $\beta$-glucosidase activity [pM mm$^{-2}$ h$^{-1}$] |
| $K_T^+$ | k 1 | $1.04^a$ | $2.19^a$ | $1.13^a$ | $56.48^a$ | $10.55^d$ | $23.58^a$ | $17.93^a$ |
| | k 2 | $1.07^b$ | $2.31^b$ | $1.14^b$ | $55.41^a$ | $9.65^c$ | $21.25^b$ | $20.02^b$ |
| | k 3 | $1.09^c$ | $2.59^c$ | $1.15^c$ | $48.14^b$ | $8.25^b$ | $16.58^c$ | $22.37^d$ |
| | k 4 | $1.12^d$ | $3.02^d$ | $1.16^d$ | $36.97^c$ | $6.53^a$ | $11.11^d$ | $21.15^c$ |
| $K_S^+$ | k 1 | $0.88^a$ | $1.79^a$ | $1.09^a$ | $64.47^a$ | $11.11^a$ | $28.16^a$ | $17.41^a$ |
| | k 2 | $0.91^b$ | $1.75^{bc}$ | $1.08^b$ | $65.11^b$ | $11.08^{bc}$ | $27.52^b$ | $19.16^b$ |
| | k 3 | $0.95^c$ | $1.76^b$ | $1.08^b$ | $64.13^a$ | $11.05^{bd}$ | $26.34^c$ | $21.86^d$ |
| | k 4 | $0.99^d$ | $1.74^c$ | $1.09^a$ | $62.99^c$ | $11.07^{cd}$ | $25.54^d$ | $20.66^c$ |

The influence of the SOC content could contribute to the phase angle variations as an indicator of the structural richness of the soil surface. SOC caused a stronger aggregate structure of the soil (Liu et al., 2014). Since high SOC contents characterized the topsoils, the differences between the cluster groups for the topsoils were greater with significant differences, which could not be observed for the subsoils. Thus, this assumption could be confirmed. Further, the subsoils were characterized by a higher bulk density (Table 4.1), which also impacted the homogeneity of the phase angles since high bulk density resulted in lower phase angles (Ranjit et al., 2015; Schwarz et al., 2018).

Most prominently, the surface color parameters showed a clear differentiation between the cluster groups (Table 4.5). With increasing $T(hm)$, L and $b^*$ values decreased, except for $G_S^+$ where $b^*$ increased from 31.21 to 32.29%. For $a^*$, no differences in the values could be detected since the values were very similar. Only for $K_T^+$, sorting in $a^*$ with values from 10.55 to 6.53% with increasing $T(hm)$ were observed.

The relationship of the cluster order to the surface color parameters L and $b^*$ can be attributed to the proportion of SOC in the soil matrix. These two values are significantly influenced by the SOC content (Heil et al., 2020; Viscarra Rossel et al., 2006). The sorting according to mean $T(hm)$ has to be considered here on two levels. First, SOC content affected the presence of easily available material for microbial activity (Bhogal et al., 2009; Blagodatskaya and Kuzyakov, 2008; Zhou et al., 2021). It can be clearly seen that with the increasing availability of SOC, the temperature increase is significantly higher (Barros et al., 2011; Bhogal et al., 2009; Chakrawal et al., 2020). Thus, the SOC content was assumed to influence $T(hm)$ positively and, therefore, microbial activity. Another influencing factor is the physical conditions related to color differences. The soil color influences the emissivity of the surface.

The darker the soil, the higher is the emissivity (Mira et al., 2007; Sánchez-Marañón et al., 2004; Schwertmann, 1993). Since a uniform emissivity of 0.95 was used for all passive IRT measurements, especially dark areas in the profile sections could be overestimated with assumed equal temperatures of the surfaces with different brightness as a result of the SOC content. Therefore, these two effects are mutually dependent so that an increase in the measured surface temperature could be related to higher microbial activity as well as to higher emissivity of the darker soil sections.

The parameter a* showed little differentiation between the clusters. Only in sample $K_T^+$, the sorting of a* is clearly inversely related to $T(hm)$ among the four clusters (Table 4.5). This relationship could also be based on the SOC content since the red content in the soil is also often used for predicting the SOC content (Heil et al., 2020; Viscarra Rossel et al., 2008). Khan et al. (2009) also showed that a* decreased significantly during a composting experiment where SOC decreased over time. However, it is unclear why similar relationships were not observed for other samples.

The distribution of the $\beta$-glucosidase activity among the cluster groups showed similar relationships to those of mean $T(hm)$. With increasing mean $T(hm)$ within the cluster groups, the mean $\beta$-glucosidase activity also increased with generally significant differences between the clusters, except in sample $G_S^+$ where the lowest $\beta$-glucosidase activity was for cluster group 2 with 6.97 pM mm$^{-2}$ h$^{-1}$ and cluster group 1 with 7.11 pM mm$^{-2}$ h$^{-1}$ (Table 4.5). The results indicate that the areas in the profile section that had the highest enzyme activity at the beginning also showed the highest temperature increase after glucose addition. In general, $\beta$-glucosidase activity indicates the production of enzymes in the breakdown of soil-borne cellobiose to glucose, which thus provides energy for microbial activity (Chen et al., 2014; Sinsabaugh and Follstad Shah, 2011). Therefore, in areas in the profile

sections, the increased amount of provided energy, indicated by high $\beta$-glucosidase activity, then positively affected microbial growth expressed as increased heat production (Salgado et al., 2018; Sinsabaugh et al., 2008; Zhang et al., 2020).

While it was difficult to establish clear relationships between mean $T(hm)$ and the other surface properties of the samples, such as temperature amplitude, surface color parameters (L, a*, and b*) or $\beta$-glucosidase activity, when considering the entire surfaces (section 4.3.2.1), more evident relationships could be established by dividing the samples into cluster groups. These indicate in particular influences by the SOC content in the soil, which played an important role revealed by the surface color parameters and regarding the formation of a crumbly structure also by the phase angle. In addition, a clear positive relationship between mean $T(hm)$ and soil moisture contents was confirmed. The $\beta$-glucosidase activity in the cluster groups indicated that initially high values were followed by a higher $T(hm)$, which is associated with increased microbial activity. The results suggest that a combined consideration of mapping techniques had much potential to explain the temperature evolution on undisturbed soil samples and to show relationships concerning spatio-temporal dynamics of microbial activity.

## 4.4  Conclusions

In this study, heat production on undisturbed soil samples was evaluated by passive IRT in a high spatial resolution of < 1 mm and a high temporal resolution in a 10-min interval in a substrate-induced approach using glucose for the stimulation of microbial activity. The heat development on the soil surfaces was examined in more detail using mathematical and geostatistical methods. However, the main objective was to capture the spatio-temporal variability of microbial heat production and describe and interpret it in detail using high-resolution mapping techniques.

The main findings of this study using passive IRT as spatio-temporal mapping tool of heat production, and active IRT, zymography, and photography for the spatial characterization of undisturbed soil samples are summed up in the following bullet points:

- The mean surface temperature increased up to a $\Delta T(hm)$ of 0.2 K after uniform glucose application on undisturbed subsoil samples and up to 0.14 K on undisturbed topsoil samples with a maximum hot moment duration of nearly 46 h.

- The spatial variability of the considered profile sections could not represent the variance of the individual soils using geostatistical methods since microbial activity takes place on the $\mu$m- to mm-scale, and this study focuses on the mm-scale.

- The spatial variability of the Kalwes soil was higher compared to the Grinderwald soil, independent from treatment with glucose or water. No differences between top- and subsoils could be determined.

- Multiple regression analyzes revealed significant relationships between glucose-treated soil surface temperature and pixelwise temperature amplitude as an indicator of soil moisture (low temperature amplitude equals high soil moisture), surface color parameters as an indicator of surface SOC contents, and initial $\beta$-glucosidase activity for the subsoils.

- Higher $R^2$ were obtained for the Grinderwald soil with values up to 0.71 for the topsoil compares to the Kalwes soil with values up to 0.44 for top- and subsoils. The $R^2$ considering all soil samples was lowest at 0.33 due to the high variability of soil surface characteristics. Thus, not all surface temperature characteristics could be explained entirely.

- A hierarchical k-means clustering based on the spatio-temporal heat production revealed that the temporal characteristics had no influence on the grouping, but the mean surface temperature was decisive.

- A clear connection to soil moisture contents could be estimated, since the high mean surface temperature was associated with high soil moisture contents. It can also be assumed that soil color parameters as a proxy for SOC contents influenced temperature development because of the varying soil-borne substrate availability. The results of the $\beta$-glucosidase activity showed that the initial biotic state of the soil contributed to the temperature increase concerning the provision of energy for microbial activity.

Thus, the combined use of the applied mapping techniques showed an increased ability to clarify spatio-temporal developments in microbial behavior on undisturbed soil samples when small-scale dependencies are considered. The surface temperature characteristics during the hot moments could not be fully explained with the help of the other soil surface properties, including the spatio-temporal clustering method. Considering that such an approach with the intersection of different surface measurement techniques related to abiotic and biotic soil properties had not been used before, the results of this study are promising. Therefore, more research needs to be done regarding microbial dynamics considering spatio-temporal soil information to fill outstanding knowledge gaps.

It is recommended to validate the passive IRT using mapping tools and test correlations, e.g., by other enzymes using zymography (e.g., chitinase or acid phosphatase) or using planar optodes that can capture $CO_2$ evolution in a spatio-temporal manner. The IRT approach offers the possibility to record soil surface heat development induced by microbial activity and dynamics. A resolution enhancement should be taken into consideration for further studies. Since microbial

activity occurs on the $\mu$m- to mm-scale, the resolution of 0.17 mm in this study might not be sufficient to refer to the small-scalic dynamics of microbial growth rates in detail. Microbial activity is linked to thermodynamic soil processes, which could be detected by applying passive IRT. A further systematic enhancement of the measurement approach could help to contribute to a more systematic understanding of microbial activity dynamics from spatial and temporal perspectives.

# 5   Synopsis

## 5.1   Concluding Discussion

The present dissertation aimed to evaluate the potential of passive IRT as a technique to investigate microbial activity in soils. It concentrated on the development of a laboratory and data processing method to detect microbial growth rates accurately. This aim is pursued by evaluating thermal images to identify regions of the soil surface with higher mineralization rates indicated by increased heat. The analysis of spatial and temporal patterns was carried out on a micro, process scale. The method development concerning the detection of microbial activity in soils using passive IRT and the evaluation of the thermal images was improved by addressing three overarching open research questions, identified in section 1.3:

a. Can IRT be applied for the detection of microbial hot spots and hot moments in soils?

b. Does IRT enable the possibility to record physical soil properties?

c. Is passive IRT capable of detecting microbial characteristics in undisturbed samples?

The most important results and contributions of this thesis, answering these research questions, are summarized and addressed in the next section.

**a. Detection of hot spots and hot moments**
The three studies in sections 2-4 addressed the detection of microbial hot spots and hot moments in top- and subsoils at different stages of processing. Section 2 considered the general applicability of passive IRT and the evaluation of measured temperature variability in temporal and spatial terms of disturbed samples while

observing the rewetting effect. In section 3, a deeper look into the process level of hot spots and hot moments was given. In a targeted laboratory method development and data preparation procedure, an evaluation of the thermal properties of the disturbed soil samples was made. This was done for the most accurate detection of hot spots and hot moments, referred to as hot movements. Section 4 addressed hot spots and hot moments on a small-scale and stepwise explanatory approach. The surface temperature change was explained by various measurement techniques referring to the soil surface. Detailed statements were made about the thermally recorded spatio-temporal heat production.

All studies showed that in a controlled environment with constant air temperature and relative air humidity conditions, microscale temperature changes were recorded in spatio-temporal terms. These temperature changes were attributed to microbial activity.

In the first study, a comparison was made between sterile and non-sterile disturbed soil samples. It was demonstrated that the non-sterile soil samples exhibited a distinct temperature peak after rewetting, which was not found in the sterile samples. This hot moment was caused by the Birch effect, which was caused by the activation of dormant microorganisms within a few hours after rewetting. In a substrate-induced approach in the second study, temporal matches of microbial growth with soil respiration data were observed. The hot moment was recorded in a time window of 20 to 60 h after substrate addition under constant ambient conditions (relative air humidity > 95%).

From a spatial perspective, differences in temperature development could be highlighted. Those differences corresponded to a temperature increase of up to 1 K. The temperature changes were not homogeneously distributed on the soil surface

but were pronounced in hot spots, which also changed in time. These are shown in particular in the time-lapse in study 2. In study 3, those spatial changes were matched using further imaging techniques. In particular, photography was used to highlight the relationship to the SOC content of the soil. Temperature changes grouped by mean could also be attributed to the change in enzyme activity imaged by $\beta$-glucosidase activity. Areas of soil samples taken from a profile, which were characterized by high initial $\beta$-glucosidase activity, showed the greatest increase in mean surface temperatures (Table 4.5 on page 124-125).

The results of this thesis support findings of previous studies focusing on heat production in soils. Wadsö et al. (2013) found that heat production detected by isothermal calorimetry was moisture-dependent with less heat production at low moisture contents and more heat production at high moisture contents. A sudden increase in the soil moisture content, especially in dry soil samples, removed the limitation of the microorganisms and stimulated sudden growth, especially of the r-strategists (Borken et al., 2003; Kieft et al., 1987). This release of energy through catabolism was also measurable as heat increase using passive IRT. In the second study, glucose was used to remove the limitation of readily degradable C, which also caused an increase in microbial activity. The increased microbial activity can be attributed to the growth of r-strategists and was also recorded as catabolic heat energy (Blagodatskaya et al., 2007; Chakrawal et al., 2020). This heat energy development was mapped over space and time.

From a spatial point of view, mapping enzyme activity, e.g., $\beta$-glucosidase activity, is an appropriate measure to validate the detected heat production by passive IRT. Zhang et al. (2020) discussed in their study that enzyme activity increases at high C inputs and also contributes to heat production during metabolization processes. These findings can also be applied to study 3. In particular, areas with

initial high enzyme activity also turned out to be thermal hot spots as shown by the results of a k-mean cluster analysis.

A decisive point that can be derived from the analyzes presented in sections 2-4. Applying passive IRT to detect microbial hot spots and hot moments from catabolic heat generation with high resolution is highly promising. The focus is on the contribution of r-strategists, which cause the largest heat effect because of rapid growth. The major results show that the analysis of thermal soil dynamics contributes significantly to the study of energy turnover in the soil by metabolization processes.

## b. Recording physical soil properties

The results of the first study (section 2), in which the application of active IRT was examined to detect physical soil properties with a focus on soil moisture contents, were then included as an additional characterization of the soil samples in study 3 (section 4). A supervised partial least square regression applying an exponential function was used to approximate and calibrate soil moisture content to the temperature amplitude calculated from the temperature profile using the active IRT Lock-In mode. The main findings of the study were:

I) soil moisture contents, expressed as volumetric water content (VWC), could be explained by the temperature amplitude ($R^2$ up to 0.88) up to 30% VWC (Fig. 2.1),

II) different default moisture levels of one soil type could be observed accurately with small-scale spatial variations (Fig. 2.2), and

III) in a sequential recording of temperature amplitudes over time, soil drying could be determined until the soil was completely dry, and the dynamics of desiccation were captured in spatio-temporal perspective (Fig. 2.3).

Another physical quantity that was determined using active IRT was the phase angle, which can be used to approximate the structural richness of a soil surface.

Larger phase angles and high variability of it show a more diverse surface structure. With this measure, statements can be made about the density, texture, and evenness of the surface (Fig. 2.3 and Fig. 2.6).

The findings of the study presented in section 2 agree with and extend the results of multiple independent studies showing a strong correlation between soil physical and thermal properties (Abu-Hamdeh, 2003; Antonucci et al., 2011; Ochsner et al., 2001; Ren et al., 2003). However, these studies did not analyze the dynamics in soil drying or moisture change and did not explicitly consider soil types to evaluate the overall transferability of the results. While Antonucci et al. (2011) found in a systematic approach that the longer active IRT detection time was, the more accurate the results were. Detailed information on different soil types with varying texture, density, or SOC contents were not presented in their study and spatio-temporal dynamics not considered. Abu-Hamdeh (2003) found that the volumetric heat capacity of soils dictated the storage and movement of heat in soils and thus influenced the temperature heat flux in soils. It increased with higher soil moisture contents and soil density in dependence of soil texture. However, their study was limited in space (point measurement of specific soil volume) and neglected the temporal perspective. The systematic application of active IRT within section 2 enables a profound view of soil physical properties, considering their thermal properties. On this basis, observational evidence could be presented that soil moisture content and the structural conditions of the soil surface influenced the thermal properties of soils.

These findings strengthen the relevance of passive IRT approaches, especially regarding the detection of catabolic heat production, as Barros et al. (1995) had already shown the relationship between microbial activity and soil moisture contents. The results were also included in the subsequent study 3 in section 4.

## c. Microbial activity in undisturbed soil samples

In section 4, the spatial and temporal characteristics of heat production in undisturbed soil samples captured by passive IRT and determinants like soil moisture contents, surface color, enzyme activity, were analyzed at different levels of observation and from different perspectives. The undisturbed soil samples were analyzed concerning their temporal component of a substrate-induced increase in microbial activity. The spatial component was evaluated geostatistically by calculating the semivariance. Based on this, the relationship of further surface properties was statistically assessed using regression models and k-means clustering. The cluster groups of each surface property were analyzed by utilizing a subsequent ANOVA with Tukey's HSD post-hoc test within the glucose-treated samples. The thermal images were shown to capture hot spots and hot moments of microbial activity in spatial and temporal perspectives (c.f. Fig. 4.2 and Fig. 4.4 on pages 106 and 121, respectively). Geostatistically, however, no small-scale hot spots could be detected since large-scale effects overlay them (c.f. Fig. 4.3 on page 113). When considering the explanatory surface properties, such as temperature amplitude, phase angle, soil color parameters, and $\beta$-glucosidase activity, soil color parameters determined heat production. The temperature amplitude also showed a uniform relationship by applying a stepwise backward regression (c.f. Table 4.4). Since the explanatory power of the regression results was not sufficient, deeper correlations were sought using a cluster analysis on the passive IRT thermograms, which were also applied to the explanatory parameters. Temperature amplitude and soil color parameters had the expected effects on heat production (c.f. Table 4.4). The patterns on the millimeter and centimeter scale, like SOC contents, soil moisture, and surface structure, determined the measured surface temperatures by passive IRT. The $\beta$-glucosidase activity also indicated a connection to the pixelwise mean surface temperature.

The study builds on the findings of 2 and 3, as well as numerous other studies showing how heat is produced in soil samples and what determinants have an im-

pact on the measured surface temperatures (Abu-Hamdeh, 2003; Antonucci et al., 2011; Ochsner et al., 2001; Sanchez et al., 2011). It supports the findings of multiple studies that show a strong dependence of soil thermal properties and their characteristics on heat production (Barros et al., 1995; Zhang et al., 2020). However, these findings were based on point measurements of a specific soil volume that may not capture spatio-temporal soil dynamics of undisturbed soil samples and thus the entire complexity of the system. Kluge et al. (2013) applied passive IRT as a non-contact approach to detect soil microbial activity, but in disturbed soil samples. However, none of the recent studies on microbial activity enabled the spatio-temporal detection of heat production induced by catabolic activity by microorganisms in undisturbed soil samples. They showed the relationship to further spatial soil surface characteristics. This is the strength and novelty of the study presented in section 4.

The study is conducted on the microscale that enables high-resolution imaging in spatial and temporal perspectives. The application of passive IRT shows promise as an approach to monitor the microbial activity of undisturbed soil samples that produce heat, particularly in the turnover of readily available soil material. It underlines the usefulness of spatio-temporal approaches and multivariate statistics to predict soil microbial activity and possibly initiates a positive trend of their application frequency.

## 5.2 Outlook

The results of this thesis showed that the detection of microbial activity in hot spots and hot moments is possible using a passive IRT approach under consideration of specific ambient conditions. Influencing factors due to the physical properties of the soil, as well as the environment, affect the thermal capture of heat production

in the soil, which are attributed to catabolic activity. Comparative measurements using active IRT, soil color parameters, or zymography increased the understanding of soil surface thermograms. Advanced process and system understanding allows a better parameterization of soil microbial activity, and thus more accurate predictions of heat production in hot spots and hot moments. However, not all processes and advances in their understanding could be obtained in the studies in sections 2–4, and thus not all knowledge gaps could be filled concerning heat production in soils. Future observational studies may focus on improving comparability with additional spatial, temporal, and spatio-temporal data sets to facilitate the detection of dynamic processes in the soil on the centimeter scale. This may be achieved by adjusting the spatial and temporal scales of the passive IRT measurements by increasing the temporal resolution up to its maximum of 60 Hz and applying a higher spatial resolution by, e.g., using a macro lens for a resolution up to 17 $\mu$m. These scales could allow more accurate detection of microbial activity, as found on the micrometer to millimeter scale (Kuzyakov and Blagodatskaya, 2015; Nunan et al., 2003), and currently used resolutions had no sufficiently detailed output. This would allow a more focused view of microbial activity and allow spatial dependencies to be highlighted, as Nunan et al. (2003) had shown in a microscopic approach.

A complete scientific understanding of heat production detected by passive IRT requires knowledge on interactions between various microscale processes, as well as feedbacks with dynamical components of the system. As these processes may buffer or amplify each other, improved understanding of the individual processes might be obtained by applying further measurement techniques for understanding the influence of the diversity of microbial community structure and their dynamical system (Chakrawal et al., 2020; Kuzyakov and Blagodatskaya, 2015; Tecon and Or, 2017). A promising path forward could be the determination of spatio-temporal $CO_2$ evolution on soil surface using the PreSens-System (PreSens Precision Sensing

GmbH, Regensburg, Germany). Fluorescence imaging enables the detection of high-resolution $CO_2$ evolution to intersect fast SOM turnover rates with catabolic heat production (Blossfeld et al., 2013; Rubol et al., 2016). Analysis of further enzymes associated with the N- or C-cycle, e.g., xylosidase, chitinase, or acid phosphatase, in a zymography approach is also an essential advance to get direct insights into the microbial community composition producing heat (Boeddinghaus et al., 2015; Heitkötter and Marschner, 2018a). Zymography can be combined with a subsequent quantitative polymerase chain reaction (qPCR) analysis to get information on the abundance of genes and transcripts of microbial community structure in hot spot and non-hot spot areas of soil profile sections (Barnard et al., 2013).

Such studies aim to understand in detail the evolution of heat in the soil and quantify microorganisms using passive IRT and assign them to groups according to functionality. The use of different substrates apart from glucose, such as citric acid, glucose combined with N, as done by Heitkötter et al. (2017), or the addition of pollutants, as shown by Kluge et al. (2013), can help evaluate the inhibition of microbial life by passive IRT as a holistic approach to the non-invasive detection of microbial activity in undisturbed soil samples.

## 5.3   Summary

Heat production is a critical component of organic matter decomposition as a measure for microbial activity in the soil C turnover. Yet, it contributes the largest uncertainty to estimate spatio-temporal dynamics of metabolic and energetic processes in the pedosphere due to technical and methodical limitations. The high complexity of the processes involved, complex linkages to microbiological processes and conditions, temporal and spatial variations, and the microscale perspective on which the processes occur are major contributors to this uncertainty. Reducing this

uncertainty is critical to improve the accuracy of future process understanding of soil metabolism.

The central aim of this thesis was to advance the application of passive IRT as a measurement technique to capture soil microbial activity by spatio-temporal analysis of heat production, the statistical implications, and the determinants of heat production. Three overarching open research questions were identified and addressed within this thesis:

a. Can IRT be applied for the detection of microbial hot spots and hot moments in soils?

b. Does IRT enable the possibility to record physical soil properties?

c. Is passive IRT capable of detecting microbial characteristics in undisturbed samples?

Three studies were presented that addressed these research questions at different stages of methodological development, with a particular emphasis on spatial and temporal patterns. The following are the major results of the thesis:

a. Microbial hot spots and hot moments are determined by heat production and are detectable by passive IRT under certain ambient conditions

- In a closed system with high relative air humidity (above 95%) with constant ambient air temperature, increased microbial heat production could be determined. At these ambient conditions, evaporation from the ground surfaces is the lowest, and thus the measured surface temperature is the least affected.

- Increased microbial activity was detectable since the primary microbial activity was superimposed by physical properties, like evapotranspiration, in terms of the Birch effect in the first hours after soil rewetting

or in a substrate-induced approach applying glucose to soil surfaces with temperature increase between 20 and 60 h after application.

- Microbial hot spots and hot moments were made visible in temporal and spatial perspectives. Temperature increases up to 1 K could be determined on a millimeter-scale in a period of about 1 h in a minutely sequential recording.

- Comparative measurements referring to the temporal perspective had shown a good agreement of the periods of increased temperature development and increased metabolization rates using respiration curves. From a spatial perspective, color parameters and enzyme activity showed that physical and biological properties also determined the temperature development spatially.

b. Soil physical properties are detectable using active IRT

- The active IRT approach (Lock-In mode) explained up to 88% of the soil moisture variations at moisture content up to 30% VWC. It was possible to record spatial differences in soil moisture content and changes over time due to, e.g., drying of the soil surface.

- Using active IRT, the phase angle, as a measure of the surface structure, could be calculated. This measure helps to interpret the surface temperature since the bulk density, texture, and evenness of the surface could be approximated.

c. Detecting hot spots and hot moments in undisturbed soil samples

- Temporal characteristics of increased microbial activity could be measured with temperature increased up to 0.2 K between 35 and 46 h after glucose application on undisturbed soil samples under controlled ambient conditions with a relative air humidity above 95%.

- Spatial soil moisture contents, indicated by the temperature amplitude, showed that moister soil profile sections contributed to a higher temperature increase on the soil surface.

- Soil color revealed a connection between SOC content and distribution and surface temperature development. However, the microbiological relationships came to light, but the physical properties were also influenced.

- Soil profile sections characterized by high initial $\beta$-glucosidase activity showed higher temperature increases, revealing a connection between enzymatic soil properties and the subsequent catabolic activity.

The findings of this thesis advanced the scientific understanding of heat production in soils and enabled by the application of passive IRT, high-resolution analysis of spatio-temporal patterns of microbial activity on the millimeter scale. Future research may also profit from the technical insights of this thesis:

- Multivariate analysis utilizing advanced comparative measurements in spatial, temporal, but also spatio-temporal perspective related to both physical and microbiological properties

- Increase of the temporal and spatial resolution of the thermal imaging

- Determining the microbial community structure and its functioning

Based on this outline, a promising path forward for future advances in the scientific understanding of microbial activity and catabolic heat production through passive IRT was presented (see also Fig. 5.1). Results of a preliminary study showed that direct analysis of the key drivers of soil thermal properties in multivariate approaches might untangle the measured surface temperature regarding metabolism in soils and give quantitative estimates of microbial community structure and their dynamics in the pedosphere.
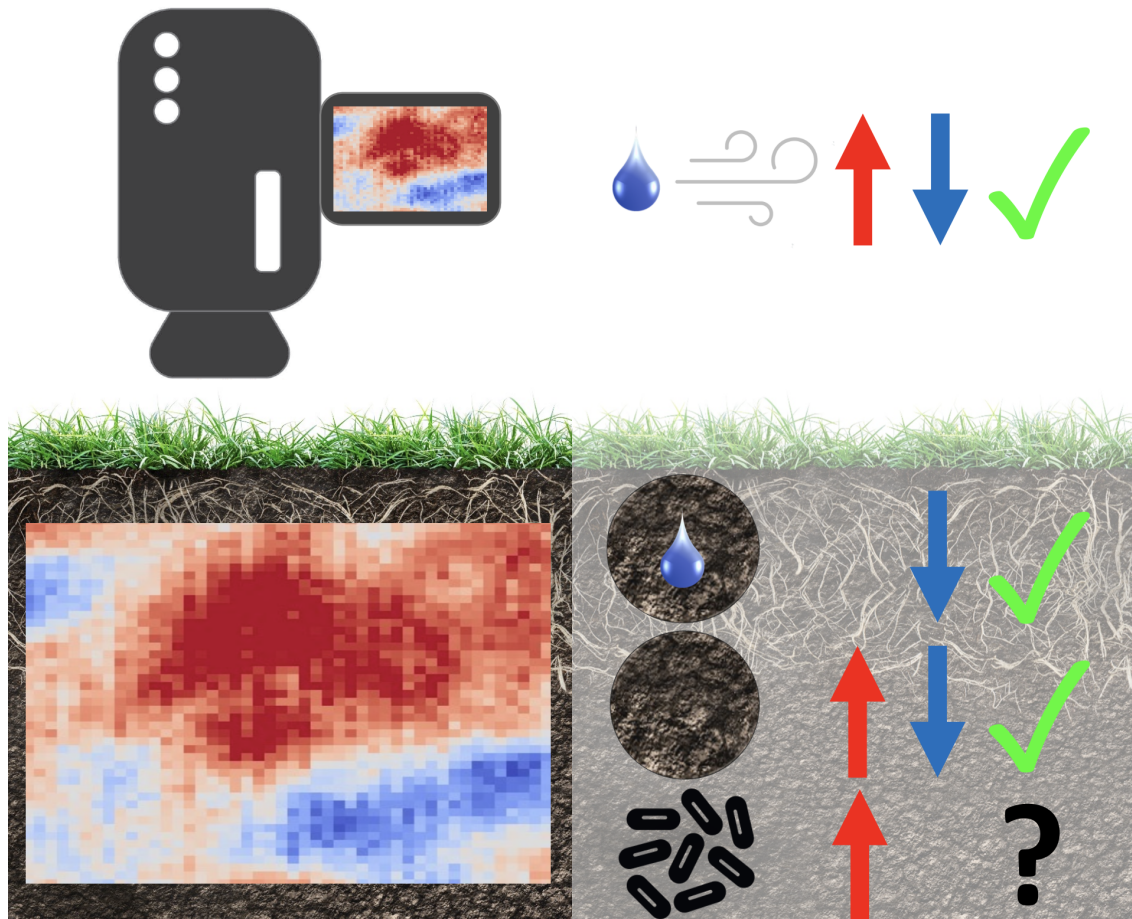
**Figure 5.1:** *Summary of major results of the thesis regarding the application of passive IRT. Ambient environmental conditions and effects on surface temperature were fully evaluated and discussed. Influences due to physical soil properties, such as soil moisture, but also surface structure were assessed. Heat production in microbial hot spots and hot moments were analyzed and evaluated. Some knowledge gaps have emerged from this research. Approaches to answer open questions about microbial heat production are summarized in section 5.2.*

# Bibliography

Abu-Hamdeh, N. H.: Thermal properties of soils as affected by density and water content, Biosystems Engineering, 86, 97–102, 2003.

Abu-Hamdeh, N. H. and Reeder, R. C.: Soil thermal conductivity: Effects of density, moisture, salt concentration, and organic matter, Soil Science Society of America Journal, 64, 1285–1290, 2000.

Aciego Pietri, J. C. and Brookes, P. C.: Substrate inputs and pH as factors controlling microbial biomass, activity and community structure in an arable soil, Soil Biology and Biochemistry, 41, 1396–1405, 2009.

Al-Shammiri, M.: Evaporation rate as a function of water salinity, Desalination, 150, 189–203, 2002.

Alnefaie, K. H. and Abu-Hamdeh, N. H.: Specific Heat and Volumetric Heat Capacity of Some Saudian Soils as affected by Moisture and Density, in: International Conference on Mechanics, Fluids, Heat, Elasticity and Electromagnetic Fields, Venice, Italy, 2013.

Altdorff, D. and Dietrich, P.: Combination of electromagnetic induction and gamma spectrometry using K-means clustering: A study for evaluation of site partitioning, Journal of Plant Nutrition and Soil Science, 175, 345–354, 2012.

An, N., Hemmati, S., and Cui, Y. J.: Assessment of the methods for determining net radiation at different time-scales of meteorological variables, Journal of Rock Mechanics and Geotechnical Engineering, 9, 239–246, 2017.

Anderson, J. P. and Domsch, K. H.: Quantification of bacterial and fungal contributions to soil respiration, Archiv Fur Mikrobiologie, 93, 113–127, 1973.

Anderson, J. P. and Domsch, K. H.: A physiological method for the quantitative measurement of microbial biomass in soils, Soil Biology and Biochemistry, 10, 215–221, 1978.

Anderson, T. H.: Microbial eco-physiological indicators to asses soil quality, Agriculture Ecosystems and Environment, 98, 285–293, 2003.

Anderson, T. H. and Domsch, K. H.: Carbon assimilation and microbial activity in soil, Zeitschrift Fur Pflanzenernahrung Und Bodenkunde, 149, 457–468, 1986.

Angert, A., Yakir, D., Rodeghiero, M., Preisler, Y., Davidson, E. A., and Weiner, T.: Using $O_2$ to study the relationships between soil $CO_2$ efflux and soil respiration, Biogeosciences, 12, 2089–2099, 2015.

Antonucci, F., Pallottino, F., Costa, C., Rimatori, V., Giorgi, S., Papetti, P., and Menesatti, P.: Development of a Rapid Soil Water Content Detection Technique Using Active Infrared Thermal Methods for In-Field Applications, Sensors, 11, 10 114–10 128, 2011.

Antonucci, F., Menesatti, P., Iori, A., Pallottino, F., D'Egidio, M. G., and Costa, C.: Thermographic medium-far ground-based proximal sensing for in-field wheat Stagonospora nodorum blotch detection, Journal of Plant Diseases and Protection, 120, 205–208, 2013.

Askaer, L., Elberling, B., Glud, R. N., Kuhl, M., Lauritsen, F. R., and Joensen, H. R.: Soil heterogeneity effects on $O_2$ distribution and $CH_4$ emissions from wetlands: In situ and mesocosm studies with planar $O_2$ optodes and membrane inlet mass spectrometry, Soil Biology and Biochemistry, 42, 2254–2265, 2010.

Avdelidis, N. P., Almond, D. P., Dobbinson, A., Hawtin, B. C., Ibarra-Castanedo, C., and Maldague, X.: Aircraft composites assessment by means of transient thermal NDT, Progress in Aerospace Sciences, 40, 143–162, 2004.

Axelsson, S. R. J.: On soil moisture mapping using IR-thermography, 1988.

Bagavathiappan, S., Lahiri, B. B., Saravanan, T., Philip, J., and Jayakumar, T.: Infrared thermography for condition monitoring - A review, Infrared Physics and Technology, 60, 35–55, 2013.

Balaras, C. A. and Argiriou, A. A.: Infrared thermography for building diagnostics, Energy and Buildings, 34, 171–183, 2002.

Baldrian, P., Merhautova, V., Petrankova, M., Cajthaml, T., and Snajdr, J.: Distribution of microbial biomass and activity of extracellular enzymes in a hardwood forest soil reflect soil moisture content, Applied Soil Ecology, 46, 177–182, 2010.

Barnard, R. L., Osborne, C. A., and Firestone, M. K.: Responses of soil bacterial and fungal communities to extreme desiccation and rewetting, Isme Journal, 7, 2229–2241, 2013.

Barreira, E. and Almeida, R.: Drying evaluation using infrared thermography, 2015.

Barros, N., Gomezorellana, I., Feijoo, S., and Balsa, R.: The effect of soil-moisture on soil microbial activity studied by microcalorimetry, Thermochimica Acta, 249, 161–168, 1995.

Barros, N., Salgado, J., and Feijoo, S.: Calorimetry and soil, Thermochimica Acta, 458, 11–17, 2007.

Barros, N., Feijoo, S., and Hansen, L. D.: Calorimetric determination of metabolic heat, $CO_2$ rates and the calorespirometric ratio of soil basal metabolism, Geoderma, 160, 542–547, 2011.

Barros, N., Hansen, L. D., Pinero, V., and Vikegard, P.: Calorimetry measures the response of soil organic matter biodegradation to increasing temperature, Journal of Thermal Analysis and Calorimetry, 123, 2397–2403, 2016.

Beare, M. H., Neely, C. L., Coleman, D. C., and Hargrove, W. L.: A substrate-induced respiration (SIR) method for measurement of fungal and bacterial biomass on plant residues, Soil Biology and Biochemistry, 22, 585–594, 1990.

Benasher, J., Matthias, A. D., and Warrick, A. W.: Assessment of evaporation from bare soil by infrared thermography, Soil Science Society of America Journal, 47, 185–191, 1983.

Bhogal, A., Nicholson, F. A., and Chambers, B. J.: Organic carbon additions: effects on soil bio-physical and physico-chemical properties, European Journal of Soil Science, 60, 276–286, 2009.

Billings, S. A. and Ballantyne Iv, F.: How interactions between microbial resource demands, soil organic matter stoichiometry, and substrate reactivity determine the direction and magnitude of soil respiratory responses to warming, Global Change Biology, 19, 90–102, 2013.

Birch, H. F.: The effect of soil drying on humus decomposition and nitrogen availability, Plant and soil, 10, 9–31, 1958.

Bittelli, M.: Measuring Soil Water Content: A Review, Horttechnology, 21, 293–300, 2011.

Blagodatskaya, E. and Kuzyakov, Y.: Mechanisms of real and apparent priming effects and their dependence on soil microbial biomass and community structure: critical review, Biology and Fertility of Soils, 45, 115–131, 2008.

Blagodatskaya, E. and Kuzyakov, Y.: Active microorganisms in soil: Critical review of estimation criteria and approaches, Soil Biology and Biochemistry, 67, 192–211, 2013.

Blagodatskaya, E. V. and Anderson, T. H.: Interactive effects of pH and substrate

quality on the fungal-to-bacterial ratio and $qCO_2$ of microbial communities in forest soils, Soil Biology and Biochemistry, 30, 1269–1274, 1998.

Blagodatskaya, E. V., Blagodatsky, S. A., Anderson, T. H., and Kuzyakov, Y.: Priming effects in Chernozem induced by glucose and N in relation to microbial growth strategies, Applied Soil Ecology, 37, 95–105, 2007.

Blossfeld, S., Schreiber, C. M., Liebsch, G., Kuhn, A. J., and Hinsinger, P.: Quantitative imaging of rhizosphere pH and $CO_2$ dynamics with planar optodes, Annals of Botany, 112, 267–276, 2013.

Boeddinghaus, R. S., Nunan, N., Berner, D., Marhan, S., and Kandeler, E.: Do general spatial relationships for microbial biomass and soil enzyme activities exist in temperate grassland soils?, Soil Biology and Biochemistry, 88, 430–440, 2015.

Borken, W. and Matzner, E.: Reappraisal of drying and wetting effects on C and N mineralization and fluxes in soils, Global Change Biology, 15, 808–824, 2008.

Borken, W., Davidson, E. A., Savage, K., Gaudinski, J., and Trumbore, S. E.: Drying and wetting effects on carbon dioxide release from organic horizons, Soil Science Society of America Journal, 67, 1888–1896, 2003.

Braissant, O., Wirz, D., Göpfert, B., and Daniels, A. U.: Use of isothermal microcalorimetry to monitor microbial activities, FEMS Microbiology Letters, 303, 1–8, 2010.

Bristow, K. L.: Measurement of thermal properties and water content of unsaturated sandy soil using dual-probe heat-pulse probes, Agricultural and Forest Meteorology, 89, 75–84, 1998.

Brockett, B. F. T., Prescott, C. E., and Grayston, S. J.: Soil moisture is the major factor influencing microbial community structure and enzyme activities across

seven biogeoclimatic zones in western Canada, Soil Biology and Biochemistry, 44, 9–20, 2012.

Busse, G., Wu, D., and Karpen, W.: Thermal wave imaging with phase sensitive modulated thermography, Journal of Applied Physics, 71, 3962–3965, 1992.

Bölscher, T., Wadsö, L., Börjesson, G., and Herrmann, A. M.: Differences in substrate use efficiency: impacts of microbial community composition, land use management, and substrate complexity, Biology and Fertility of Soils, 52, 547–559, 2016.

Bölscher, T., Paterson, E., Freitag, T., Thornton, B., and Herrmann, A. M.: Temperature sensitivity of substrate-use efficiency can result from altered microbial physiology without change to community composition, Soil Biology and Biochemistry, 109, 59–69, 2017.

Cambardella, C. A., Moorman, T. B., Novak, J. M., Parkin, T. B., Karlen, D. L., Turco, R. F., and Konopka, A. E.: Field-Scale Variability of Soil Properties in Central Iowa Soils, Soil Science Society of America Journal, 58, 1501–1511, 1994.

Chakrawal, A., Herrmann, A. M., Santruckova, H., and Manzoni, S.: Quantifying microbial metabolism in soils using calorespirometry - A bioenergetics perspective, Soil Biology and Biochemistry, 148, 21, 2020.

Chen, R., Senbayram, M., Blagodatsky, S., Myachina, O., Dittert, K., Lin, X., Blagodatskaya, E., and Kuzyakov, Y.: Soil C and N availability determine the priming effect: microbial N mining and stoichiometric decomposition theories, Global Change Biology, 20, 2356–2367, 2014.

Ciais, P., Sabine, C., Bala, G., Bopp, L., Brovkin, V., Canadell, J., Chhabra, A., DeFries, R., Galloway, J., and Heimann, M.: Carbon and other biogeochemical

cycles, in: Climate change 2013: the physical science basis. Contribution of Working Group I to the Fifth Assessment Report of the Intergovernmental Panel on Climate Change, pp. 465–570, Cambridge University Press, 2014.

Critter, S. A. M., Simoni, J. D., and Airoldi, C.: Microcalorimetric study of glucose degradation in some brazilian soils, Thermochimica Acta, 232, 145–154, 1994.

Critter, S. A. M., Freitas, S. S., and Airoldi, C.: Calorimetry versus respirometry for the monitoring of microbial activity in a tropical soil, Applied Soil Ecology, 18, 217–227, 2001.

De Vries, D. A.: Simultaneous transfer of heat and moisture in porous media, Eos, Transactions American Geophysical Union, 39, 909–916, 1958.

De Vries, D. A.: Thermal properties of soils, Physics of plant environment, 1963.

Dechesne, A., Pallud, C., and Grundmann, G. L.: Spatial distribution of bacteria at the microscale in soil, The Spatial Distribution of Microbes in the Environment, pp. 87–107, 2007.

Don, A., Steinberg, B., Schoening, I., Pritsch, K., Joschko, M., Gleixner, G., and Schulze, E. D.: Organic carbon sequestration in earthworm burrows, Soil Biology and Biochemistry, 40, 1803–1812, 2008.

Drotz, S. H., Sparrman, T., Nilsson, M. B., Schleucher, J., and Oquist, M. G.: Both catabolic and anabolic heterotrophic microbial activity proceed in frozen soils, Proceedings of the National Academy of Sciences of the United States of America, 107, 21 046–21 051, 2010.

Ekschmitt, K., Liu, M. Q., Vetter, S., Fox, O., and Wolters, V.: Strategies used by soil biota to overcome soil organic matter stability - why is dead organic matter left over in the soil?, Geoderma, 128, 167–176, 2005.

Fierer, N., Schimel, J. P., and Holden, P. A.: Variations in microbial community composition through two soil depth profiles, Soil Biology and Biochemistry, 35, 167–176, 2003.

Fierer, N., Bradford, M. A., and Jackson, R. B.: Toward an ecological classification of soil bacteria, Ecology, 88, 1354–1364, 2007.

Fokaides, P. A. and Kalogirou, S. A.: Application of infrared thermography for the determination of the overall heat transfer coefficient (U-Value) in building envelopes, Applied Energy, 88, 4358–4365, 2011.

Franzluebbers, A. J.: Water infiltration and soil structure related to organic matter and its stratification with depth, Soil and Tillage Research, 66, 197–205, 2002.

Gansert, D. and Blossfeld, S.: The application of novel optical sensors (optodes) in experimental plant ecology, in: Progress in botany, pp. 333–358, Springer, 2008.

Ghuman, B. and Lal, R.: Thermal conductivity, thermal diffusivity, and thermal capacity of some nigerian soils, Soil Science, 139, 74–80, 1985.

Griffiths, B. S., Ritz, K., Ebblewhite, N., and Dobson, G.: Soil microbial community structure: Effects of substrate loading rates, Soil Biology and Biochemistry, 31, 145–153, 1999.

Grinzato, E., Vavilov, V., and Kauppinen, T.: Quantitative infrared thermography in buildings, Energy and Buildings, 29, 1–9, 1998.

Grinzato, E., Ludwig, N., Cadelano, G., Bertucci, M., Gargano, M., and Bison, P.: Infrared Thermography for Moisture Detection: A Laboratory Study and In-situ Test, Materials Evaluation, 69, 97–104, 2011.

Grudzielanek, A. M. and Cermak, J.: Capturing Cold-Air Flow Using Thermal Imaging, Boundary-Layer Meteorology, 157, 321–332, 2015.

Grundmann, G. L. and Debouzie, D.: Geostatistical analysis of the distribution of $NH_4^+$ and $NO_2^-$-oxidizing bacteria and serotypes at the millimeter scale along a soil transect, Fems Microbiology Ecology, 34, 57–62, 2000.

Gu, B., Schmitt, J., Chen, Z., Liang, L., and McCarthy, J. F.: Adsorption and desorption of natural organic matter on iron oxide: mechanisms and models, Environmental Science and Technology, 28, 38–46, 1994.

Hain, M., Bartl, J., and Jacko, V.: Active infrared thermography in non-destructive testing, in: Proc. of the 7th International Conference on Measurement, Bratislava, Institute of Measurement Science SAS, pp. 339–343, 2009.

Han, J. B. and Zhou, Z. F.: Dynamics of Soil Water Evaporation during Soil Drying: Laboratory Experiment and Numerical Analysis, Scientific World Journal, 2013.

Heeraman, D. A., Hopmans, J. W., and Clausnitzer, V.: Three dimensional imaging of plant roots in situ with x-ray computed tomography, Plant and Soil, 189, 167–179, 1997.

Heil, J., Häring, V., Marschner, B., and Stumpe, B.: Advantages of fuzzy k-means over k-means clustering in the classification of diffuse reflectance soil spectra: A case study with West African soils, Geoderma, 337, 11–21, 2019.

Heil, J., Marschner, B., and Stumpe, B.: Digital photography as a tool for microscale mapping of soil organic carbon and iron oxides, Catena, 193, 12, 2020.

Heinze, S., Ludwig, B., Piepho, H. P., Mikutta, R., Don, A., Wordell-Dietrich, P., Helfrich, M., Hertel, D., Leuschner, C., Kirfel, K., Kandeler, E., Preusser, S., Guggenberger, G., Leinemann, T., and Marschner, B.: Factors controlling the variability of organic matter in the top- and subsoil of a sandy Dystric Cambisol under beech forest, Geoderma, 311, 37–44, 2018.

Heitkötter, J. and Marschner, B.: Soil zymography as a powerful tool for exploring hotspots and substrate limitation in undisturbed subsoil, Soil Biology and Biochemistry, 124, 210–217, 2018a.

Heitkötter, J. and Marschner, B.: Is There Anybody Out There? Substrate Availability Controls Microbial Activity outside of Hotspots in Subsoils, Soil Systems, 2, 12, 2018b.

Heitkötter, J., Heinze, S., and Marschner, B.: Relevance of substrate quality and nutrients for microbial C-turnover in top- and subsoil of a Dystric Cambisol, Geoderma, 302, 89–99, 2017.

Heng, B. C. P., Chandler, J. H., and Armstrong, A.: Applying close range digital photogrammetry in soil erosion studies, Photogrammetric Record, 25, 240–265, 2010.

Herrmann, A. M., Coucheney, E., and Nunan, N.: Isothermal Microcalorimetry Provides New Insight into Terrestrial Carbon Cycling, Environmental Science and Technology, 48, 4344–4352, 2014.

Hesselink van Suchtelen, F.: Energetics and microbiology of the soil, Arch Pflanzenbau, 7, 519–541, 1931.

Hirmas, D. R., Gimenez, D., Mome, E. A., Patterson, M., Drager, K., Platt, B. F., and Eck, D. V.: Quantifying Soil Structure and Porosity Using Three-Dimensional Laser Scanning, in: Digital Soil Morphometrics, edited by Hartemink, A. E. and Minasny, B., Progress in Soil Science, pp. 19–35, Springer, Dordrecht, 2016.

Hodge, A., Robinson, D., and Fitter, A.: Are microorganisms more effective than plants at competing for nitrogen?, Trends in Plant Science, 5, 304–308, 2000.

Holst, G. and Grunwald, B.: Luminescence lifetime imaging with transparent oxygen optodes, Sensors and Actuators B-Chemical, 74, 78–90, 2001.

Hovmöller, E.: The Trough-and-Ridge Diagram, Tellus, 1, 62–66, 1949.

Hummel, J. W., Sudduth, K. A., and Hollinger, S. E.: Soil moisture and organic matter prediction of surface and subsurface soils using an NIR soil sensor, Computers and Electronics in Agriculture, 32, 149–165, 2001.

Huth, S., Breitenstein, O., Huber, A., Dantz, D., Lambert, U., and Altmann, F.: Lock-in IR-thermography - A novel tool for material and device characterization, in: Gettering and Defect Engineering in Semiconductor Technology, edited by Raineri, V., Priolo, F., Kittler, M., and Richter, H., vol. 82-84 of *Solid State Phenomena*, pp. 741–746, Trans Tech Publications Ltd, Zurich-Uetikon, 2002.

Ibarra-Castanedo, C., Piau, J. M., Guilbert, S., Avdelidis, N. P., Genest, M., Bendada, A., and Maldague, X. P. V.: Comparative Study of Active Thermography Techniques for the Nondestructive Evaluation of Honeycomb Structures, Research in Nondestructive Evaluation, 20, 1–31, 2009.

Joergensen, R. and Wichern, F.: Alive and kicking: Why dormant soil microorganisms matter, Soil Biology and Biochemistry, 116, 419–430, 2018.

Joergensen, R. G., Mader, P., and Fliessbach, A.: Long-term effects of organic farming on fungal and bacterial residues in relation to microbial energy metabolism, Biology and Fertility of Soils, 46, 303–307, 2010.

Jones, D. L. and Murphy, D. V.: Microbial response time to sugar and amino acid additions to soil, Soil Biology and Biochemistry, 39, 2178–2182, 2007.

Jones, D. L., Kemmitt, S. J., Wright, D., Cuttle, S. P., Bol, R., and Edwards, A. C.: Rapid intrinsic rates of amino acid biodegradation in soils are unaffected by agricultural management strategy, Soil Biology and Biochemistry, 37, 1267–1275, 2005.

Jones, H. G.: Use of thermography for quantitative studies of spatial and temporal variation of stomatal conductance over leaf surfaces, Plant Cell and Environment, 22, 1043–1055, 1999.

Jílková, V., Jandová, K., and Kukla, J.: Responses of microbial activity to carbon, nitrogen, and phosphorus additions in forest mineral soils differing in organic carbon content, Biology and Fertility of Soils, 2021.

Kerridge, B. L., Hornbuckle, J. W., Christen, E. W., and Faulkner, R. D.: Using soil surface temperature to assess soil evaporation in a drip irrigated vineyard, Agricultural Water Management, 116, 128–141, 2013.

Khan, M. A. I., Ueno, K., Horimoto, S., Komai, F., Someya, T., Inoue, K., Tanaka, K., and Ono, Y.: CIELAB color variables as indicators of compost stability, Waste Management, 29, 2969–2975, 2009.

Kieft, T. L., Soroker, E., and Firestone, M. K.: Microbial biomass response to a rapid increase in water potential when dry soil is wetted, Soil Biology and Biochemistry, 19, 119–126, 1987.

Kluge, B., Peters, A., Krüger, J., and Wessolek, G.: Detection of soil microbial activity by infrared thermography (IRT), Soil Biology and Biochemistry, 57, 383–389, 2013.

Kuzyakov, Y. and Blagodatskaya, E.: Microbial hotspots and hot moments in soil: Concept & review, Soil Biology and Biochemistry, 83, 184–199, 2015.

Lal, R.: Soil Carbon Sequestration Impacts on Global Climate Change and Food Security, Science, 304, 1623–1627, 2004.

LaRowe, D. E. and Van Cappellen, P.: Degradation of natural organic matter: A thermodynamic analysis, Geochimica Et Cosmochimica Acta, 75, 2030–2042, 2011.

Lehmann, J., Solomon, D., Kinyangi, J., Dathe, L., Wirick, S., and Jacobsen, C.: Spatial complexity of soil organic matter forms at nanometre scales, Nature Geoscience, 1, 238–242, 2008.

Liang, C., Schimel, J. P., and Jastrow, J. D.: The importance of anabolism in microbial control over soil carbon storage, Nature Microbiology, 2, 6, 2017.

Liu, M.-Y., Chang, Q.-R., Qi, Y.-B., Liu, J., and Chen, T.: Aggregation and soil organic carbon fractions under different land uses on the tableland of the Loess Plateau of China, CATENA, 115, 19–28, 2014.

Ljungholm, K., Norén, B., and Wadsö, I.: Microcalorimetric Observations of Microbial Activity in Normal and Acidified Soils, Oikos, 33, 24–30, 1979.

Ludwig, N., Redaelli, V., Rosina, E., and Augelli, F.: Moisture detection in wood and plaster by IR thermography, Infrared Physics and Technology, 46, 161–166, 2004.

Lützow, M. v., Kögel-Knabner, I., Ekschmitt, K., Matzner, E., Guggenberger, G., Marschner, B., and Flessa, H.: Stabilization of organic matter in temperate soils: mechanisms and their relevance under different soil conditions – a review, European Journal of Soil Science, 57, 426–445, 2006.

Martz, M., Heil, J., Marschner, B., and Stumpe, B.: Effects of soil organic carbon (SOC) content and accessibility in subsoils on the sorption processes of the model pollutants nonylphenol (4-$n$-NP) and perfluorooctanoic acid (PFOA), Science of the Total Environment, 672, 162–173, 2019.

McClain, M. E., Boyer, E. W., Dent, C. L., Gergel, S. E., Grimm, N. B., Groffman, P. M., Hart, S. C., Harvey, J. W., Johnston, C. A., Mayorga, E., McDowell, W. H., and Pinay, G.: Biogeochemical hot spots and hot moments at the interface of terrestrial and aquatic ecosystems, Ecosystems, 6, 301–312, 2003.

McDowell, W. H., Zsolnay, A., Aitkenhead-Peterson, J. A., Gregorich, E. G., Jones, D. L., Jödemann, D., Kalbitz, K., Marschner, B., and Schwesig, D.: A comparison of methods to determine the biodegradable dissolved organic carbon from different terrestrial sources, Soil Biology and Biochemistry, 38, 1933–1942, 2006.

McNamara, N. P., Black, H. I. J., Beresford, N. A., and Parekh, N. R.: Effects of acute gamma irradiation on chemical, physical and biological properties of soils, Applied Soil Ecology, 24, 117–132, 2003.

Meola, C. and Carlomagno, G. M.: Recent advances in the use of infrared thermography, Measurement Science and Technology, 15, R27–R58, 2004.

Meola, C., Carlomagno, G. M., Squillace, A., and Vitiello, A.: Non-destructive evaluation of aerospace materials with lock-in thermography, Engineering Failure Analysis, 13, 380–388, 2006.

Mira, M., Valor, E., Boluda, R., Caselles, V., and Coll, C.: Influence of soil water content on the thermal infrared emissivity of bare soils: Implication for land surface temperature determination, Journal of Geophysical Research-Earth Surface, 112, 11, 2007.

Mollmann, K. P. and Vollmer, M.: Infrared thermal imaging as a tool in university physics education, European Journal of Physics, 28, S37–S50, 2007.

Moran, C. J., Pierret, A., and Stevenson, A. W.: X-ray absorption and phase contrast imaging to study the interplay between plant roots and soil structure, Plant and Soil, 223, 101–117, 2000.

Njoku, E. G., Jackson, T. J., Lakshmi, V., Chan, T. K., and Nghiem, S. V.: Soil moisture retrieval from AMSR-E, Ieee Transactions on Geoscience and Remote Sensing, 41, 215–229, 2003.

Nordgren, A.: Apparatus for the continuous, long-term monitoring of soil respiration rate in large numbers of samples, Soil Biology and Biochemistry, 20, 955–957, 1988.

Nunan, N., Wu, K. J., Young, I. M., Crawford, J. W., and Ritz, K.: Spatial distribution of bacterial communities and their relationships with the micro-architecture of soil, Fems Microbiology Ecology, 44, 203–215, 2003.

Obroślak, R. and Dorozhynskyy, O.: Selection of a semivariogram model in the study of spatial distribution of soil moisture, Journal of Water and Land Development, 35, 161–166, 2017.

Ochsner, T. E., Horton, R., and Ren, T. H.: A new perspective on soil thermal properties, Soil Science Society of America Journal, 65, 1641–1647, 2001.

Odgers, N. P., Libohova, Z., and Thompson, J. A.: Equal-area spline functions applied to a legacy soil database to create weighted-means maps of soil organic carbon at a continental scale, Geoderma, 189, 153–163, 2012.

Pausch, J. and Kuzyakov, Y.: Photoassimilate allocation and dynamics of hotspots in roots visualized by $^{14}$C phosphor imaging, Journal of Plant Nutrition and Soil Science, 174, 12–19, 2011.

Pierret, A., Kirby, M., and Moran, C.: Simultaneous X-ray imaging of plant root growth and water uptake in thin-slab systems, Plant and Soil, 255, 361–373, 2003.

Qiu, G. Y. and Ben-Asher, J.: Experimental Determination of Soil Evaporation Stages with Soil Surface Temperature, Soil Science Society of America Journal, 74, 13–22, 2010.

Quinn, T.: The calculation of the emissivity of cylindrical cavities giving near black-body radiation, British Journal of Applied Physics, 18, 1105, 1967.

Ranjit, S., Kang, K., and Kim, W.: Investigation of lock-in infrared thermography for evaluation of subsurface defects size and depth, International Journal of Precision Engineering and Manufacturing, 16, 2255–2264, 2015.

Rawls, W. J., Pachepsky, Y. A., Ritchie, J. C., Sobecki, T. M., and Bloodworth, H.: Effect of soil organic carbon on soil water retention, Geoderma, 116, 61–76, 2003.

Reischke, S., Rousk, J., and Baath, E.: The effects of glucose loading rates on bacterial and fungal growth in soil, Soil Biology and Biochemistry, 70, 88–95, 2014.

Ren, T., Ochsner, T. E., Horton, R., and Ju, Z.: Heat-Pulse Method for Soil Water Content Measurement, Soil Science Society of America Journal, 67, 1631–1634, 2003.

Rey, A., Petsikos, C., Jarvis, P., and Grace, J.: Effect of temperature and moisture on rates of carbon mineralization in a Mediterranean oak forest soil under controlled and field conditions, European Journal of Soil Science, 56, 589–599, 2005.

Rockland, L. B.: Saturated salt solutions for static control of relative humidity between 5°C and 40°C, Analytical Chemistry, 32, 1375–1376, 1960.

Rousk, J., Hill, P. W., and Jones, D. L.: Priming of the decomposition of ageing soil organic matter: concentration dependence and microbial control, Functional Ecology, 29, 285–296, 2015.

Ruamps, L. S., Nunan, N., and Chenu, C.: Microbial biogeography at the soil pore scale, Soil Biology and Biochemistry, 43, 280–286, 2011.

Rubol, S., Dutta, T., and Rocchini, D.: 2D visualization captures the local heterogeneity of oxidative metabolism across soils from diverse land-use, Science of the Total Environment, 572, 713–723, 2016.

Saidy, A. R., Smernik, R. J., Baldock, J. A., Kaiser, K., and Sanderman, J.: The sorption of organic carbon onto differing clay minerals in the presence and absence of hydrous iron oxide, Geoderma, 209-210, 15–21, 2013.

Salgado, J. C. S., Meleiro, L. P., Carli, S., and Ward, R. J.: Glucose tolerant and glucose stimulated $\beta$-glucosidases – A review, Bioresource Technology, 267, 704–713, 2018.

Sanchez, J. M., French, A. N., Mira, M., Hunsaker, D. J., Thorp, K. R., Valor, E., and Caselles, V.: Thermal Infrared Emissivity Dependence on Soil Moisture in Field Conditions, Ieee Transactions on Geoscience and Remote Sensing, 49, 4652–4659, 2011.

Schimel, J. and Schaeffer, S.: Microbial control over carbon cycling in soil, Frontiers in Microbiology, 3, 2012.

Schindelin, J., Arganda-Carreras, I., Frise, E., Kaynig, V., Longair, M., Pietzsch, T., Preibisch, S., Rueden, C., Saalfeld, S., Schmid, B., Tinevez, J.-Y., White, D. J., Hartenstein, V., Eliceiri, K., Tomancak, P., and Cardona, A.: Fiji: an open-source platform for biological-image analysis, Nature Methods, 9, 676–682, 2012.

Schlesinger, W. H. and Andrews, J. A.: Soil respiration and the global carbon cycle, Biogeochemistry, 48, 7–20, 2000.

Schmidt, H. and Eickhorst, T.: Detection and quantification of native microbial populations on soil-grown rice roots by catalyzed reporter deposition-fluorescence in situ hybridization, Fems Microbiology Ecology, 87, 390–402, 2014.

Schmidt, M. W. I., Torn, M. S., Abiven, S., Dittmar, T., Guggenberger, G., Janssens, I. A., Kleber, M., Kögel-Knabner, I., Lehmann, J., Manning, D. A. C.,

Nannipieri, P., Rasse, D. P., Weiner, S., and Trumbore, S. E.: Persistence of soil organic matter as an ecosystem property, nature, 478, 49–56, 2011.

Schwarz, K., Heitkötter, J., Heil, J., Marschner, B., and Stumpe, B.: The potential of active and passive infrared thermography for identifying dynamics of soil moisture and microbial activity at high spatial and temporal resolution, Geoderma, 327, 119–129, 2018.

Schwarz, K., Heil, J., Marschner, B., and Stumpe, B.: Hot movements on soil surfaces – Innovative insights into microbial dynamics using passive infrared thermography, Geoderma, 385, 114 879, 2021.

Schwertmann, U.: Relations Between Iron Oxides, Soil Color, and Soil Formation, in: Soil Color, pp. 51–69, 1993.

Sinsabaugh, R. L. and Follstad Shah, J. J.: Ecoenzymatic stoichiometry of recalcitrant organic matter decomposition: the growth rate hypothesis in reverse, Biogeochemistry, 102, 31–43, 2011.

Sinsabaugh, R. L., Lauber, C. L., Weintraub, M. N., Ahmed, B., Allison, S. D., Crenshaw, C., Contosta, A. R., Cusack, D., Frey, S., Gallo, M. E., Gartner, T. B., Hobbie, S. E., Holland, K., Keeler, B. L., Powers, J. S., Stursova, M., Takacs-Vesbach, C., Waldrop, M. P., Wallenstein, M. D., Zak, D. R., and Zeglin, L. H.: Stoichiometry of soil enzyme activity at global scale, Ecology Letters, 11, 1252–1264, 2008.

Skopp, J., Jawson, M. D., and Doran, J. W.: Steady-State Aerobic Microbial Activity as a Function of Soil-Water Content, Soil Science Society of America Journal, 54, 1619–1625, 1990.

Slaets, J. I., Boeddinghaus, R. S., and Piepho, H.: Linear mixed models and geo-

statistics for designed experiments in soil science: Two entirely different methods or two sides of the same coin?, European Journal of Soil Science, 72, 47–68, 2021.

Sparling, G.: Microcalorimetry and other methods to assess biomass and activity in soil, Soil Biology and Biochemistry, 13, 93–98, 1981.

Spohn, M. and Kuzyakov, Y.: Distribution of microbial- and root-derived phosphatase activities in the rhizosphere depending on P availability and C allocation - Coupling soil zymography with $^{14}$C imaging, Soil Biology and Biochemistry, 67, 106–113, 2013.

Spohn, M. and Kuzyakov, Y.: Spatial and temporal dynamics of hotspots of enzyme activity in soil as affected by living and dead roots - a soil zymography analysis, Plant and Soil, 379, 67–77, 2014.

Spohn, M., Carminati, A., and Kuzyakov, Y.: Soil zymography - A novel in situ method for mapping distribution of enzyme activity in soil, Soil Biology and Biochemistry, 58, 275–280, 2013.

Steinweg, J. M., Dukes, J. S., and Wallenstein, M. D.: Modeling the effects of temperature and moisture on soil enzyme activity: Linking laboratory assays to continuous field data, Soil Biology and Biochemistry, 55, 85–92, 2012.

Stoeckli, M., Staab, D., Wetzel, M., and Brechbuehl, M.: iMatrixSpray: A Free and Open Source Sample Preparation Device for Mass Spectrometric Imaging, CHIMIA International Journal for Chemistry, 68, 146–149, 2014.

Stumpe, B. and Marschner, B.: Factors controlling the biodegradation of 17 beta-estradiol, estrone and 17 alpha-ethinylestradiol in different natural soils, Chemosphere, 74, 556–562, 2009.

Sánchez-Marañón, M., Soriano, M., Melgosa, M., Delgado, G., and Delgado, R.:

Quantifying the effects of aggregation, particle size and components on the colour of Mediterranean soils, European Journal of Soil Science, 55, 551–565, 2004.

Tecon, R. and Or, D.: Biophysical processes supporting the diversity of microbial life in soil, Fems Microbiology Reviews, 41, 599–623, 2017.

Theodorakeas, P., Cheilakou, E., Ftikou, E., and Koui, M.: Passive and active infrared thermography: An overview of applications for the inspection of mosaic structures, 2015.

Tian, Q. X., Yang, X. L., Wang, X. G., Liao, C., Li, Q. X., Wang, M., Wu, Y., and Liu, F.: Microbial community mediated response of organic carbon mineralization to labile carbon and nitrogen addition in topsoil and subsoil, Biogeochemistry, 128, 125–139, 2016.

Torsvik, V., Sørheim, R., and Goksøyr, J.: Total bacterial diversity in soil and sediment communities — A review, Journal of Industrial Microbiology, 17, 170–178, 1996.

Trevors, J. T.: Sterilization and inhibition of microbial activity in soil, Journal of Microbiological Methods, 26, 53–59, 1996.

Unger, S., Máguas, C., Pereira, J. S., David, T. S., and Werner, C.: The influence of precipitation pulses on soil respiration - Assessing the "Birch effect" by stable carbon isotopes, Soil Biology and Biochemistry, 42, 1800–1810, 2010.

Usamentiaga, R., Venegas, P., Guerediaga, J., Vega, L., Molleda, J., and Bulnes, F. G.: Infrared Thermography for Temperature Measurement and Non-Destructive Testing, Sensors, 14, 12 305–12 348, 2014.

Utne, I. B., Brurok, T., and Rodseth, H.: A structured approach to improved condition monitoring, Journal of Loss Prevention in the Process Industries, 25, 478–488, 2012.

Vance, E. D., Brookes, P. C., and Jenkinson, D. S.: An extraction method for measuring soil microbial biomass-C, Soil Biology and Biochemistry, 19, 703–707, 1987.

Verstraeten, W. W., Veroustraete, F., van der Sande, C. J., Grootaers, I., and Feyen, J.: Soil moisture retrieval using thermal inertia, determined with visible and thermal spaceborne data, validated for European forests, Remote Sensing of Environment, 101, 299–314, 2006.

Villaseñor-Mora, C. and González-Vega, A.: Measuring soil water potential using IR thermal imaging, SPIE Newsroom, 1, 2015.

Viscarra Rossel, R. A. and Webster, R.: Predicting soil properties from the Australian soil visible–near infrared spectroscopic database, European Journal of Soil Science, 63, 848–860, 2012.

Viscarra Rossel, R. A., Minasny, B., Roudier, P., and McBratney, A. B.: Colour space models for soil science, Geoderma, 133, 320–337, 2006.

Viscarra Rossel, R. A., Fouad, Y., and Walter, C.: Using a digital camera to measure soil organic carbon and iron contents, Biosystems Engineering, 100, 149–159, 2008.

Viscarra Rossel, R. A., Behrens, T., Ben-Dor, E., Brown, D. J., Demattê, J. A. M., Shepherd, K. D., Shi, Z., Stenberg, B., Stevens, A., Adamchuk, V., Aïchi, H., Barthès, B. G., Bartholomeus, H. M., Bayer, A. D., Bernoux, M., Böttcher, K., Brodský, L., Du, C. W., Chappell, A., Fouad, Y., Genot, V., Gomez, C., Grunwald, S., Gubler, A., Guerrero, C., Hedley, C. B., Knadel, M., Morrás, H. J. M., Nocita, M., Ramirez-Lopez, L., Roudier, P., Campos, E. M. R., Sanborn, P., Sellitto, V. M., Sudduth, K. A., Rawlins, B. G., Walter, C., Winowiecki, L. A., Hong, S. Y., and Ji, W.: A global spectral library to characterize the world's soil, Earth-Science Reviews, 155, 198–230, 2016.

Vollmer, M. and Möllmann, K.: Fundamentals of infrared thermal imaging, Infrared Thermal Imaging: Fundamentals, Research and Applications, pp. 1–72, 2010.

Vor, T., Dyckmans, J., Flessa, H., and Beese, F.: Use of microcalorimetry to study microbial activity during the transition from oxic to anoxic conditions, Biology and Fertility of Soils, 36, 66–71, 2002.

Vos, M., Wolf, A. B., Jennings, S. J., and Kowalchuk, G. A.: Micro-scale determinants of bacterial diversity in soil, Fems Microbiology Reviews, 37, 936–954, 2013.

Wadsö, L., Johansson, S., Pilgård, A., and Alfredsen, G.: The activity of rot fungi (Postia placenta) during drying and rewetting cycles measured by isothermal calorimetry, Engineering in Life Sciences, 13, 536–540, 2013.

Wallbrink, C., Wade, S. A., and Jones, R.: The effect of size on the quantitative estimation of defect depth in steel structures using lock-in thermography, Journal of Applied Physics, 101, 8, 2007.

Wiggenhauser, H.: Active IR-applications in civil engineering, Infrared Physics and Technology, 43, 233–238, 2002.

Wu, D. and Busse, G.: Lock-in thermography for nondestructive evaluation of materials, Revue Générale de Thermique, 37, 693–703, 1998.

Yan, J., Pan, G., Li, L., Quan, G., Ding, C., and Luo, A.: Adsorption, immobilization, and activity of $\beta$-glucosidase on different soil colloids, J. Colloid and Interf. Sci., 348, 565–570, 2010.

Ye, R. and Wright, A. L.: Multivariate analysis of chemical and microbial properties in histosols as influenced by land-use types, Soil and Tillage Research, 110, 94–100, 2010.

Young, I. M. and Crawford, J. W.: Interactions and self-organization in the soil-microbe complex, Science, 304, 1634–1637, 2004.

Young, J. F.: Humidity control in the laboratory using salt solutions - a review, Journal of applied chemistry, 17, 241–245, 1967.

Zanetti, S. S., Cecílio, R. A., Alves, E. G., Silva, V. H., and Sousa, E. F.: Estimation of the moisture content of tropical soils using colour images and artificial neural networks, CATENA, 135, 100–106, 2015.

Zhang, S., Shao, M., and Li, D.: Prediction of soil moisture scarcity using sequential Gaussian simulation in an arid region of China, Geoderma, 295, 119–128, 2017.

Zhang, X., Kuzyakov, Y., Zang, H., Dippold, M. A., Shi, L., Spielvogel, S., and Razavi, B. S.: Rhizosphere hotspots: Root hairs and warming control microbial efficiency, carbon utilization and energy production, Soil Biology and Biochemistry, 148, 107 872, 2020.

Zhou, J., Wen, Y., Shi, L. L., Marshall, M. R., Kuzyakov, Y., Blagodatskaya, E., and Zang, H. D.: Strong priming of soil organic matter induced by frequent input of labile carbon, Soil Biology and Biochemistry, 152, 11, 2021.

# Appendix

## Appendix I

**Table A1.1:** *Relevant properties of soil samples used for the soil moisture calibration (experiment A1).*

| Soil Sample | SOC[a] | Sand[b] | Silt[b] | Clay[b] |
|:---:|:---:|:---:|:---:|:---:|
| | | [%] | | |
| A | 2.5 | 38 | 54 | 8 |
| B | 3.0 | 7 | 85 | 8 |
| C | 0.4 | 12 | 68 | 20 |
| 1 | 1.5 | 87 | 7 | 6 |
| 2 | 0.8 | 93 | 2 | 5 |
| 3 | 0.2 | 95 | 2 | 3 |
| 4 | 1.1 | 90 | 5 | 5 |
| 5 | 1.2 | 94 | 1 | 5 |
| 6 | 0.1 | 90 | 3 | 7 |
| 7 | 1.4 | 78 | 12 | 10 |
| 8 | 0.2 | 92 | 4 | 4 |
| 9 | 0.1 | 87 | 5 | 8 |
| 10 | 0.1 | 83 | 8 | 9 |
| 11 | 0.3 | 90 | 8 | 2 |
| 12 | 0.2 | 95 | 2 | 3 |
| 13 | 2.8 | 39 | 34 | 27 |
| 14 | 1.2 | 17 | 36 | 47 |
| 15 | 0.7 | 17 | 71 | 12 |
| 16 | 0.2 | 10 | 77 | 13 |
| 17 | 0.1 | 91 | 4 | 5 |

**Table A1.1:** *Relevant properties of soil samples used for the soil moisture calibration (experiment A1).*

| Soil Sample | SOC[a] | Sand[b] | Silt[b] | Clay[b] |
|:-----------:|:------:|:-------:|:-------:|:-------:|
|             |        | [%]     |         |         |
| 18          | 0.2    | 92      | 7       | 1       |
| 19          | 0.4    | 91      | 7       | 2       |
| 20          | 0.3    | 97      | 1       | 2       |
| 21          | 0.2    | 98      | 1       | 1       |
| 22          | 3.2    | 85      | 7       | 8       |
| 23          | 1.1    | 93      | 3       | 4       |
| 24          | 1.0    | 9       | 69      | 22      |
| 25          | 0.3    | 60      | 21      | 19      |
| 26          | 0.2    | 55      | 30      | 15      |
| 27          | 0.4    | 56      | 29      | 15      |
| 28          | 0.6    | 91      | 6       | 3       |
| 29          | 0.9    | 88      | 7       | 5       |
| 30          | 1.4    | 94      | 1       | 5       |
| 31          | 0.4    | 98      | 1       | 1       |
| 32          | 0.4    | 47      | 30      | 23      |
| 33          | 0.3    | 44      | 32      | 24      |
| 34          | 0.1    | 51      | 21      | 28      |
| 35          | 2.3    | 49      | 46      | 5       |
| 36          | 0.2    | 45      | 50      | 5       |
| 37          | 1.0    | 3       | 83      | 14      |
| 38          | 0.3    | 1       | 77      | 22      |
| 39          | 0.2    | 2       | 82      | 16      |
| 40          | 0.2    | 2       | 75      | 23      |

**Table A1.1:** *Relevant properties of soil samples used for the soil moisture calibration (experiment A1).*

| Soil Sample | SOC[a] | Sand[b] | Silt[b] | Clay[b] |
|:---:|:---:|:---:|:---:|:---:|
| | | [%] | | |
| 41 | 1.5 | 55 | 30 | 15 |
| 42 | 1.1 | 43 | 35 | 22 |
| 43 | 0.6 | 27 | 45 | 28 |
| 44 | 0.3 | 48 | 32 | 20 |
| 45 | 1.4 | 73 | 10 | 17 |
| 46 | 0.2 | 69 | 17 | 14 |
| 47 | 1.4 | 43 | 38 | 19 |
| 48 | 0.4 | 48 | 31 | 21 |
| 49 | 1.8 | 38 | 32 | 30 |

[a] Vario EL Elementar Analyser (Elementar Analysesysteme GmbH, Hanau, Germany

[b] Analysette (Fritsch GmbH, Idar-Oberstein, Germany)

# Appendix II
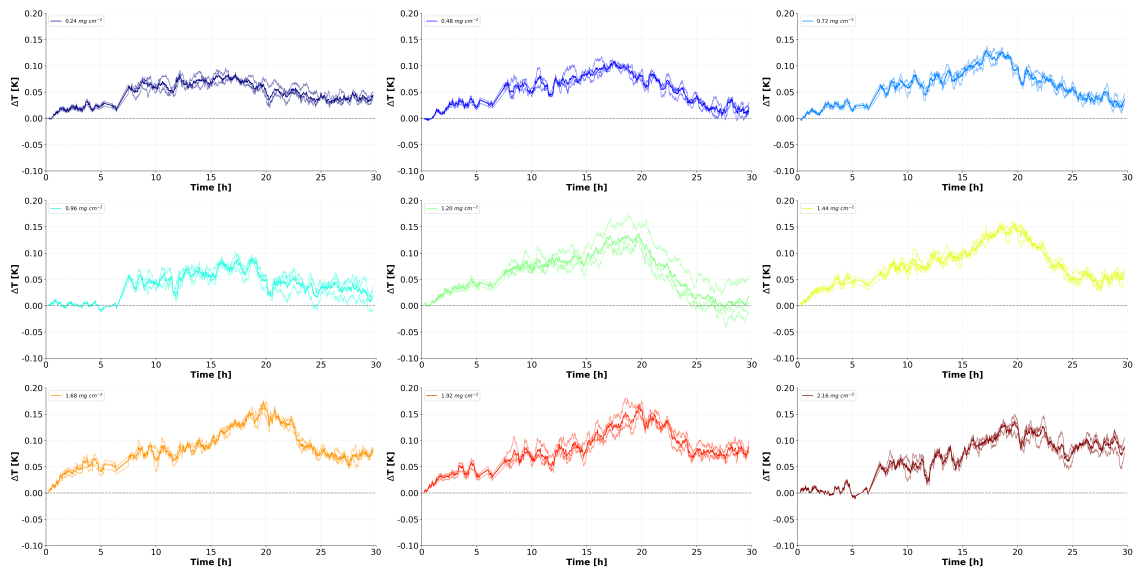


**Figure A2.1:** *Temporal courses of mean $\Delta T$ of the replicates and their mean values [K] of soil P after application of nine glucose concentrations ($G_P$) at CHC (Extension of Figure 2.1).*
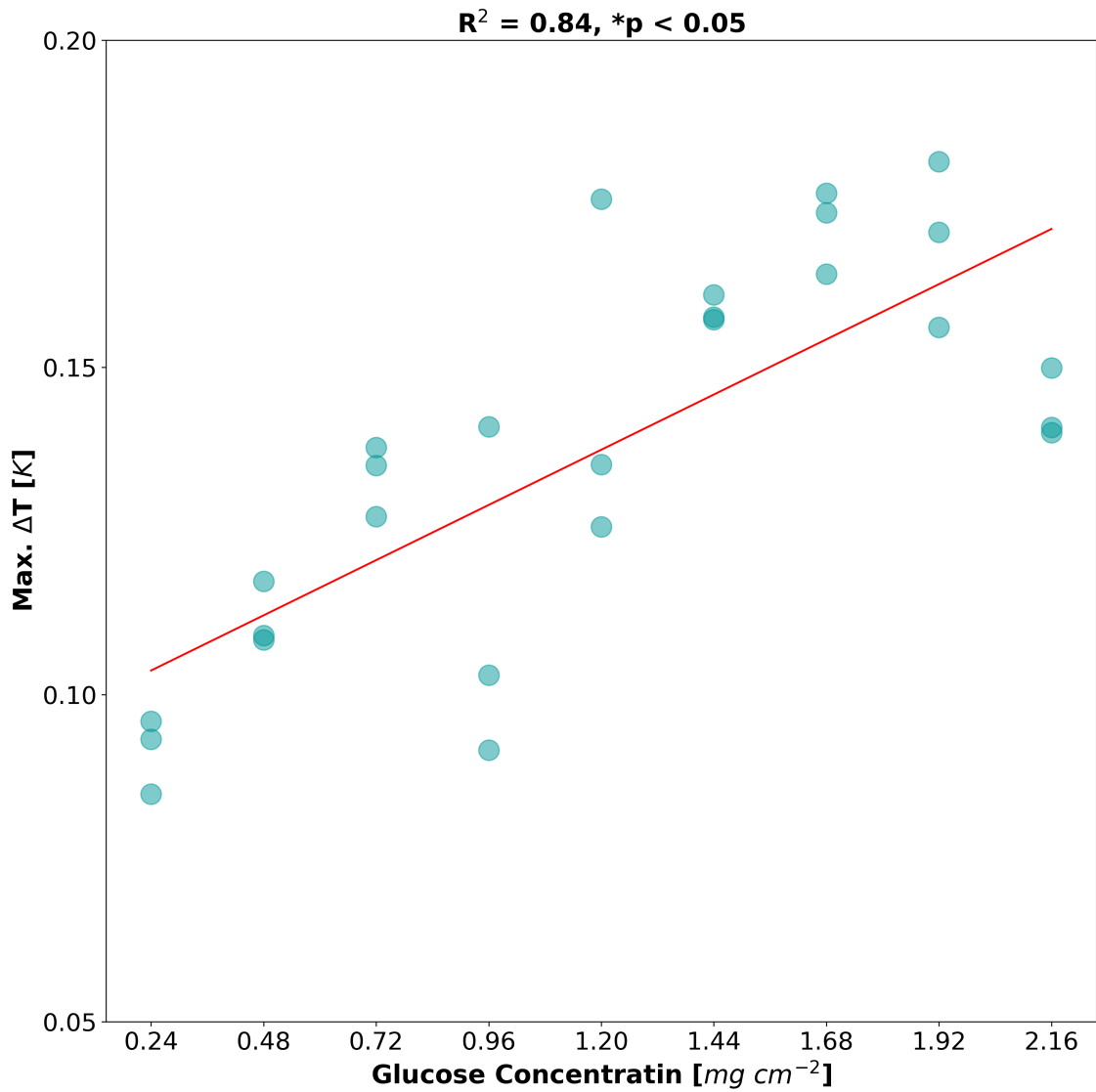
**Figure A2.2:** *Linear relationship between the nine glucose concentrations [mg cm⁻²] and maximum increase of ΔT [K] corresponding to the data in Figure 2.1.*

# Appendix III
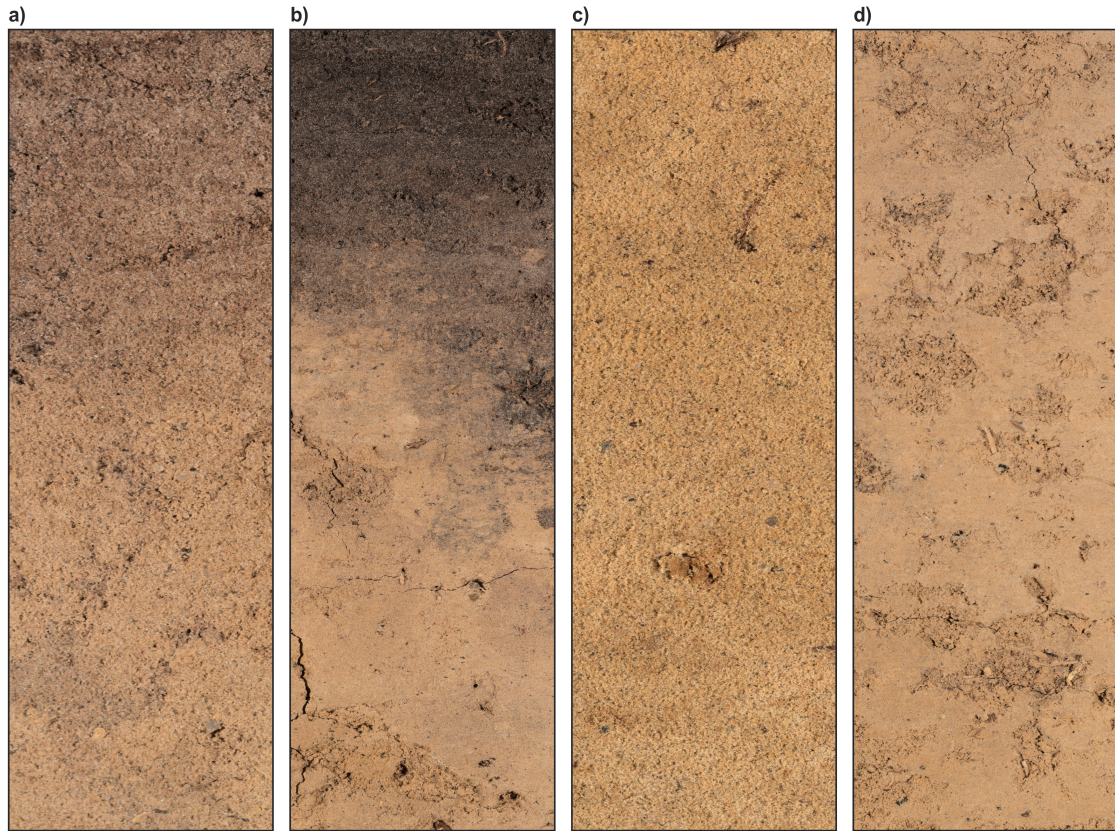


**Figure A3.1:** *RGB images of rewetted glucose-treated soil surfaces with a) Grinderwald topsoil ($G_T^+$), b) Kalwes topsoil ($K_T^+$), c) Grinderwald subsoil ($G_S^+$), and d) Kalwes subsoil ($K_S^+$).*
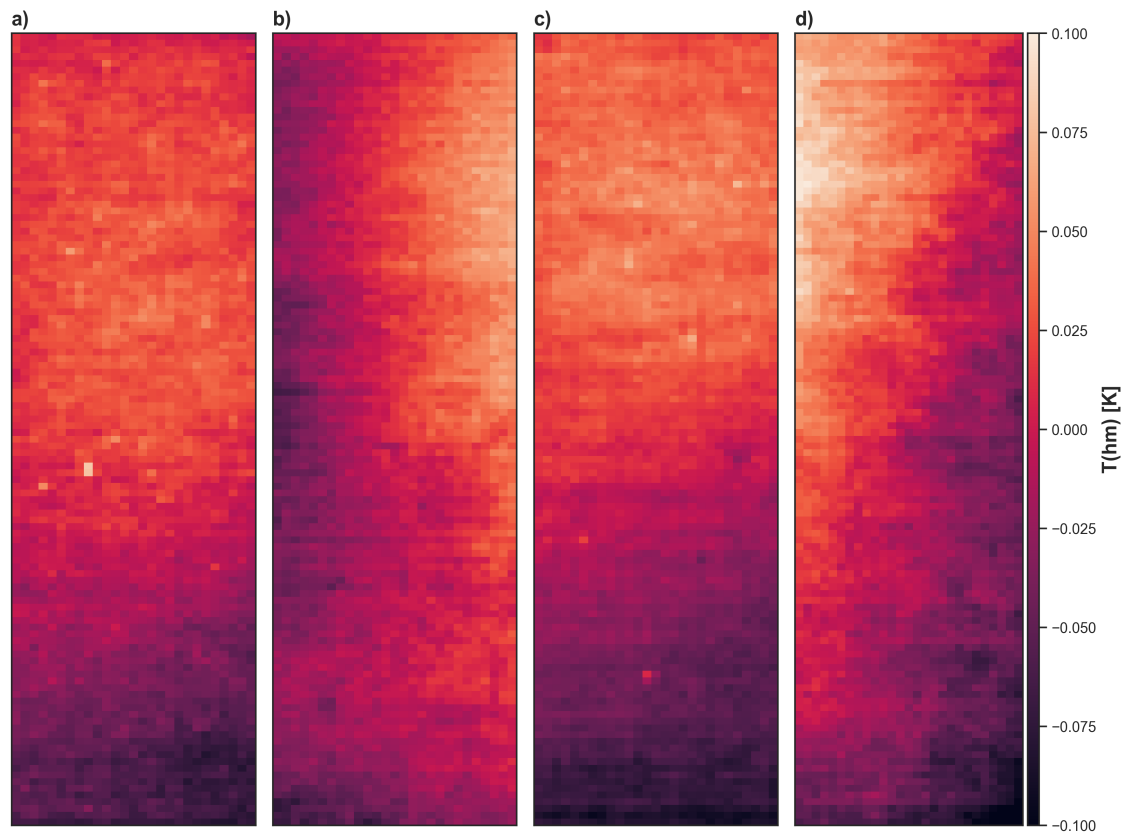
**Figure A3.2:** *Pixelwise mean values of passive IRT images of rewetted glucose-treated soil surfaces considering the time period of the hot moment ($T(hm)$) referring to Grinderwald topsoil ($G_T^+$) (a), Kalwes topsoil ($K_T^+$) (b), Grinderwald subsoil ($G_S^+$) (c), and Kalwes subsoil ($K_S^+$) (d).*
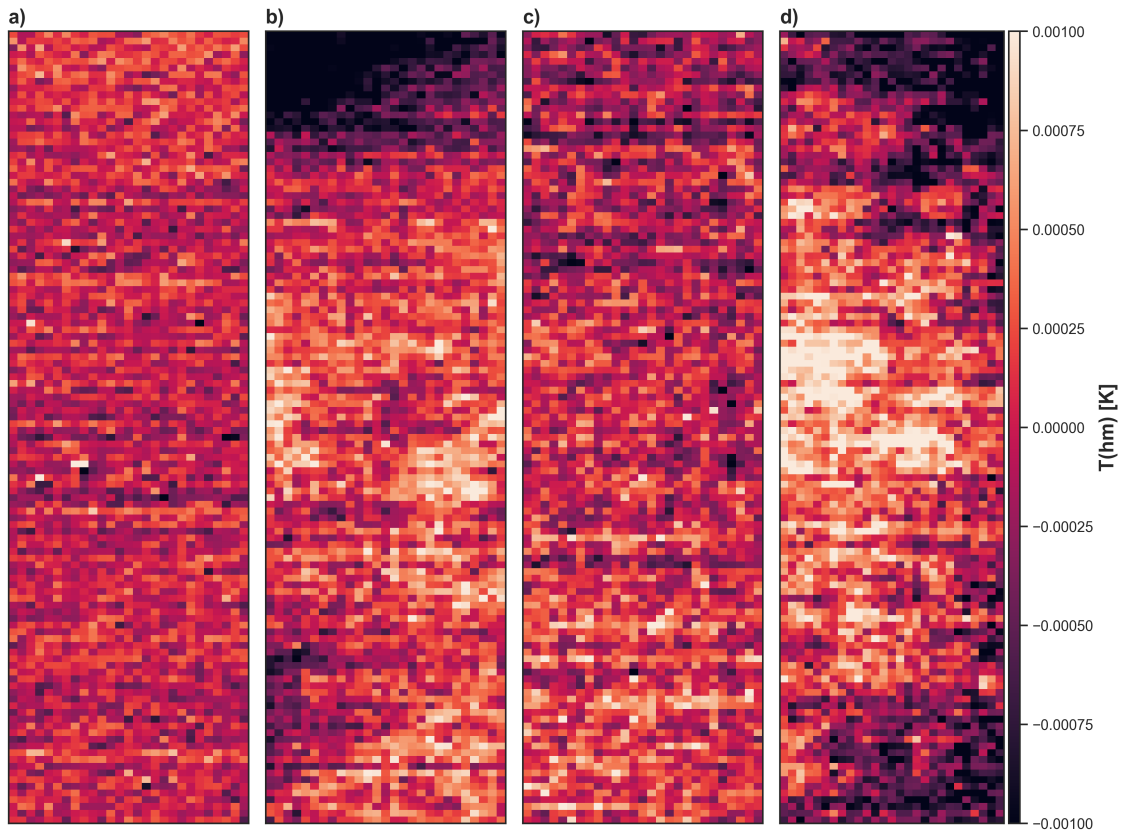
**Figure A3.3:** *Pixelwise variance of passive IRT images of rewetted glucose-treated soil surfaces considering the time period of the hot moment ($T(hm)$) referring to Grinderwald topsoil ($G_T^+$) (a), Kalwes topsoil ($K_T^+$) (b), Grinderwald subsoil ($G_S^+$) (c), and Kalwes subsoil ($K_S^+$) (d).*
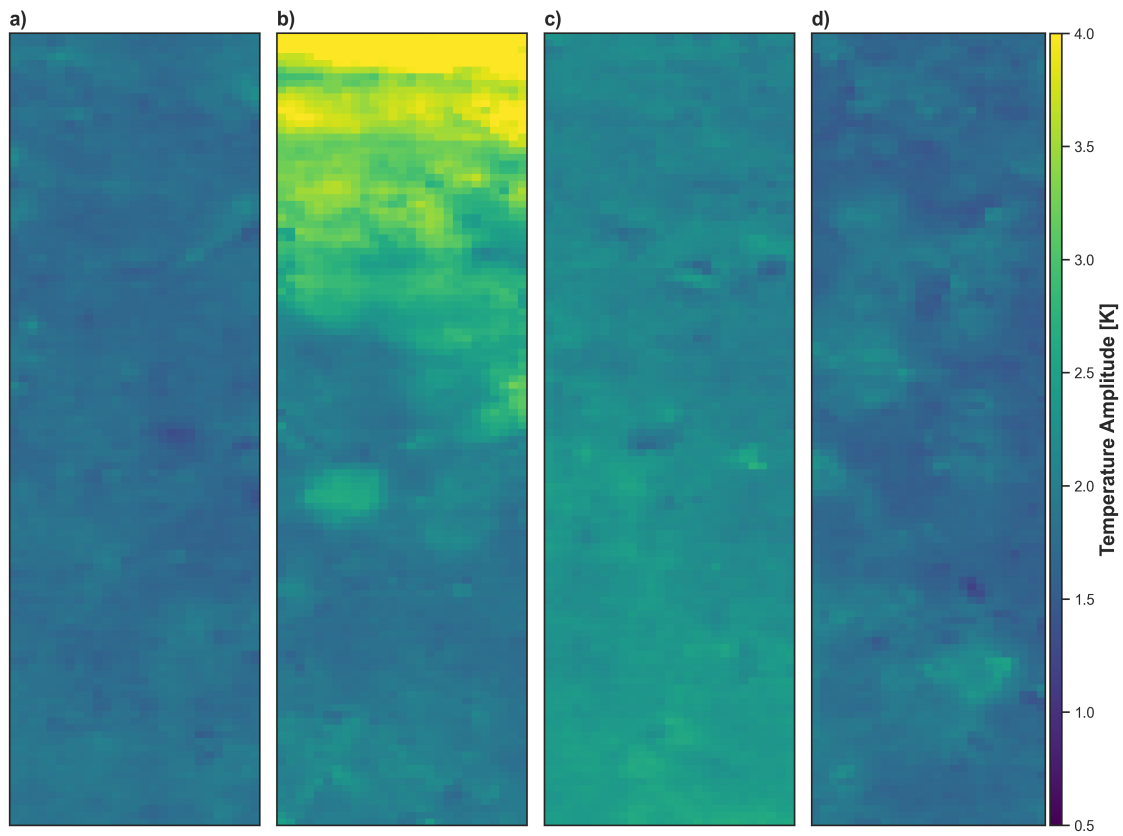
**Figure A3.4:** *Initial temperature amplitude of glucose-treated soil surfaces captured with the active IRT approach referring to Grinderwald topsoil ($G_T^+$) (a), Kalwes topsoil ($K_T^+$) (b), Grinderwald subsoil ($G_S^+$) (c), and Kalwes subsoil ($K_S^+$) (d).*
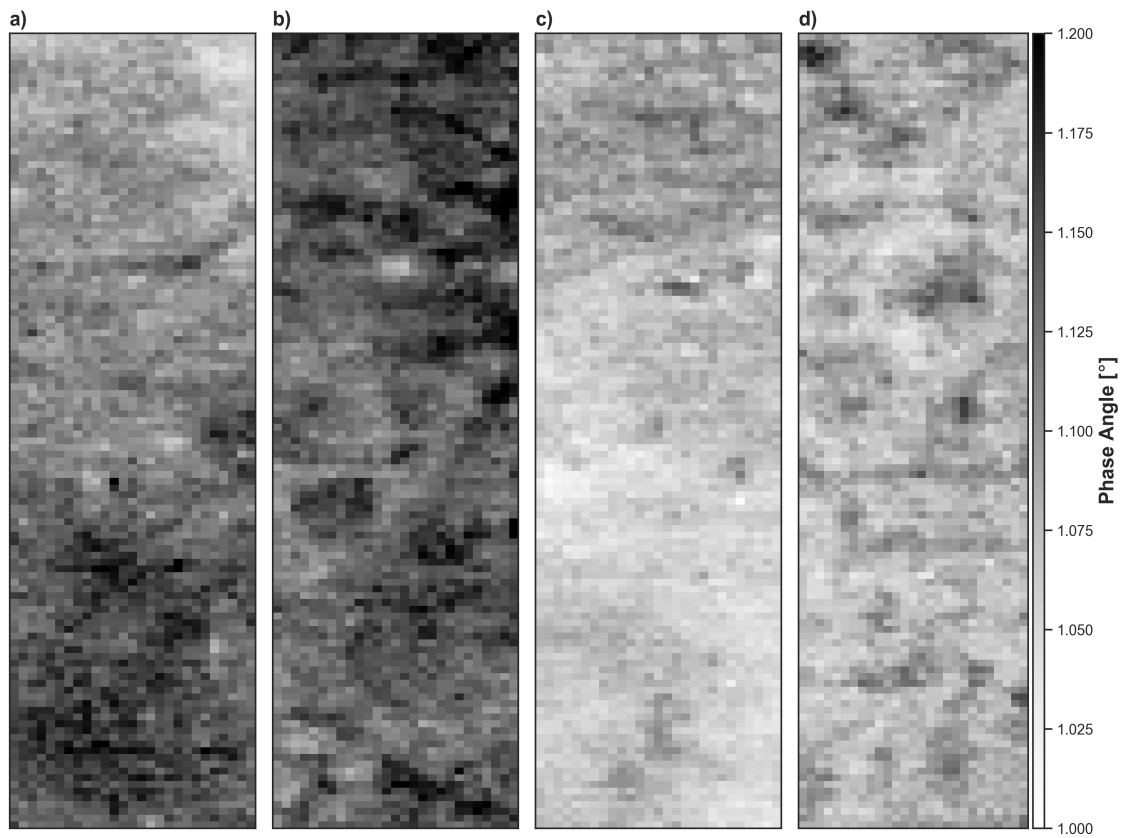
**Figure A3.5:** *Initial phase angle of glucose-treated soil surfaces captured with the active IRT approach referring to Grinderwald topsoil ($G_T^+$) (a), Kalwes topsoil ($K_T^+$) (b), Grinderwald subsoil ($G_S^+$) (c), and Kalwes subsoil ($K_S^+$) (d).*
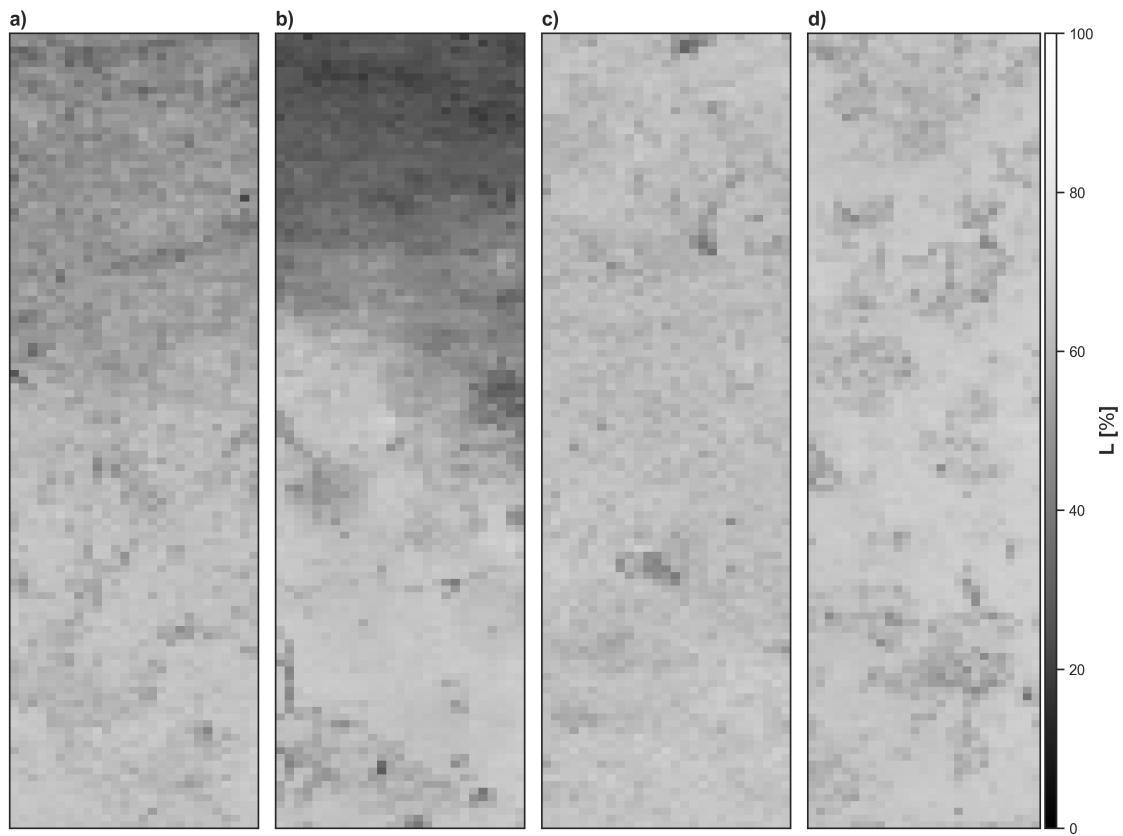
**Figure A3.6:** *Color value L of glucose-treated soil surfaces gained from photography referring to Grinderwald topsoil ($G_T^+$) (a), Kalwes topsoil ($K_T^+$) (b), Grinderwald subsoil ($G_S^+$) (c), and Kalwes subsoil ($K_S^+$) (d).*
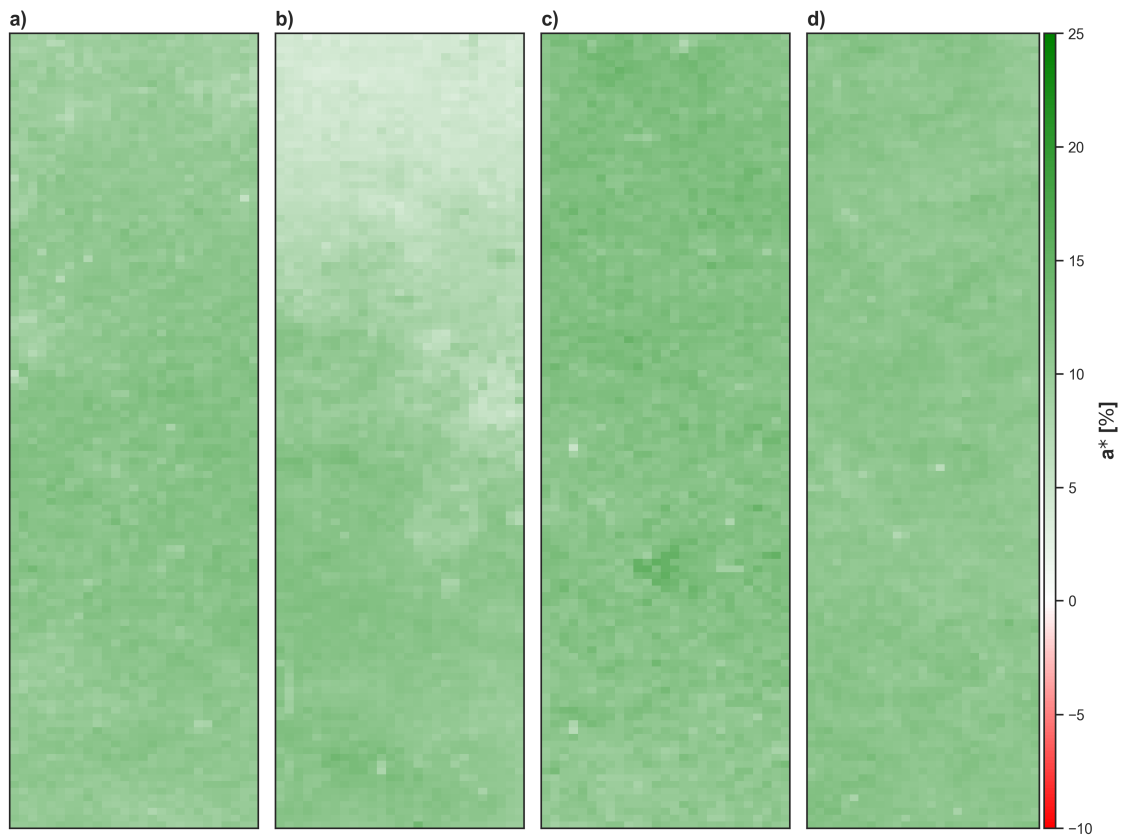
**Figure A3.7:** *Color value a* $^*$ *of glucose-treated soil surfaces gained from photography referring to Grinderwald topsoil ($G_T^+$) (a), Kalwes topsoil ($K_T^+$) (b), Grinderwald subsoil ($G_S^+$) (c), and Kalwes subsoil ($K_S^+$) (d).*
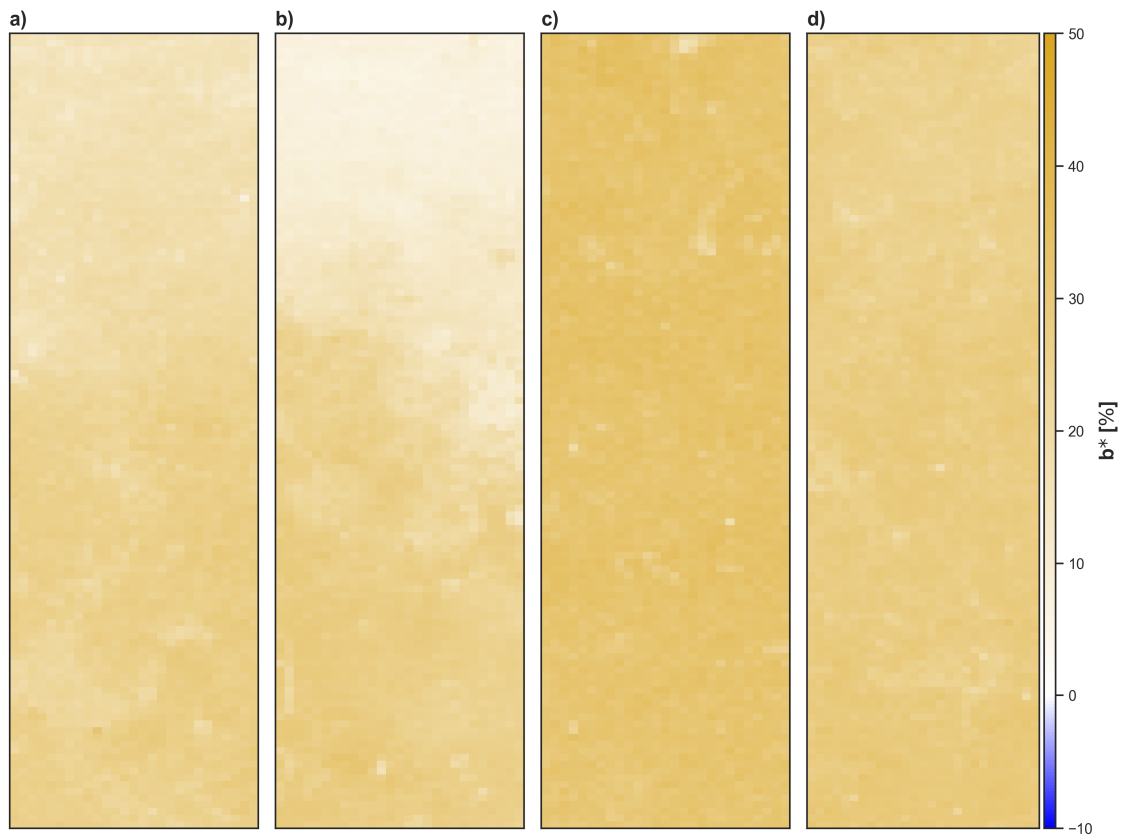
**Figure A3.8:** *Color value b\* of glucose-treated soil surfaces gained from photography referring to Grinderwald topsoil ($G_T^+$) (a), Kalwes topsoil ($K_T^+$) (b), Grinderwald subsoil ($G_S^+$) (c), and Kalwes subsoil ($K_S^+$) (d).*
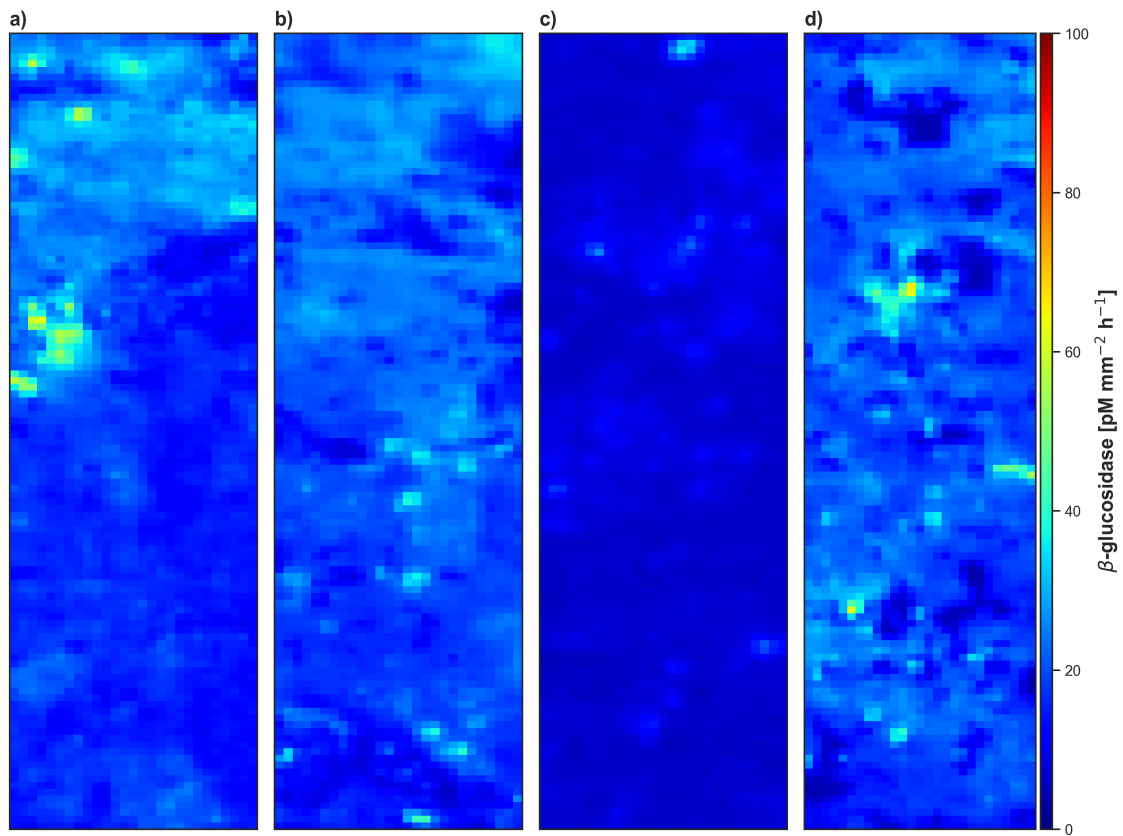
**Figure A3.9:** *Initial β-glucosidase activity of glucose-treated soil surfaces measured by zymography referring to Grinderwald topsoil ($G_T^+$) (a), Kalwes topsoil ($K_T^+$) (b), Grinderwald subsoil ($G_S^+$) (c), and Kalwes subsoil ($K_S^+$) (d).*

# Appendix IV

**List of publications**

1. K. Schwarz, J. Heitkötter, J. Heil, B. Marschner, B. Stumpe: The potential of active and passive infrared thermography for identifying dynamics of soil moisture and microbial activity at high spatial and temporal resolution, Geoderma, 327, 119 - 129, doi: 10.1016/j.geoderma.2020.114879, 2021.

   Peer-Review: The manuscript was submitted for publication in Geoderma on 23 February 2018 and after peer-review with two anonymous reviewers, it was accepted for publication on 29 April 2018.

   Modifications: References to figures, tables, sections and appendix are modified. Unifying the spelling of *hotspots* to *hot spots* and harmonizing capitalization of p and R.

2. K. Schwarz, J. Heil, B. Marschner, B. Stumpe: Hot movements on soil surfaces – Innovative insights into microbial dynamics using passive infrared thermography, Geoderma, 385, 114879, doi: 10.1016/j.geoderma.2018.04.028, 2018.

   Peer-Review: The manuscript was submitted for publication in Geoderma on 29 May 2020 and after peer-review with two anonymous reviewers, it was accepted for publication on 28 November 2020.

   Modifications: References to figures, tables, sections and appendix are modified.

3. K. Schwarz, T. Reinersmann, J. Heil, B. Marschner, B. Stumpe: High resolution mapping of surface heat evolution combined with other imaging approaches for analyzing spatial heterogeneity and temporal dynamics of microbial hot spots and hot moments in undisturbed soil samples, submitted to Geoderma, 2021.

Peer-Review: The manuscript was submitted for publication in Geoderma on 26 June 2021.

Modifications: References to figures, tables, sections and appendix are modified.

# ACKNOWLEDGEMENTS

Der Lebenslauf ist in der Online-Version aus Gründen des Datenschutzes nicht enthalten.

"If A is a success in life, then A equals x plus y plus z. Work is x; y is play; and z
is keeping your mouth shut"

*Albert Einstein*


"I have studied these things - you have not."

*Sir Isaac Newton*